Advanced Echocardiographic Imaging In Dogs With Myxomatous Mitral Valve Disease

Giulio Menciotti

Thesis submitted to the faculty of the Virginia Polytechnic Institute and State University
in partial fulfillment of the requirements for the degree of

Doctor of Philosophy
In
Biomedical and Veterinary Sciences

Michele Borgarelli – Committee Chair
Jonathan A. Abbott
Raffaella De Vita
Carlo Guglielmini
Jens Häggström
William R. Huckle

May 5, 2017

Blacksburg, Virginia

Keywords: canine, heart, diagnostic, imaging

Advanced Echocardiographic Imaging In Dogs With Myxomatous Mitral Valve Disease

Giulio Menciotti

Academic Abstract

Myxomatous mitral valve degeneration (MMVD) is the most common canine cardiac disease.

In the studies presented in this dissertation, we used advanced echocardiographic techniques to elucidate several aspects of MMVD in dogs. Our hypothesis was that the mitral valve (MV) morphology could have a role in the development of MMVD. First, we tested whether we could use real time three-dimensional transthoracic echocardiography (RT–3DTTE), and an offline software for MV analysis to evaluate canine MV. We described that the technique was feasible and repeatable, we evaluated the morphology of the MV in healthy dogs, and we provided reference values for MV morphologic variables in this species. Then, we used the same technique to compare healthy dogs to dogs affected by MMVD. We found that dogs affected by MMVD have more circular and flatter valve. We then analyzed the MV of healthy Cavalier King Charles Spaniels (CKCSs), given the high predisposition of this breed for MMVD. Our findings indicate that compared to healthy dogs of other breeds, the MV of healthy CKCSs is flatter and has less leaflet tenting, corroborating our hypothesis that an altered MV morphology could represent a predisposing factor for disease development. We also used RT–3DTTE to characterize the area of the regurgitant MV orifice of dogs affected with MMVD, finding that the technique requires further standardization in order to become clinically useful.

The elevation of pulmonary venous pressure caused by MMVD can, in some dogs, cause pulmonary arterial hypertension (PH), which is a risk factor associated with worse outcome in dogs with MMVD. Diagnosis of PH in dogs with MMVD is usually made by estimating pulmonary pressure using Doppler echocardiography. We are currently evaluating the accuracy of this technique, compared to invasive measurement of pulmonary pressure. Only preliminary data are presented regarding this study, as the disclosure of the blinding would have infringed the power of the study. Our preliminary results demonstrate that there is only moderate agreement between the two techniques, indicating that caution should be used when deriving the non-invasive estimation of systolic pulmonary pressure in order to make clinical decisions.

Advanced Echocardiographic Imaging In Dogs With Myxomatous Mitral Valve Disease

Giulio Menciotti

General Audience Abstract

The studies collected in this dissertation focus on myxomatous mitral valve disease (MMVD), which is the most common heart disease in dogs, and the most common cause of cardiac-related death in this species. This disease mainly affects one of the heart valves, i.e. the mitral valve (MV), impeding its normal functionality. In the studies presented in this dissertation, we used advanced non-invasive ultrasonographic techniques to investigate the mechanisms involved in this disease. We hypothesized that a different shape of the MV in some dogs could contribute to the development of the disease. We used 3D ultrasounds to build models of the MV and analyze the shape of it. We first demonstrated that using this technique in dogs was feasible and repeatable, and that the MV of normal dogs was elliptical and saddle-shaped. We then compared the shape of the MV of normal dogs, to the shape of the MV of dogs affected with MMVD. We found that dogs with the disease have a MV that is flatter and more circular. In our next study, we examined the shape of the MV of a breed of dogs that is predisposed to develop MMVD: Cavalier King Charles Spaniels (CKCSs). Our study found that healthy CKCSs have an overall flatter MV when compared with the other breeds, and that the normal MV of CKCSs is similar to the MV of affected dogs of other breeds. This finding support our hypothesis that an abnormal shape of the MV could contribute to the development of the disease. In another study, we saw to evaluate whether we could use 3D ultrasounds for investigating the shape of the hole that creates on affected MV. We concluded that this technique still requires more standardization before being used for evaluation of dogs.
In another study, of which some preliminary results are presented in this dissertation, we are testing how accurate it is to evaluate the pressure of the pulmonary artery using ultrasonography. We are doing this by comparing this technique to a direct measurement of the pressures with a catheter in the pulmonary artery. We found that measurements obtained with the two techniques do not agree very well, which most likely indicates the evaluation of the pulmonary artery pressure using ultrasonography requires caution.

alla mia Famiglia, lontana e vicina, fonte inesauribile di sostegno, incoraggiamento e motivazione.

to my Family, faraway and close, inexhaustible well of moral support, encouragement and motivation.

Acknowledgments

Like every important achievement, the work presented in this dissertation would have been impossible without the help and support of several people.

I owe my first acknowledgment to Carlo Guglielmini, who first introduced me to Cardiology and to Research; by proposing me to apply for the PhD position at Virginia Tech he not only showed me his trust, but also provided me with a great example of outstanding mentorship.

Immediately after, I need to acknowledge Helen Poser, who went above and beyond both as instructor and friend, preparing me at the best for starting this PhD.

Jonathan Abbott and Jens Häggström, for your invaluable hints and suggestions on every single study I performed, and for being wonderful scientists, cardiologists, and persons.

Sunshine Lahmers, Sonya Wesselowski, Michael Aherne, Jess Douthat, Nicky Kandzior, who during these years contributed incredibly to the hard work of collecting data, while keeping up with all the other daily clinical duties. You are the best team-mates!!

William Huckle, who taught me to never give up on science, and to have cautious confidence in my results.

My entire PhD committee, for overlooking my progresses and experiments, and for providing me with a great guidance through the entire PhD.

Becky Jones, your role in our Graduate Program cannot be described by the name of a working position. You represent a bright steady point for every student to look at while they are navigating in the stormy waters for obtaining their degree.

All the owners who, across two continents, responded to our several calls for enrolling dogs in the studies.

Sandra Müller and Stephanie Apple, who undertook with great enthusiasm and curiosity their first approach to research in our lab. You had been great lab-mates.

Safak, Roberto, Davide L, Emanuele, Eftila, Tugce, Marina, Davide P, are only a handful of the tens of amazing, supporting people met during these years, who contributed immensely to reaching this goal by being companions of endless memorable moments.

Lucy, you welcomed me as family and have always been nice and supportive with me.

My mom, dad, and brother, for encouraging me to undertake this challenge at first, and for constantly giving me the advice I need. You all will always be my role model.

Alejandra. No written acknowledgment could truly express your role in my life during these last years, and how much motivation and strength you give me. Your smile and enthusiasm push me through every single day.

Michele. *Mentor* and *Advisor*. Two words that were coined after you. I owe you <u>everything</u> I have achieved in these last four years, and everything that will come after. Most importantly, you taught me the greatness of humility, at work and in life. I will always be grateful to you.

Table of Contents

List of figures

List of tables

List of abbreviations

2DE	Two-dimensional echocardiography
ACVIM	American College of Veterinary Internal Medicine
AHCWR	Annulus height to commissural width ratio
AnH	Annulus height
ANOVA	Analysis of variance
AROA	Anatomic regurgitant orifice area
BW	Body weight
CKCS	Cavalier King Charles Spaniel
CO	Cardiac output
CV	Coefficient of variation
EROA	Effective regurgitant orifice area
LA	Left atrium
LA Vol/BW	Left atrial volume indexed to body weight
LA:Ao	Left atrial to aortic root ratio
LV	Left ventricle
MMVD	Myxomatous mitral valve disease
MR	Mitral regurgitation
MRSS	Mitral regurgitation severity score
MV	Mitral valve
nALA	Normalized anterior leaflet area
nALL	Normalized anterior leaflet length
nALPMD	Normalized anterolateral-posteromedial annulus diameter
nAnA	Normalized annulus area
nAnCirc	Normalized annulus circumference
nAPD	Normalized antero-posterior annulus diameter
nCmD	Normalized commissural diameter
NPA	Non-planar angle
nPLA	Normalized posterior leaflet area
nTnV	Normalized tenting volume
PA	Pulmonary artery
PASP	Doppler estimated pulmonary artery systolic pressure
PH	Pulmonary hypertension
PI	Pulmonary insufficiency
PLL	Posterior leaflet length
RT–3DTTE or RT3DE	Real-time three-dimensional transthoracic echocardiography
SI	Annulus sphericity index
SLU	Swedish University of Agricultural Sciences
TnA	Tenting area
TnH	Tenting height
TR	Tricuspid regurgitation
VMCVM	VA-MD College of Veterinary Medicine
VPS	Volumes per second

Attribution

The studies presented in this dissertation would have not been possible without the collaboration of several investigators, which are listed as co-authors of the manuscripts presented. The individual contribution of each author in each study is hereby presented:

1. Assessment of mitral valve morphology using three-dimensional echocardiography. Feasibility and reference values.
   G. Menciotti: study design, performed 3D echocardiographic measurements, performed statistical data analysis and interpretation, wrote manuscript, served as corresponding author for the review process.
   M. Borgarelli: study design, echocardiographic images acquisition, contributed to data interpretation, contributed to manuscript preparation and revision.
   M. Aherne: echocardiographic images acquisition, contributed to manuscript preparation and revision.
   J. Häggström: contributed to study design, contributed to data interpretation, contributed to manuscript preparation and revision.
   I. Ljungvall: contributed to manuscript preparation and revision.
   S.M. Lahmers: contributed to data interpretation, contributed to manuscript preparation and revision.
   J.A. Abbott: contributed to study design, echocardiographic images acquisition, contributed to data interpretation, contributed to manuscript preparation and revision.
2. Mitral valve morphology assessed by three-dimensional transthoracic echocardiography in healthy dogs and dogs with myxomatous mitral valve disease.
   G. Menciotti: study design, performed 3D echocardiographic measurements, performed statistical data analysis and interpretation, wrote manuscript, served as corresponding author for the review process.
   M. Borgarelli: study design, echocardiographic images acquisition, contributed to data interpretation, contributed to manuscript preparation and revision.
   M. Aherne: echocardiographic images acquisition, contributed to manuscript preparation and revision.
   S. Wesselowski: echocardiographic images acquisition, contributed to manuscript preparation and revision.
   J. Häggström: contributed to study design, contributed to data interpretation, contributed to manuscript preparation and revision.
   I. Ljungvall: contributed to manuscript preparation and revision.
   S.M. Lahmers: contributed to data interpretation, contributed to manuscript preparation and revision.
   J.A. Abbott: contributed to study design, echocardiographic images acquisition, contributed to data interpretation, contributed to manuscript preparation and revision.
3. Comparison of the Mitral Valve Morphology between Cavalier King Charles Spaniels and other Dog Breeds using Real-time 3D Transthoracic

Echocardiography.
G. Menciotti: study design, performed 3D echocardiographic measurements, performed statistical data analysis and interpretation, wrote manuscript, will serve as corresponding author for the review process.
M. Borgarelli: study design, echocardiographic images acquisition, contributed to data interpretation, contributed to manuscript preparation and revision.
M. Aherne: echocardiographic images acquisition, will contribute to manuscript preparation.
P. Camacho: contributed to echocardiographic images acquisition, will contribute to manuscript preparation.
J. Häggström: echocardiographic images acquisition, contributed to study design, contributed to data interpretation, contributed to manuscript preparation and revision.
I. Ljungvall: echocardiographic images acquisition, will contribute to manuscript preparation.
S.M. Lahmers: contributed to data interpretation, will contribute to manuscript preparation.
J.A. Abbott: contributed to study design, echocardiographic images acquisition, contributed to data interpretation, contributed to manuscript preparation and revision.

4. Anatomic Regurgitant Orifice Area Obtained Using 3D-Echocardiography As An Indicator of Severity of Mitral Regurgitation in Dogs With Myxomatous Mitral Valve Disease.
   S. Müller: performed 3D echocardiographic measurements, contributed to manuscript preparation and currently contributing in manuscript revision.
   G. Menciotti: study design, trained S. Müller in echocardiographic images interpretation and measurement, performed 3D echocardiographic measurements, performed statistical data analysis and interpretation, contributed to manuscript preparation and currently serving as corresponding author for the review process.
   M. Borgarelli: study design, echocardiographic images acquisition, contributed to data interpretation, contributed to manuscript preparation and currently contributing in manuscript revision.
5. Accuracy of Noninvasively Determined Pulmonary Artery Pressure in Dogs with Myxomatous Mitral Valve Disease (MMVD).
   G. Menciotti: study design, data collection, data analysis, report preparation.
   M. Borgarelli: study design, echocardiographic examination, non-invasive measurement of systolic pulmonary artery pressure.
   M. Aherne: cardiac catheterization.
   J. A. Abbott: contributed to study design, cardiac catheterization, invasive pressure tracings measurements.

Introduction

Relevance of myxomatous mitral valve disease in the dog

Myxomatous mitral valve disease (MMVD) is the most common canine cardiovascular disease [1,2]. The disease is more prevalent in small breed dogs than in large breed ones, and some small breeds are reported with an incidence close to 100% over a dog's lifetime [3–5]. Reports about the prevalence of the disease are however largely influenced by the methodic used for the diagnosis (pathologic examination vs. cardiac auscultation vs. echocardiographic examination). Detweiler and Patterson in 1965, in an epidemiological study combining clinical and necropsy findings focused on dogs' cardiac diseases, described a prevalence of "chronic valvular disease" of almost 55% of all the dogs with heart disease, increasing from 8-11% of dogs in the 5-8 years old group, to 20-25% in the 9-12 years old group, and between 30% and 40% in dogs older than 13 years of age [1]. Although in general small breeds are more affected than large breeds, Cavalier King Charles Spaniels have been reported as having an even higher prevalence of the disease. Particularly, in this breed is estimated that 50% of the dogs will develop the condition at about 6 years of age or earlier [5,6], with recorded prevalence of 100% over 10 years of age [6].

The pathophysiology of the disease as well as the valvular degenerative process are well described. Valves affected by the myxomatous degeneration undergo a process in which both the cellularity, and the matrix deposition increase [7,8], eventually completely disrupting the otherwise highly organized ultrastructural architecture of the leaflets. In myxomatous valves, the normal interstitial cells shift towards a myofibroelastic phenotype, and increased α-actin positive staining phenotype [9,10], along with expression of matrix metalloproteinases and collagenolytic enzymes. The consequent decrease in collagen, along with the increase in glycosaminoglycans in

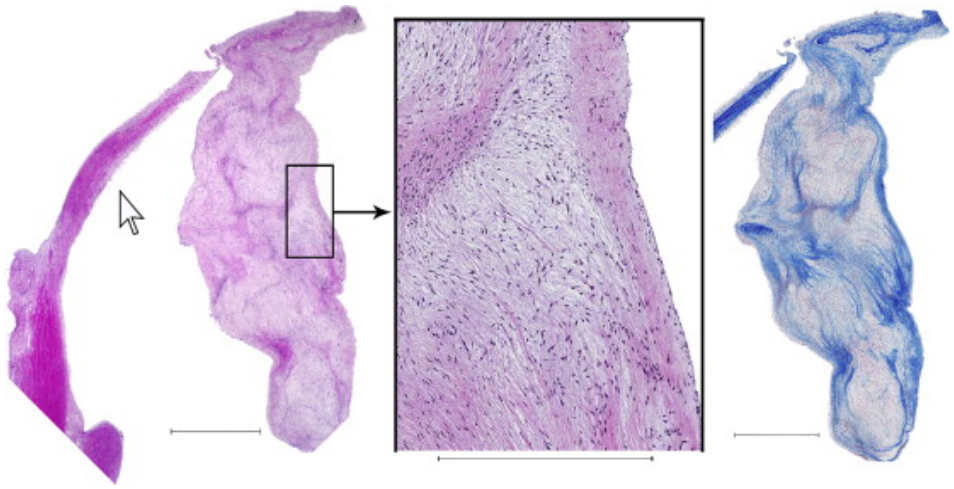

Fig. 1 Photomicrograph of the distal posterior mitral valve leaflet from a 12 year old, male, Maltese dog with severe myxomatous valve disease (Whitney stage IV pathology), illustrating the most prominent structural features of this condition- increased thickness of the spongiosa from glycosaminoglycan and proteoglycan deposition, and degeneration of the fibrosa. Left frame (H & E; Bar = 1 mm) and right frame (Masson trichrome; bar = 1 mm) reveal total loss of the leaflet's normal layered arrangement. Collagen bundles in the fibrosa have undergone disintegration. Only scattered remnants remain which are variably displaced throughout the thickened valve stroma, forming swirls throughout the leaflet. These changes contribute to the gross appearance of increased opacities in the leaflet, and focal nodular thickening in the leaflet edge. A large, second-order chorda tendinae associated with this leaflet appears on the left side of the left frame. Center frame is higher magnification taken from the area of interest within the box of the left frame. Markedly increased glycosaminoglycan deposition transforms the spongiosa into a relatively granular appearing stroma, which contains stellate and spindle-shaped cells, and scant mononuclear infiltration within the increased myxomatous content. H & E; Bar = 500 mm). From: P. Fox, J Vet Cardiol, 2012;14:103–26

diseased area of the valve [11], affect the mechanical and likely the transduction properties of the valve. Collagen fibrils, in fact, usually align to the main tensile force acting on a tissue; in diseased areas of the myxomatous valves, they become not only more sparse, but they also lose their spatial organization [12], therefore decreasing the mechanical stability of the structure (Fig. 1). These microscopic structural derangements ultimately lead to macroscopic alterations of the MV and its apparatus, ranging in severity and extension as described and classified by Pomerance and Whitney [13]. The combination of micro and macroscopic alterations represents a flaw in the otherwise perfectly tuned apparatus of the MV, resulting in incomplete apposition of the mitral leaflets and therefore the first clinical evidence of the disease, mitral regurgitation. However, it is worth mention that given the still unclear etiopathogenesis of the disease, and the profound interrelations between abnormal valvular stress and alteration of the MV ultrastructure, it is

difficult to discern which alterations are primary characteristics of the disease process, and which are secondary to the mechanical imbalance created in the disease status. Experiments on ovine models in fact, were able to demonstrate that inducing MR by piercing a mitral leaflet is enough to trigger ultrastructural leaflet remodeling similar to the one found in MMVD [14]. Regarding annular morphology instead, the changes observed in the same experimental procedure were different from the morphological changes reported in natural occurring ischemic and myxomatous MR [15,16]. This could indicate that the annular morphological changes found in these diseases are more likely primary, rather than secondary to the MR.

The presence and severity of MMVD in some breeds, i.e. Cavalier King Charles Spaniels (CKCSs) and Dachshunds, is highly heritable [17–19]. Particularly, in a Swedish cohort of CKCSs, both the proportion of offspring with heart murmurs, and the intensity of the murmurs, were related to the ones of the parental generation [18]. An analysis of the data recorded in the context of the United Kingdom breed club heart monitoring scheme, revealed high heritability of the murmur presence and intensity in four years old CKCSs [17]. For these reasons, is now widely accepted that MMVD has a genetically determined component, and identifying and breeding against traits that predispose to the disease is crucial. However, using only cardiac auscultation to guide selective breeding in United Kingdom and Sweden had been somewhat disappointing [20,21]. On the contrary, encouraging results were obtained by the Danish CKCSs breeding program, which used an association of echocardiography and cardiac auscultation as screening method [22].

The morphology of the mitral valve apparatus

"The mitral apparatus is a complex, finely coordinated mechanism […]" (Perloff and Roberts 1972) [23] which involves the interactions of left atrial wall, mitral annulus, mitral leaflets, chordae tendinae, papillary muscles, and left ventricular wall. In the case of a healthy individual, these components act in harmony in order to provide unidirectional flow from the left atrium to the left ventricle tens of thousands of times a day.

Evidence of the non-planarity of the canine mitral annulus can be extrapolated from invasive experiments using dogs models for analyzing the annular motion during the cardiac cycle in the early 1970's [24]. In this study, a picture of the lateral roentgenogram of the lead beads sutured to the MV annulus of an experimental dog, clearly do not follow a flat ring fashion, but no mention to this annular characteristic can be found in the text of the manuscript. In 1987 Levine postulated that the MV annulus was not a mere flat ring, but could resemble more an hyperbolic paraboloid, a configuration commonly called "*saddle-shape*" [25]. Few years later he could clearly demonstrate the saddle-shape of the mitral annulus and its implications in the diagnosis of mitral prolapse in vivo [26]. Curiously, using an ingenious system for *image acquisition, analysis, and offline modeling*, a tomographic reconstruction of the MV was generated and the saddle-shape of the MV annulus was clearly evident (Fig. 2).

However, a strong push towards further investigations of MV biomechanics derived slightly later from the use of ring annuloplasty in the context of MV repair. When enough data on this technique was collected, investigators realized that early MV repairs were "[…] associated with significant number of repair failures result[ing] from chordal, leaflet, and suture line disruption,

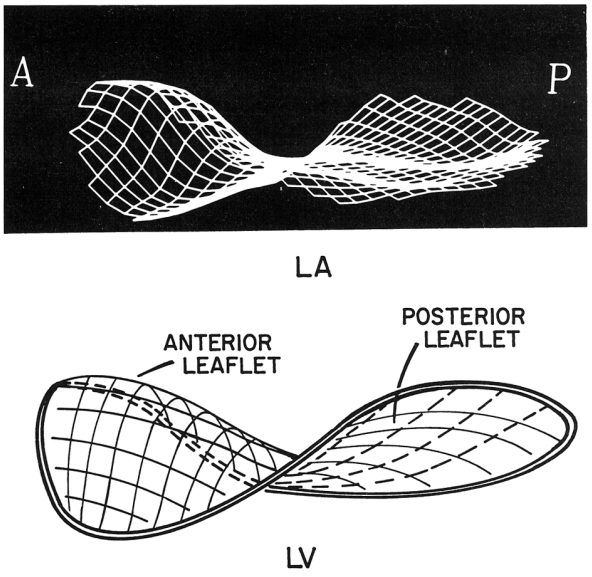

Fig. 2 Illustration of topographical map of the leaflet surface fitted to traces of the closed leaflets from one subject (upper panel), with corresponding line drawing (lower panel). A, anterior; P, posterior; LA, left atrium; LV, left ventricle. From: R. Levine et al. Circulation, 1989;80:289-298

which suggest that mechanical leaflet stress plays a significant role [27]" [28]. The importance of the morphological characteristics of the mitral annulus in the valvular biomechanics were investigated both by finite element modeling and in experimental settings [16,25,28–35]. The common finding across the methodologies is that the annular shape is a fundamental determinant of the stress acting on the MV leaflets. Particularly, the non-planarity of the annulus plays a key role in minimizing peak leaflet stress, compared to a flat annular configuration. Results of the computational studies were confirmed by in-vivo analysis: the calculated annular parameter resulting in optimal leaflet stress in the model, were found to be very close to the ones measured in healthy individuals, even across different mammalian species [35]. Further endorsement arrived then from studies focused on annuloplasty rings with different configurations, where saddle-shaped rings, compared to flat ones, were found to augment the non-planar shape of the mitral annulus [32] therefore increasing the overall leaflet curvature [28], experiencing lower forces [29], and improving leaflet coaptation [31]. At the same time, although intrinsically linked to MV annular morphology, also the configuration and morphology of the MV leaflets is fundamental in minimizing the stress on the leaflets themselves. Particularly, leaflet billowing contributes along with the annular shape in optimizing leaflet curvature and creating a

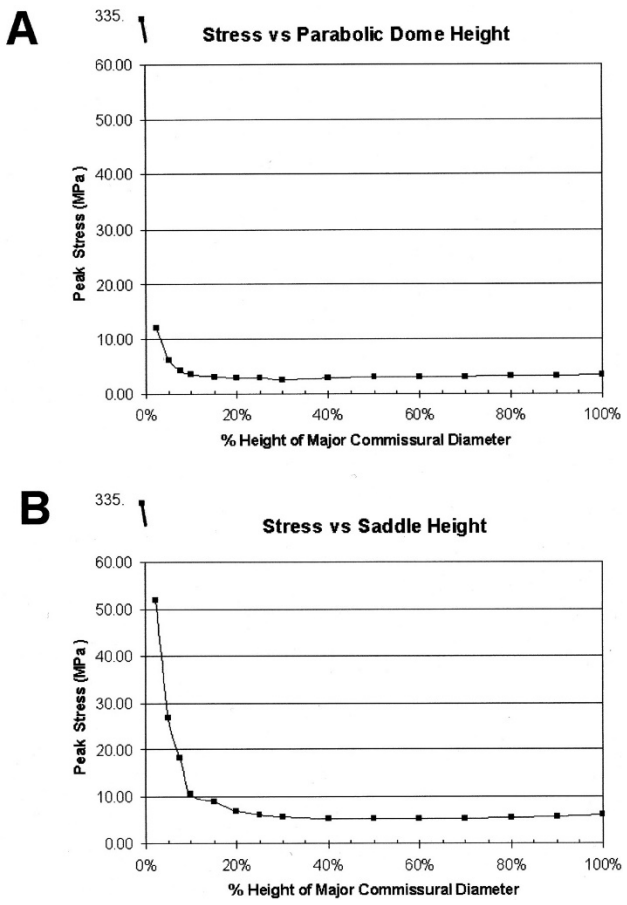

Fig. 3 Plot of peak stress versus percent height. The elliptic paraboloid (A) and the hyperbolic paraboloid (B; saddle) are shown. A, Peak stress for the billowing leaflet model. B, Peak stress for the nonplanar annulus model. A flat disc results when the parameters for each model, hb [parameter controlling for leaflet billowing] and ha [parameter controlling for annulus height] respectively, are set to 0. The peak stress of the flat disc is 335 MPa in A and B. From: I. Salgo et al. Circulation, 2002;106:711-717

serve as diagnostic factors and breeding criteria.

lower-energy status with the annulus and chordae tendinae, minimizing stresses on the leaflets [36] (Fig. 3).

In vitro experiments on canine MVs demonstrated that applying an abnormal stress on the leaflets could trigger the expression of effector proteins and markers of myxomatous degeneration [37]. Also, it has been demonstrated that the abnormal stress caused by piercing otherwise normal ovine leaflets causes expression of proteins that suggest active matrix and collagen reorganization [14].

Therefore, investigating the morphology of the MV and its apparatus could provide new insights in the etiopathogenesis and diagnosis of MMVD in dogs, identifying new characteristics of the disease which could

Three-dimensional echocardiography

The importance of the geometric complexity of cardiac structures, and of their reciprocal relationship has always been clear. Therefore, the push for the development of three-dimensional (3D) reconstruction from ultrasonographic images started back in the early 1970s [38]. Through a constant improvement of informatics calculation speed, and ultrasonographic transducer technology, the first mechanically rotating transducers were developed, which then left the step to electronic matrix transducers. The following step was for systems to become capable of acquiring and showing three-dimensional images at the same time, which lead to the birth of the so-called real-time 3D echocardiography. Nowadays, pretty much all the transducers used in 3D echocardiography are *"fully sampled matrix transducers",* which can be imagined like a grid (matrix) of thousands of elements, working together for acquiring and transmitting volumes to the main ultrasound unit. Several acquisition modalities have been implemented, the most common being:

- live 3D
- live 3D zoom
- full volume acquisition

Pros and cons of the different modalities are well described in the textbook of Buck et al. by the triangle of interdependency: Volume size, temporal resolution, and spatial resolution represent three interdependent characteristics of real-time 3D volumes [39] (Fig. 4). Particularly, increasing one of these three factors will inevitably have the tradeoff of reducing the other two. For this reason, for example, acquiring images in live 3D mode would have a high temporal resolution, i.e. high frame rates expressed in volumes-per-seconds (vps), but the volumes that can be imaged are small, and indirectly proportional to the spatial resolution obtained; in live 3D zoom mode, an even smaller volume is imaged, obtaining in exchange high temporal and spatial resolutions.

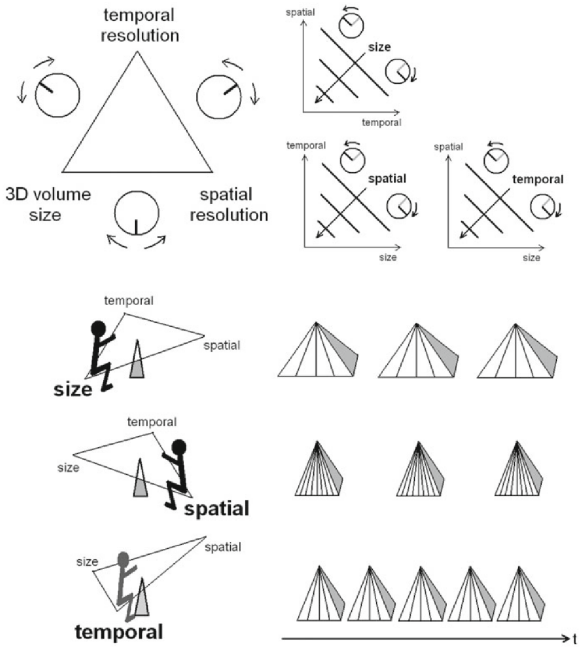

Fig. 4 Principle of interdependency of 3D volume size, temporal and spatial resolution. Upper left: The interdependency is expressed by a triangle where all three parameters are connected to each other. The dial knobs between each pair of parameters indicate the option for weighting more to the one or the other. Upper right: The three diagrams illustrate the effect of the dialing for all possible settings of the three parameters. The upper diagram shows for a given 3D volume size the effect of dialing more towards increased spatial resolution causing lower temporal resolution and vice versa. With increasing 3D volume size (in direction of the size arrow), however, both temporal and spatial resolution have to decrease. Lower part: Interdependency between the three parameters is illustrated by the triangle balanced on a center axis point. The preference set to a large 3D volume size (top) causes lower temporal resolution (as indicated by the separation between pyramids on the right) and lower spatial resolution (as indicated by the three wide-spread lines). The preference set to higher spatial resolution (middle) causes smaller 3D volume size at a lower temporal resolution (the higher spatial resolution indicated by a larger number of lines with higher density). The preference set to higher temporal resolution (bottom) causes smaller 3D volume size and lower number and density of lines. From: T. Buck, A. Franke, M. Monaghan. Three-dimensional Echocardiography. Chapter 2 Basic principles and practical application p. 32 – 2015 Springer Berlin Heidelber

The full-volume acquisition instead, as suggested by the name, allows the acquisition of bigger volumes, maintaining relatively high frame rates and spatial resolution. In this technique, the imaged area is divided into several smaller sectors which are sequentially acquired during consecutive cardiac cycles, appropriately timed using the ECG (ECG triggering), and then stitched together in order to reconstruct the entire volume. The biggest downside of this technique is the possible misalignment of the different sectors, also called *stitching artifact*. This artifact can originate when the position of the cardiac structures relative to the probe varies during the same phase of consecutive cardiac cycles. This is usually originated when the cycle length changes beat-

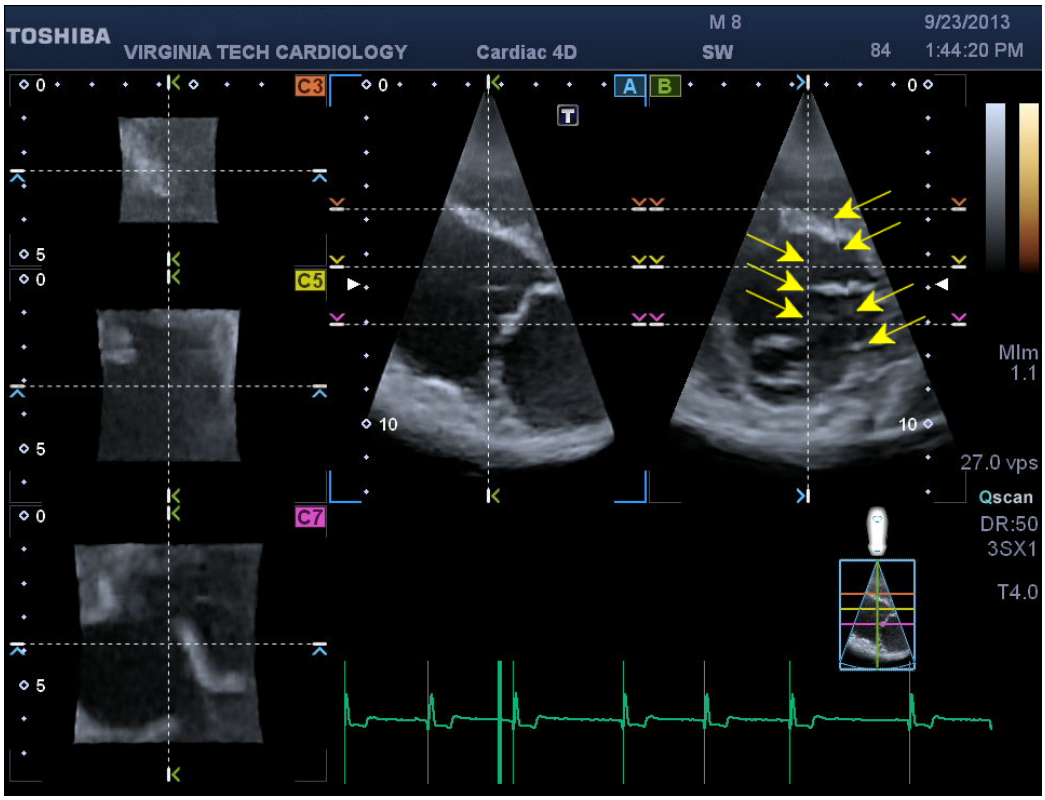

Fig. 5 Example of a stitching artifact on a "pre–4D" acquisition. On the right of the image two orthogonal images are simultaneously shown, representing a right parasternal long-axis and short-axis image of the left ventricle at the level of the mitral valve, respectively. On the left, three transverse plane are represented. It can be notice in the image on the right (short-axis) that the different sectors comprising the image are misaligned generating a stitching artifact along the lines indicated by the yellow arrows. The ECG trace on the bottom reveals the presence of sinus arrhythmia, likely causing the stitching artifact.

to-beat (arrhythmias), and when there is excessive movement of the thoracic cavity during respiration (Fig. 5). The entity of the stitching varies. Misalignment that are only slight, and affect only few sectors, are usually tolerated. In humans and in anesthetized subjects, this artifact is usually avoided by performing the acquisition while having the patients holding their breath, or pausing respiration. In conscious animals, this is clearly challenging. In our experience, gently holding a hand on the chest of the dog to minimize thoracic movement, often is enough to reduce the amount of cardiac translation motion relative to the probe, and therefore the amount of stitching. Another challenge in using this technique in dogs arises from the high prevalence of sinus arrhythmia, which continuously changes the cycle length, producing full-volume images with stitching artifacts. Therefore, it is important to perform the full-volume acquisition when the

rhythm is more regular, and sometimes a slight stimulation of the dog intended to temporarily decrease the vagal tone, can help to obtain stitching-free images. The first veterinary clinical study using 3D echocardiography, was published in 2010 [40]. Real-time three-dimensional transthoracic echocardiography (RT–3DTTE) was used for estimating end-systolic and end-diastolic LV volumes and comparing them to conventional methods (two 2D methods and the Teichholz method from M-Mode images), finding good agreement between the 2D techniques and RT–3DTTE, and confirming an overestimation of the LV volumes by the Teichholz method. In the same study, the estimation of LA sizes using RT–3DTTE was also investigated and compared to LA/Ao measures, finding increasing differences between the two techniques with atrial dilatation. Subsequently, a dedicated comparison of LA measurements using RT–3DTTE in 32 healthy dogs [41], revealed that none of the analyzed 2D methods for estimating LA sizes indexed to the BW has good correlation with body-weight indexed LA volume obtained using RT–3DTTE. In the same study, the better estimate of the volume calculated using RT–3DTTE was obtained by allometric scaling of the 2D measurements [41]. Lately, an analysis of LV volumes in healthy dogs and dogs affected by MMVD was performed [42], and found that end-diastolic and end-systolic LV volumes significantly expand only in dogs that are severely affected, and that the central portion of the LV, compared to the basilar and the apical ones, is the main contributor to this increase in volumes. Furthermore, the LV was found to change shape into a more spherical one, with potential implications on the geometry of the MV apparatus. To the best of our knowledge, our group was the first to use 3D echocardiography for systematically analyzing canine's MVs in the studies reported in this dissertation.

All the three-dimensional datasets used in the original studies presented in this dissertation (pp. 20–76), have been acquired using a full-volume acquisition over four consecutive beats. Briefly,

from a left apical acoustic window, correct alignment was assessed by a multi-plane real-time view (called "pre – 4D" in our machine), showing two orthogonal long-axis planes along with three short-axis sections; the transducer position was optimized so that the two long-axis views showed standard apical four- and two-chamber views (Fig. 6). Depth, azimuth and elevation were then adjusted in order to focus the ultrasound beam on the mitral apparatus and include the left ventricular outflow tract. Acquisition modality was then switched to the multi-beat acquisition mode (called "full – 4D" in our machine), and 3D full-volume datasets were acquired from four consecutive beats. Three consecutive datasets were stored. When possible, cineloops free from artifacts were selected for storage [43].

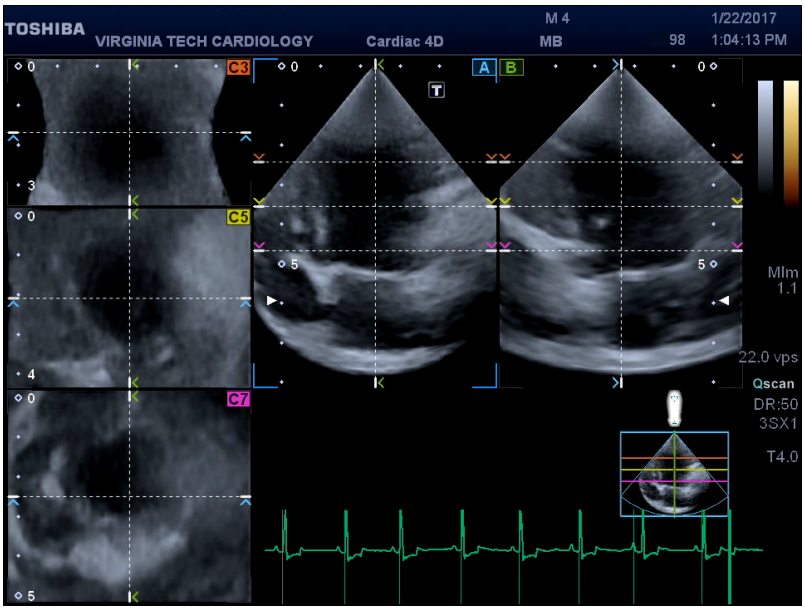

Fig. 6 Acquisition of RT–3DTTE full-volume datasets for analysis of the MV. Five different planes are visualized simultaneously. On the right the two long-axis views show an apical four-chamber view on the left (plane labeled A by the ultrasound unit) and two-chambers view on the right (plane labeled B). Three short axis section are also shown simultaneously on the left.

Offline analysis of three-dimensional mitral valve datasets

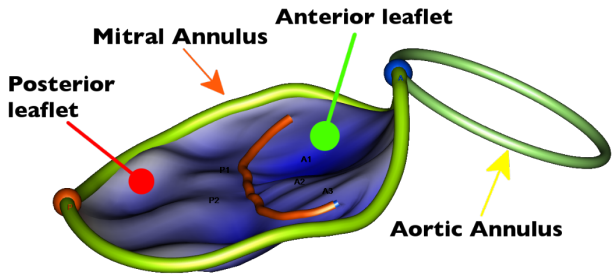

Fig. 7 Mitral valve model generated by offline analysis of a dog's RT–3DTTE dataset seen from a side. The mitral annulus (orange arrow) and aortic annulus (yellow arrow) are indicated, as well as the anterior (green arrow) and posterior (red arrow) mitral leaflets.

Once the full-volume datasets are acquired, they can be manipulated in order to obtain different pieces of information. Modern ultrasound units allow some degree of processing of the 3D datasets like cropping, multiplanar reconstructions, perspective views, or distances and areas measurements. However, the use of dedicated software specifically created for the manipulation of these datasets, usually provides the opportunity of a much thorough, complex, and standardized analysis. Two software packages were used for manipulation of 3D datasets in the studies comprising this dissertation: *4D MV–Analysis*, and *4D Cardio–View*, both from *TomTec Imaging Systems*, Unterschleißheim, Germany. The first software guides the operator through the identification of some specific landmarks on the 3D datasets, and uses an automated tracking algorithm to identify the MV leaflets. A manual review process allows the operator to correct possible tracking errors. A 3D model of the MV is then generated (Fig. 7), and a set of standardized variables are measured on the model. More details about this software, and hyperlinks to online additional content, are presented in the "Methods" section of the paper: Assessment of mitral valve morphology using three-dimensional echocardiography. Feasibility and reference values (pp. 20–31). The *TomTec 4D Cardio–View* on the other hand is a more generic software which allows cropping, slicing, and measuring of 3D echocardiographic datasets. One of

the function of this software, which was used for our study, is the simultaneous visualization of three orthogonal planes. The planes can be moved across the dataset in order to identify structures of interest, which are then measured from a preferred "en face" view. This approach had been proven useful in humans for evaluation of sizes and characteristics of ventricular septal defects [44], and atrial septal defects [45]. We used this method to obtain en face views of mitral regurgitant orifices in dogs affected by MMVD, and measure the anatomical regurgitant orifice area (AROA). More details about this software and the methodology used, are presented in the "Methods" section of the paper: Anatomic Regurgitant Orifice Area Obtained Using 3D-Echocardiography As An Indicator of Severity of Mitral Regurgitation in Dogs With Myxomatous Mitral Valve Disease (pp. 59–76)

Pulmonary hypertension in dogs affected by myxomatous mitral valve disease

Pulmonary hypertension is a well-recognized condition in both humans and dogs [46]. Historically, PH has been classified as primary or secondary depending on the presence or absence of identifiable causes. In dogs, primary PH is a rare condition. Secondary PH can be due to several causes, including Dirofilariasis, left-sided heart failure, chronic lung disease and pulmonary thromboembolism. Left-sided heart failure is one of the most common causes of PH in dogs [47–50]. Studies have reported that the prevalence of PH in dogs with MMVD ranges from 14 to 48%, representing a clinically relevant condition in dogs with this disease [50–52]. Pulmonary hypertension due to left-sided heart failure is initially the consequence of passive back transmission of increased left ventricular filling pressure to the pulmonary circulation. This stage is generally considered to be reversible. When elevation of left-ventricular filling pressure is sustained, a "reactive" increase in pulmonary pressure can occur. This "reactive" phase is due to an increase in pulmonary vascular resistance in response to vasoconstrictive stimuli mainly mediated by the endothelium, like endothelin–1 release and decrease response to endogenous nitric oxide [53]. If the high pressure is maintained, medial hypertrophy with muscolarization of arterioles and pulmonary vein "arterialization" [54,55], and intimal fibrosis and dilation both at the arterial and at the venous side can occur, resulting in a decreased vasodilatory response [55]. In dogs with MMVD, a Doppler estimated systolic pulmonary pressure (PASP) at or above 48 mmHg, is suggestive of irreversible PH [56]. Interestingly, in humans a similar pressure gradient is also associated with poor outcome [57]. In humans with MR, PH has been associated with an approximately double the risk of death and heart failure [57], and in patients with cardiomyopathies an increase in the hazard of death by 25% has been reported for each 5-mmHg increase in mean pulmonary arterial pressure [58]. Furthermore, as an effect of sustained PH,

right ventricular failure can occur, providing as well a two-fold increase in risk of premature death [59]. A recent study confirmed that also in dogs with MMVD, PH is associated with a worse prognosis, that a PASP greater than 55mmHg is an independent predictor of poor outcome with a hazard ratio of 1.8, and that for patients with PASP > 50mmHg the risk of death increases linearly with the increase in PASP [60].

Right heart catheterization is considered the "gold standard" for diagnosis of PH in humans [61]. This technique provides accurate measurements of systolic, diastolic and mean pulmonary pressure and gives information on right ventricular function. However, in veterinary medicine, right heart catheterization is rarely performed in routine practice, and PH is generally diagnosed based on the presence of clinical and echocardiographic signs. Using the simplified Bernoulli equation (Pressure gradient = 4 x V^2), Doppler echocardiography allows for the definitive diagnosis and quantification of PH. As long as the right ventricular outflow tract is not obstructed, systolic pulmonary pressure can be estimated by measuring the velocity of the tricuspid regurgitation jet (TR). The diastolic pressure can be estimated by examining the pulmonary insufficiency jet (PI). In order to obtain estimations of the systolic or diastolic pulmonary pressure, right atrial and right ventricular diastolic pressures should be added to the calculated values. The right atrial and right ventricular diastolic pressures can be obtained by right heart cardiac catheterization or estimated by clinical signs and/or echocardiographic findings. However, most of the published studies in veterinary medicine use only the pressure gradient to establish the diagnosis of PH, since adding the estimation of atrial or ventricular pressures is reported as having controversial effects on improving the accuracy of this estimation [62,63]. There is no agreement on the optimal PASP cut-offs for the diagnosis of PH. Normal systolic pulmonary pressure in dogs at sea level should be less than 30 mmHg and normal diastolic pressure should be less than 15

mmHg [64]. The cut-off proposed by various authors varies from 2.5 to 3.5 m/sec for TR and from 2 to 2.2 m/sec for PI. The majority of authors accept a cut-off of 2.8 m/sec for TR and 2.2 m/sec for PI [46,65]. Early investigations of the accuracy of Doppler echocardiographic estimates of right ventricular and PASP provided impressively high correlations [66,67]. However, it has been suggested that the results of these carefully controlled studies may not reflect the reality of clinical practice [68]. Furthermore, correlation is a measure of linear association, not a measure of diagnostic accuracy; high correlations can be identified when agreement between methods is poor [69]. Indeed, the accuracy of Doppler echocardiographic estimates has recently been re-evaluated [68,70,71]. A metanalysis of published data yielded summary measures of correlation and diagnostic accuracy that were described as modest [71]. Moreover, in a single-center study in which 792 paired echocardiographic and catheterization values were evaluated, limits of agreement were broad and, relative to the catheterization standard, echocardiographic data resulted in misclassification of clinical categories of pulmonary artery pressures in more than 50% of cases [68]. The accuracy of Doppler echocardiography for estimating pulmonary artery pressures has been recently investigated in a canine model of PH [72]. In this study, only moderate correlation was found between PASP and invasively determined systolic pulmonary artery pressure, with the bias between the two techniques increasing along with the entity of pulmonary hypertension. Also, of great clinical importance, the PASP would both under- and overestimate the actual pulmonary pressure and very wide limits of agreements were reported [72]. The accuracy of Doppler echocardiographic estimates of pulmonary artery pressure has not been evaluated in dogs with naturally occurring MMVD. Because of the high prevalence of PH reported in dogs with MMVD, and the fact that early in the course of its development, PH in patients with MMVD may be amenable to therapeutic intervention [56], the accuracy of Doppler

echocardiography in estimating pulmonary pressure in dogs with naturally occurring MMVD is of great clinical importance.

Aims

The common aim of the studies reported in this thesis was to perform a systematic evaluation of the MV of dogs using RT–3DTTE. Particularly, we wanted to explore whether this technique could provide new insights for better understanding the etiopathogenesis of the disease and its diagnosis, with possible future implications in the management of the disease.

Specific aims were to:

- Evaluate feasibility and reproducibility of assessing the MV of dogs using RT–3DTTE and offline analysis with dedicated software.
- Describe the morphology of the MV and its apparatus in healthy dogs, and provide reference values for morphologic parameters of the MV.
- Evaluate morphologic differences between the MV of healthy dogs, and the MV of dogs affected by MMVD at different disease stages.
- Evaluate morphologic differences between the MV of healthy CKCSs and healthy dogs of other breeds.
- Evaluate the feasibility and reproducibility of calculating the AROA in dogs with MMVD, and evaluate whether AROA measurements are related to dogs' disease stage.

Also, preliminary results of a study intended to evaluate the accuracy of estimating pulmonary arterial pressure using the simplified Bernoulli equation in dogs affected by MMVD are presented.

Manuscripts

Journal of Veterinary Cardiology (2016) **18**, 156—167

ELSEVIER

Journal of Veterinary Cardiology
ESVC

www.elsevier.com/locate/jvc

Assessment of mitral valve morphology using three-dimensional echocardiography. Feasibility and reference values☆

G. Menciotti, DVM [a,*], M. Borgarelli, DVM, PhD [a], M. Aherne, MVB, GradDipVetStud [a], J. Häggström, DVM, PhD [b], I. Ljungvall, DVM, PhD [b], S.M. Lahmers, DVM, PhD [a], J.A. Abbott, DVM [a]

[a] *Department of Small Animal Clinical Sciences, Virginia—Maryland College of Veterinary Medicine, Blacksburg, VA 24061, USA*
[b] *Department of Clinical Sciences, Swedish University of Agricultural Science, Uppsala, Sweden*

Received 6 July 2015; received in revised form 23 November 2015; accepted 23 November 2015

KEYWORDS
Canine;
Heart;
Diagnostic;
Imaging

Abstract *Objectives:* To evaluate the feasibility of real time transthoracic three-dimensional echocardiography (RT3DE) for evaluation of normal canine mitral valves (MVs), and to provide reference values for this technique.
Animals: Forty-three cardiologically healthy, not sedated dogs.
Methods: Transthoracic RT3DE mitral datasets were acquired during two consecutive 6-month periods. The datasets were analyzed using commercially available software. An MV model was drawn using a semiautomated procedure and MV variables were obtained and calculated. The ratio between annulus height and

☆ A unique aspect of the Journal of Veterinary Cardiology is the emphasis of additional web-based images permitting the detailing of procedures and diagnostics. These images can be viewed (by those readers with subscription access) by going to http://www.sciencedirect.com/science/journal/17602734. The issue to be viewed is clicked and the available PDF and image downloading is available via the Summary Plus link. The supplementary material for a given article appears at the end of the page. Downloading the videos may take several minutes. Readers will require at least Quicktime 7 (available free at http://www.apple.com/quicktime/download/) to enjoy the content. Another means to view the material is to go to http://www.doi.org and enter the doi number unique to this paper which is indicated at the end of the manuscript.

* Corresponding author.
E-mail address: gmencio@gmail.com (G. Menciotti).

http://dx.doi.org/10.1016/j.jvc.2015.11.002

commissural diameter was used as an index of the annulus' saddle-shaped non-planarity. After evaluation of associations between measured variables and body size, the datasets were used to generate reference intervals. Coefficients of variation (CVs), variance components, and repeatability coefficients were calculated for the evaluation of intra-observer, inter-observer, and day-to-day variability.
Results: Datasets could be analyzed in 34 of 43 (79%) dogs. 68 percent of datasets obtained during the first 6-month period could be analyzed and 90% obtained during the second period could be analyzed. An allometric relationship was identified for most MV variables. The MV annulus appeared elliptical and saddle-shaped. Inter- and intra-observer CVs were less than 20%. Coefficient of variation greater than 20% was calculated for the inter-day variation for some variables. Operator and observer were primarily responsible for the variation of most of the variables.
Conclusions: Evaluation of canine mitral valves by transthoracic RT3DE is feasible. Canine MVs of healthy dogs analyzed using RT3DE are elliptical and saddle-shaped. Reference intervals for the measured MV variables are proposed.

Abbreviations

AHCWR	annulus height to commissural width ratio
ALA	anterior leaflet area
ALL	anterior leaflet length
ALPMD	anterolateral—posteromedial annulus diameter
AnA	annulus area
AnCirc	annulus circumference
AnH	annulus height
APD	antero-posterior annulus diameter
BW	body weight
CmD	commissural diameter
CV	coefficient of variation
MV	mitral valve
NPA	non-planar angle
PLA	posterior leaflet area
PLL	posterior leaflet length
RT3DE	real time transthoracic three-dimensional echocardiography
SI	annulus sphericity index
TnA	tenting area
TnH	tenting height
TnV	tenting volume

Introduction

The mitral valve (MV) apparatus has a complex, three-dimensional structure [1—3]. The effect of geometry on valve stress is well established, [4,5] and for this reason, MV replacement and repair techniques that preserve or approximate normal valve morphology are associated with superior outcomes [6—8]. Furthermore, it has been hypothesized that structural alteration of the MV apparatus has a role in the pathogenesis of myxomatous MV disease [5,9]. Specifically, changes in MV morphology can alter forces acting on valvular structures, and possibly trigger the activation of signaling pathways responsible for the valve degeneration and leakage [9—13]. Studying the morphology of the MV and its apparatus in vivo is challenging because the complexity of valvular structure makes two-dimensional echocardiographic investigation incomplete and sometimes difficult to interpret. Real-time three-dimensional echocardiography (RT3DE), allows acquisition and visualization of volumes, rather than tomographic planes, in real-time, providing the operator with a comprehensive, in vivo image of valvular structures. Moreover, off-line analysis of acquired volumes, provides different perspectives on valvular structures, and discloses features that could otherwise be missed with conventional 2D examination. In humans, RT3DE is superior to conventional 2D echocardiography for evaluation of the MV and is becoming an essential component of the diagnostic evaluation of patients prior to MV valvular surgery [14—19].

The first objective of this study was to evaluate the feasibility of using transthoracic RT3DE for assessing the canine MV and its apparatus with a dedicated software.[c] Secondly, we wanted to evaluate inter- and intra-observer variability of the variables measured on the MV using this technique. Finally, we wanted to evaluate the morphology of the MV, and provide RT3DE reference values and ranges for MV variables in healthy dogs.

[c] 4D MV-Analysis 3.1, TomTec Imaging Systems, Unterschleissheim, Germany.

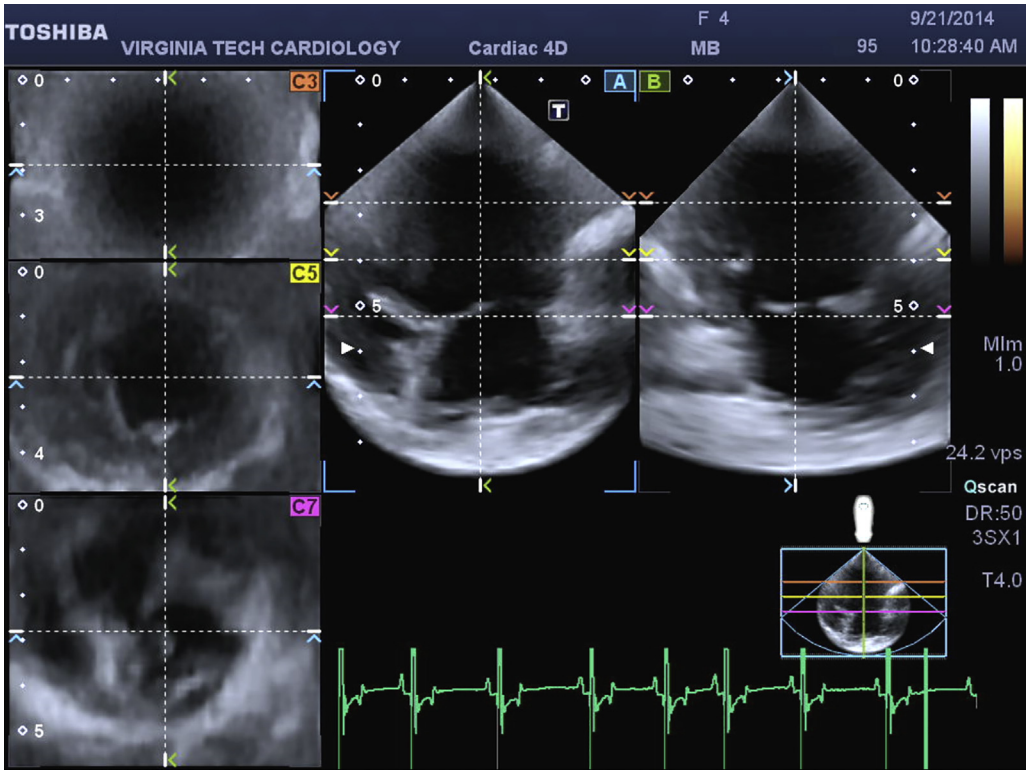

Fig. 1 Pre 4D mode. Five different planes are visualized simultaneously. Two long-axis views (on the right), and three short-axis views. For standardizing the acquisition process, the probe was oriented so that the two long-axis views showed an apical four-chamber view on the left (plane labeled A by the ultrasound unit) and two-chambers view on the right (plane labeled B).

Animals, materials and methods

Animals

During a 1-year period, we prospectively enrolled dogs recruited from students and staff of the Virginia—Maryland College of Veterinary Medicine, as well as dogs presented for echocardiographic examination to the Veterinary Teaching Hospital of the same institution. The study period was subdivided into two equal 6-month periods, in order to identify changes in feasibility that might reflect operator experience. For inclusion, dogs must have weighed between 5 kg and 40 kg, and were considered healthy based on owner interview, physical examination, cardiac auscultation, and conventional echocardiography. Exclusion criteria were: history of heart disease, a heart murmur with an intensity greater than 2 on the 6 grade scale, echocardiographic evidence of heart disease, clinical evidence of systemic or significant organ related diseases, or current administration of medications known to affect the cardiovascular system. The presence of trivial pulmonic or tricuspid regurgitation did not constitute exclusion criteria in our patients. We excluded dogs that were uncooperative and that would have required sedation in order to undergo echocardiographic examination. This study was approved by the Institutional Animal Care and Use Committee at Virginia Tech, VA (IACUC #14-141).

Echocardiographic examination

Dogs were gently restrained in right and left lateral recumbency on an echocardiographic scanning table in order to acquire standard 2D, M-mode, Doppler and RT3DE datasets using an ultrasound unit.[d] An electrocardiogram was recorded simultaneously with the echocardiographic examination. Standard echocardiographic planes were visualized [20], and images and cineloops were stored for off-line analyses. Briefly, color Doppler mapping of a right parasternal long-axis view was used in order to evaluate the presence or absence of mitral regurgitation and to subjectively assess the MV for evidence of thickening or prolapse. M-mode examination of the left ventricle was directed by a 2D right-parasternal short-axis view, while the left atrial to aortic root ratio was obtained

[d] Artida, Toshiba Medical Systems, Tokyo, Japan.

from 2D echocardiographic images of the base of the heart as previously described [21]. Color Doppler mapping of a left-parasternal apical four-chamber view was used to further evaluate the competence of the MV and for acquiring RT3DE datasets using a fully sampled matrix array transducer.[e] With regard to the RT3DE datasets, correct alignment was assessed by a multi-plane real-time view (pre 4D), showing two orthogonal long-axis planes along with three short-axis sections; the transducer position was optimized so that the two long-axis views showed standard apical four- and two-chamber views (Fig. 1). Depth, azimuth and elevation were then adjusted in order to focus the ultrasound beam on the mitral apparatus and include the left ventricular outflow tract. Acquisition modality was then switched to full 4D mode, and 3D volume datasets were acquired using information from four consecutive beats. Three consecutive datasets were stored. When possible, cineloops free from artifacts were selected for storage. Six dogs were randomly selected from those recruited from students and staff using a random number generator, and they underwent a second echocardiographic examination within 8 hours from the first one, in order to analyze the variability between two acquisitions. All datasets were acquired by a single operator (MB).

Image analysis

Each study was analyzed off-line by a single operator (GM) using a workstation equipped with a dedicated software.[c] Three-dimensional datasets were imported and an MV model was drawn using a semi-automated procedure. Two orthogonal planes corresponding to a four- and a two-chamber view were visualized and their orientation was manually adjusted (Fig. 2), if necessary; end-diastolic and end-systolic frames were identified and marked, and a mid-systolic frame was selected for the analysis as required by the software. The visible aspects of the mitral annulus were identified and labeled in the two aforementioned planes (Fig. 2A and B). The center of the aortic valve was identified and labeled in the short-axis plane, and, in an apical five-chamber view, the visible aspect of the aortic annulus was also identified and labeled (Fig. 2C). Finally, as defined by TomTec software, the coaptation point of mitral leaflets was identified in the same view. The model was developed from these landmarks (Videos 1 and 2) after which the

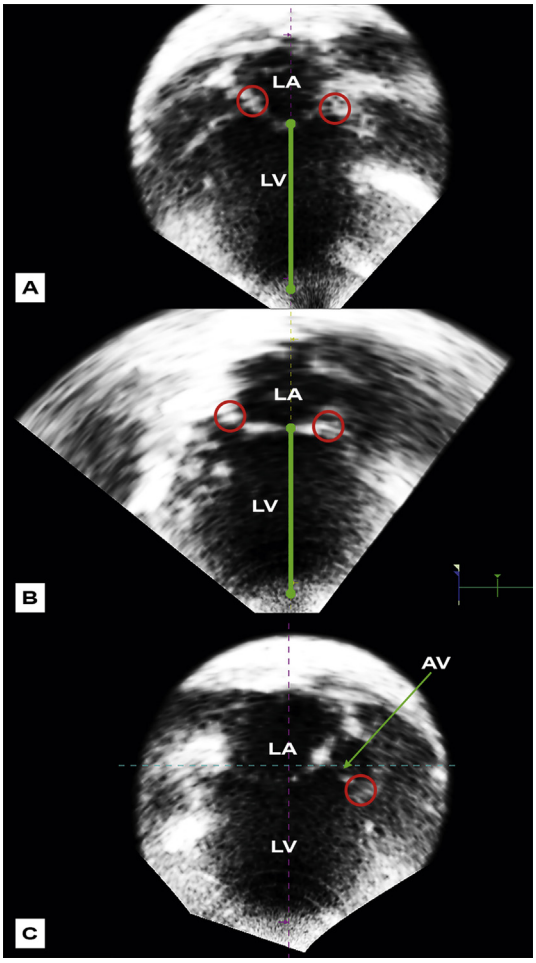

Fig. 2 Image alignment and landmarks identification. (A and B) Two orthogonal planes are visualized and a line is positioned to align the center of the mitral valve and the left ventricular apex (green bar). On the same images, the visible aspects of the mitral annulus are marked (red circles). (C) A third plane is then automatically visualized, and the visible aspect of the aortic annulus is identified (red circle). LA, left atrium; LV, left ventricle; AV, aortic valve.

dataset was manually reviewed in order to verify the correct tracing of the mitral annulus and leaflets contours, and to correct contingent tracing errors. The following variables were automatically measured and derived (Figs. I—XII, data available in Supplemental Data on-line): antero-posterior annulus diameter (APD), antero-lateral—posteromedial annulus diameter (ALPMD), commissural diameter (CmD), annulus sphericity index (SI) calculated as APD/ALPMD, annulus height (AnH), annulus circumference (AnCirc), annulus area (AnA), tenting height (TnH), tenting area (TnA), tenting volume (TnV), anterior leaflet length (ALL), anterior leaflet area (ALA), posterior leaflet length (PLL), posterior leaflet area (PLA), non-planar angle (NPA). The

[e] PST-25SX matrix-array transducer, Toshiba Medical Systems, Tokyo, Japan.

Table 1 R^2 and p-values of the linear regression analyses.

Dependent variable[a]	Independent variable					
	BW		BSA		$\log_{10}$BW	
	R^2	p-value	R^2	p-value	R^2	p-value
APD	0.50	<0.0001	0.51	<0.0001	0.55	<0.0001
ALPMD	0.45	<0.0001	0.47	<0.0001	0.54	<0.0001
CmD	0.42	<0.0001	0.44	<0.0001	0.51	<0.0001
SI	0.02	0.4697	0.01	0.5077	0.01	0.6473
AnH	0.05	0.1951	0.06	0.1511	0.07	0.1209
AnCirc	0.49	<0.0001	0.51	<0.0001	0.57	<0.0001
AnA	0.47	<0.0001	0.49	<0.0001	0.58	<0.0001
TnH	0.00	0.8150	0.01	0.6607	0.00	0.7588
TnA	0.02	0.4888	0.03	0.3630	0.05	0.1931
TnV	0.04	0.2318	0.06	0.1659	0.16	0.0204
ALL	0.36	0.0002	0.38	0.0001	0.41	<0.0001
ALA	0.36	0.0002	0.39	<0.0001	0.47	<0.0001
PLL	0.07	0.1253	0.08	0.1075	0.11	0.0571
PLA	0.24	0.0029	0.25	0.0025	0.34	0.0003
NPA	0.02	0.4561	0.01	0.5409	0.00	0.7167
AHCWR	0.01	0.4924	0.01	0.5311	0.01	0.5916

Each echocardiographic variable was regressed against body weight (BW) and body surface area (BSA); additionally a linear regression was performed after $\log_{10}$ transformation of both variables. Where a significant association to body size ($p < 0.05$) was present, regression of $\log_{10}$ transformed variables consistently had a higher R^2, suggesting an allometric relationship.
APD, antero-posterior annulus diameter; ALPMD, anterolateral—posteromedial annulus diameter; CmD, commissural diameter; SI, annulus sphericity index calculated as APD/ALPMD; AnH, annulus height; AnCirc, annulus circumference; AnA, annulus area; TnH, tenting height; TnA, tenting area; TnV, tenting volume; ALL, anterior leaflet length; ALA, anterior leaflet area; PLL, posterior leaflet length; PLA, posterior leaflet area; NPA, non-planar angle; AHCWR, annulus height to commissural width ratio.
[a] Log_{10} transformed variables were used in the regression against $\log_{10}$BW.

variables TnH and TnA are reported by the software as absolute numbers and represent the distance between APD and the valve closure line, and the 2D area lying between APD and the leaflet contours in AP direction, respectively; TnV is the volume enclosed by the MV annulus and the leaflets.[f] The ratio of AnH and CmD (annulus height to commissural width ratio [AHCWR]) was calculated. The relationship between annular height and CmD expressed by this ratio has been used as an index of saddle-shaped non-planarity of the mitral annulus [5]. For each of six randomly selected dogs, the first acquired dataset was analyzed twice by two different observers (GM and MB), and the second acquired dataset was analyzed twice by one observer (GM) and once by the other (MB) in order to assess inter- and intra-observer variability, as well as inter-acquisition variability. Repeated analyses of the datasets by the same observer and repeated analyses by the two different observers were conducted at least 1 day apart from each other and in random order. It was not possible to conceal patient identifiers from the investigators, but both observers were blinded to the results of previous analyses, as well as analyses performed by the other observer.

Data analysis

Data were analyzed using a commercially available software.[g] Normal distribution of data was visually assessed using normal quartile plots. Differences in sex proportions between the group of analyzed dogs, and the group of not analyzed ones were evaluated using Fisher's exact test; differences in age and body weight (BW) between these two groups were evaluated using a Mann—Whitney U test and an unpaired Student's t-test, respectively. Simple linear regression analysis was used in order to investigate the association between each variable and body size. Each variable was regressed against BW and body surface area; additionally, a $\log_{10}$ transformation was applied both to the echocardiographic variable and to BW, and a linear regression of the two transformed variables was evaluated. For those variables showing a significant association to body size, R-

[f] Adapted from TomTec Imaging Systems, personal communication, March 2015.

[g] JMP Pro 11, SAS Institute Inc., Cary, NC, 1989—2013.

Table 2 Sex, age, BW, HR, and VR of the enrolled and analyzed dogs.

	Sex (M/F)	Age (y)	BW (kg)	HR (bpm)	VR (vps)
Enrolled (n = 43)	15/28	3.9 (1.0–12.9)	18.4 ± 7.3	112.8 ± 25.8	23.4 (19.5–32.3)
Analyzed (n = 34)	11/23	4.3 (1.1–12.9)	18.4 ± 6.1	113.2 ± 25.6	23.6 (19.5–32.3)

Normal distributed data are presented as mean ± standard deviation, while not normally distributed one are presented as median (minimum–maximum).
BW, body weight; HR: heart rate (beats per minute [bpm]); Vps, volumes per second; VR, volume rate (volumes per second).

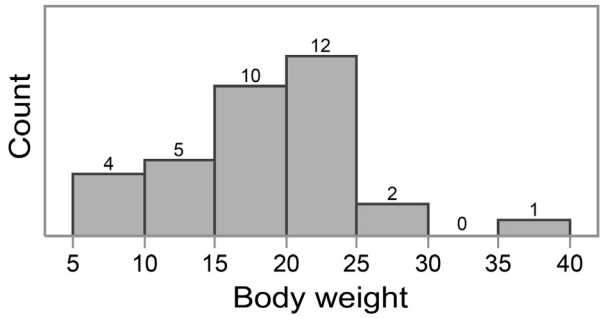

Fig. 3 Number of included dogs by weight group.

squared values, used a measure of goodness of fit of the model, were consistently higher for linear regressions of $\log_{10}$ transformed variables (Table 1). Based on this finding, an allometric relationship was assumed and the terms of the allometric equation $Y = a \times (BW)^b$ were defined from the regression as follows: the slope of the regression is the scaling exponent (b), while the antilog ($\log^{-1}$) of the intercept, is the proportionality constant (a). For these variables, predicted values and 95% prediction intervals for a range of BWs were developed. Normality of data was visually assessed and confirmed with a Shapiro–Wilk test. Normally distributed data are presented as mean ± standard deviation (SD), while non-normally distributed data are presented as median (minimum–maximum). Fisher's exact test was used to compare the proportions of analyzable datasets between the two study periods. A $p < 0.05$ was considered significant. Coefficients of variation (CV) were calculated from the datasets analyzed twice by the same operator, the datasets analyzed by two different operators, and the datasets acquired from the same dog at different times, in order to evaluate intra-observer, inter-observer and inter-acquisition variability. The CVs were calculated using the square root of the variance and the mean derived from repeated measurements on each dog; average and SD of the six CVs derived for each variable were then calculated. Furthermore, a nested random effects model was used for estimating the variance components of dog, day of acquisition (inter-acquisition), observer (inter-observer), and repeated measurements on the same image (intra-observer), on the variation of 3D variables, and for calculating repeatability coefficients [22].

Results

During the entire 1-year study period, 43 dogs met the inclusion criteria. Thirty-two dogs were owned by students and staff of the veterinary college,

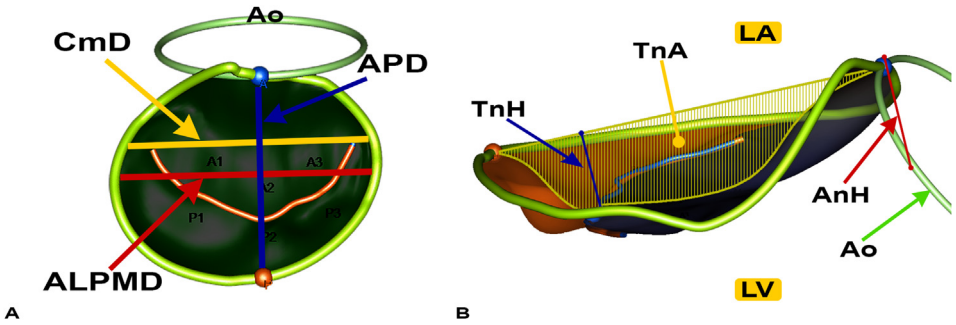

Fig. 4 Mitral valve models. (A) Atrial view of the mitral valve model. The elliptical shape can be noticed. CmD, commissural diameter; Ao, aortic annulus; APD, antero-posterior annulus diameter; ALPMD, antero-rolateral–posteromedial annulus diameter. (B) Lateral view of the mitral model. The saddle shape can be noticed. LA, left atrial side of the valve; LV, left ventricular side of the valve; TnH, tenting height; TnA, tenting area (dashed); AnH, annulus height; Ao, aortic annulus.

Table 3 Mean values, 95% prediction intervals and terms of the allometric equation for dogs of varying weights.

BW	APD	ALPMD	CmD	AnCirc	AnA	TnV	ALL	ALA	PLA
4	1.64 (1.32–2.04)	1.82 (1.48–2.26)	1.72 (1.35–2.2)	5.80 (4.7–7.15)	2.46 (1.63–3.69)	0.37 (0.12–1.22)	1.03 (0.72–1.47)	1.34 (0.77–2.34)	1.49 (0.83–2.72)
6	1.86 (1.49–2.31)	2.05 (1.66–2.54)	1.95 (1.53–2.5)	6.56 (5.32–8.09)	3.15 (2.08–4.73)	0.48 (0.16–1.59)	1.20 (0.83–1.7)	1.76 (1.01–3.06)	1.86 (1.03–3.39)
8	2.03 (1.63–2.52)	2.23 (1.81–2.77)	2.14 (1.67–2.73)	7.15 (5.8–8.83)	3.75 (2.48–5.63)	0.57 (0.19–1.91)	1.34 (0.93–1.9)	2.12 (1.22–3.69)	2.17 (1.21–3.97)
10	2.17 (1.75–2.7)	2.39 (1.93–2.96)	2.29 (1.8–2.93)	7.65 (6.21–9.44)	4.30 (2.84–6.45)	0.66 (0.22–2.21)	1.45 (1.01–2.06)	2.46 (1.41–4.28)	2.45 (1.36–4.48)
12	2.30 (1.85–2.86)	2.52 (2.04–3.12)	2.43 (1.9–3.11)	8.09 (6.56–9.98)	4.80 (3.17–7.2)	0.75 (0.25–2.48)	1.55 (1.08–2.2)	2.77 (1.59–4.82)	2.71 (1.51–4.95)
14	2.41 (1.94–3)	2.64 (2.13–3.27)	2.55 (2–3.26)	8.48 (6.87–10.46)	5.27 (3.48–7.91)	0.82 (0.27–2.74)	1.64 (1.14–2.33)	3.07 (1.76–5.34)	2.94 (1.64–5.38)
17	2.56 (2.06–3.18)	2.79 (2.26–3.46)	2.71 (2.12–3.47)	8.99 (7.29–11.09)	5.93 (3.92–8.9)	0.93 (0.31–3.11)	1.76 (1.22–2.5)	3.48 (2–6.06)	3.27 (1.82–5.98)
20	2.69 (2.16–3.35)	2.93 (2.37–3.63)	2.85 (2.24–3.65)	9.44 (7.66–11.65)	6.55 (4.33–9.83)	1.04 (0.35–3.45)	1.87 (1.3–2.66)	3.88 (2.23–6.75)	3.57 (1.99–6.53)
25	2.88 (2.32–3.58)	3.13 (2.53–3.88)	3.06 (2.4–3.91)	10.10 (8.19–12.46)	7.50 (4.96–11.25)	1.20 (0.4–3.99)	2.03 (1.41–2.89)	4.49 (2.58–7.82)	4.03 (2.25–7.37)
30	3.05 (2.45–3.79)	3.30 (2.67–4.09)	3.24 (2.54–4.15)	10.68 (8.66–13.17)	8.38 (5.54–12.57)	1.35 (0.45–4.48)	2.17 (1.51–3.09)	5.06 (2.91–8.81)	4.45 (2.48–8.14)
35	3.20 (2.57–3.98)	3.45 (2.8–4.28)	3.40 (2.67–4.35)	11.19 (9.07–13.8)	9.21 (6.08–13.81)	1.49 (0.5–4.95)	2.30 (1.6–3.27)	5.60 (3.22–9.75)	4.84 (2.7–8.85)
40	3.33 (2.68–4.14)	3.59 (2.91–4.45)	3.55 (2.78–4.54)	11.65 (9.45–14.37)	9.99 (6.59–14.98)	1.62 (0.54–5.4)	2.42 (1.68–3.43)	6.12 (3.51–10.65)	5.21 (2.9–9.52)
Proportionality constant (a)	1.07 (0.86–1.33)	1.21 (0.98–1.50)	1.11 (0.87–1.42)	3.81 (3.09–4.70)	1.06 (0.70–1.59)	0.15 (0.05–0.5)	0.62 (0.43–0.88)	0.54 (0.31–1.42)	0.70 (0.39–1.28)
Scaling exponent (b)	0.308	0.295	0.315	0.303	0.608	0.645	0.369	0.658	0.544

Individual mean values and reference intervals for a body weight (BW) can be calculated using the equation: $Y = a \times (BW)^b$ where Y is the variable of interest, and a and b are proportionality constant and scaling exponent, respectively, relative to that variable.

APD, antero-posterior annulus diameter; ALPMD, anterolateral–posteromedial annulus diameter; CmD, commissural diameter; AnCirc, annulus circumference; AnA, annulus area; TnV, tenting volume; ALL, anterior leaflet length; ALA, anterior leaflet area; PLA, posterior leaflet area.

while 11 were referred to the veterinary teaching hospital of the same institution. Data regarding sex, age, BW, heart rate, and volume rate are presented in Table 2, while distribution of the dogs into the different weight classes is presented in Fig. 3. Females (n = 23) were overrepresented compared to males (n = 11). Datasets were of analyzable quality in 34 patients (79%); however, when the study was divided into two 6-month time periods, 68% of datasets (analyzable/acquired: 15/22 datasets) could be analyzed during the first period, while 90% of the datasets acquired during the second period were of sufficient quality to be analyzed (analyzable/acquired: 19/21 datasets). This increase was not statistically significant ($p = 0.08$). There was no significant difference in sex proportions ($p = 0.70$), age ($p = 0.61$), and BW ($p = 0.99$) between the 34 analyzed dogs and the 9 not analyzed.

As shown in Fig. 4, the MV of healthy dogs, as visualized in-vivo using RT3DE had an elliptical annulus, with the APD smaller than the ALPMD, resulting in an SI of 0.916 ± 0.06. The MV annulus had a saddle-shape, with its anterior part elevated compared to the rest of the valve by 0.576 ± 0.168 cm (AH), and was non-planar with an NPA of 152.31 ± 14.63° and AHCWR of 0.209 ± 0.054. In mid-systole, when all the analyses were performed, the leaflets were concave when viewed from the atrial side of the annulus. While the anterior leaflet was longer than the posterior in almost all (32 of 34) of our dogs (ALL/PLL ratio: 1.682 ± 0.507), the area of the anterior leaflet was greater than that of the posterior leaflet in 19 of 34 dogs (ALA/PLA ratio 1.122 ± 0.403).

The following variables were significantly associated with BW after logarithmic transformation, APD ($r^2 = 0.55$, $p < 0.0001$), ALPMD ($r^2 = 0.54$, $p < 0.0001$), CmD ($r^2 = 0.51$, $p < 0.0001$), AnCirc ($r^2 = 0.57$, $p < 0.0001$), AnA ($r^2 = 0.58$, $p < 0.0001$), TnV ($r^2 = 0.16$, $p = 0.0204$), ALL ($r^2 = 0.41$, $p < 0.0001$), ALA ($r^2 = 0.47$, $p < 0.0001$), PLA ($r^2 = 0.34$, $p < 0.001$). For these variables, 95% prediction intervals for representative classes of BW were derived and reported in Table 3. The following variables were not related to body sizes and are reported as mean ± SD: SI = 0.96 ± 0.06, AnH = 0.57 ± 0.17 cm, TnH = 0.45 ± 0.20 cm, TnA = 0.85 ± 0.39 cm^2, PLL = 1.13 ± 0.26 cm, NPA = 152.31 ± 14.63°, and AHCWR = 0.21 ± 0.05.

Results of the repeatability analyses are reported in Tables 4 and 5. Inter- and intra-observer CVs were less than 20% for all the variables analyzed, while CVs greater than 20% were calculated for inter-acquisition TH, TA, TV, and ALA variability. Variance component analysis identified observer as the principal source of variation for APD, ALPMD, TnV, TnA, CmD, ALA, and ALL. Operator was identified as the principal source of variation of NPA, AnCirc, AnA, AnH, TnH, PLA, PLL, and AHCWR. The inter-acquisition, or day-to-day variation, was the main component for the variation in the measurements of SI.

Discussion

In this study, we demonstrated that transthoracic RT3DE is a feasible technique for in vivo morphologic assessment of the MV in healthy dogs. In humans, RT3DE is an established technique for evaluating MV, and it has been demonstrated to provide fundamental additional information, compared to conventional 2D echocardiography, when assessing patients with valvular diseases [23]. In veterinary medicine, RT3DE has been

Table 4 Intra-observer, inter-observer and inter-acquisition coefficients of variation of the variables measured.

Variable	Coefficients of variation (%, mean ± standard deviation)		
	Intra-observer	Inter-observer	Inter-acquisition
APD	4 ± 2	7 ± 3	9 ± 2
ALPMD	4 ± 2	3 ± 2	8 ± 2
CmD	4 ± 4	5 ± 5	10 ± 4
SI	5 ± 3	5 ± 4	5 ± 3
AnH	17 ± 8	9 ± 9	17 ± 8
AnCirc	3 ± 3	4 ± 3	7 ± 3
AnA	6 ± 4	9 ± 6	13 ± 4
TnH	15 ± 11	12 ± 8	28 ± 11
TnA	14 ± 12	17 ± 10	26 ± 12
TnV	10 ± 4	15 ± 15	23 ± 4
ALL	6 ± 3	8 ± 7	15 ± 3
ALA	11 ± 7	14 ± 11	26 ± 7
PLL	3 ± 3	10 ± 11	8 ± 3
PLA	11 ± 6	17 ± 16	10 ± 6
NPA	6 ± 6	5 ± 5	10 ± 6
AHCWR	17 ± 11	12 ± 11	20 ± 11

APD, antero-posterior annulus diameter; ALPMD, anterolateral—posteromedial annulus diameter; CmD, commissural diameter; SI, annulus sphericity index calculated as APD/ALPMD; AnH, annulus height; AnCirc, annulus circumference; AnA, annulus area; TnH, tenting height; TnA, tenting area; TnV, tenting volume; ALL, anterior leaflet length; ALA, anterior leaflet area; PLL, posterior leaflet length; PLA, posterior leaflet area; NPA, non-planar angle; AHCWR, annulus height to commissural width ratio.

Table 5 Results of the variance components analysis.

Variance components analysis				
Variable[a]	Component	Variance component	% Of total	RC
ADP(i)	Dog	0.01	23.60	0.20
	Acquisition	0.00	13.77	0.15
	Inter-observer	0.01	35.48	0.25
	Intra-observer	0.01	27.14	0.22
	Total	0.02	100.00	0.41
ALPMD(i)	Dog	0.00	0.00	0.00
	Acquisition	0.00	14.16	0.12
	Inter-observer	0.01	47.13	0.22
	Intra-observer	0.01	38.71	0.20
	Total	0.01	100.00	0.33
CmD(i)	Dog	0.00	0.00	0.00
	Acquisition	0.00	18.52	0.14
	Inter-observer	0.01	53.60	0.24
	Intra-observer	0.00	27.87	0.17
	Total	0.01	100.00	0.33
SI	Dog	0.00	0.00	0.00
	Acquisition	0.00	44.94	0.18
	Inter-observer	0.00	11.27	0.09
	Intra-observer	0.00	43.80	0.18
	Total	0.01	100.00	0.27
AnH	Dog	0.00	12.73	0.15
	Acquisition	0.00	0.00	0.00
	Inter-observer	0.00	0.00	0.00
	Intra-observer	0.02	87.27	0.38
	Total	0.02	100.00	0.41
AnCirc(i)	Dog	0.02	14.02	0.41
	Acquisition	0.01	7.89	0.31
	Inter-observer	0.05	31.70	0.61
	Intra-observer	0.07	46.39	0.74
	Total	0.15	100.00	1.09
AnA(i)	Dog	0.01	12.96	0.22
	Acquisition	0.01	10.39	0.20
	Inter-observer	0.02	36.38	0.37
	Intra-observer	0.02	40.26	0.39
	Total	0.05	100.00	0.62
TnH	Dog	0.00	0.00	0.00
	Acquisition	0.01	30.45	0.22
	Inter-observer	0.00	10.77	0.13
	Intra-observer	0.01	58.77	0.31
	Total	0.02	100.00	0.41
TnA	Dog	0.00	0.00	0.00
	Acquisition	0.01	6.07	0.22
	Inter-observer	0.05	51.35	0.64
	Intra-observer	0.04	42.58	0.59
	Total	0.11	100.00	0.90
TnV(i)	Dog	0.00	13.20	0.09
	Acquisition	0.00	0.00	0.00
	Inter-observer	0.01	73.86	0.22
	Intra-observer	0.00	12.94	0.09
	Total	0.01	100.00	0.26
ALL(i)	Dog	0.01	36.31	0.23
	Acquisition	0.00	14.87	0.15
	Inter-observer	0.01	40.34	0.25
	Intra-observer	0.00	8.48	0.11
	Total	0.02	100.00	0.39
ALA(i)	Dog	0.01	27.03	0.26
	Acquisition	0.00	7.22	0.13
	Inter-observer	0.02	52.13	0.36
	Intra-observer	0.00	13.61	0.18
	Total	0.03	100.00	0.50
PLL	Dog	0.00	5.98	0.17
	Acquisition	0.01	13.95	0.25
	Inter-observer	0.01	12.01	0.24
	Intra-observer	0.04	68.06	0.56
	Total	0.06	100.00	0.68
PLA(i)	Dog	0.00	3.30	0.11
	Acquisition	0.01	21.83	0.29
	Inter-observer	0.00	6.51	0.16
	Intra-observer	0.03	68.36	0.51
	Total	0.05	100.00	0.62
NPA	Dog	27.52	15.62	14.54
	Acquisition	54.83	31.12	20.52
	Inter-observer	0.00	0.00	0.00
	Intra-observer	93.83	53.26	26.85
	Total	176.18	100.00	36.79
AHCWR	Dog	0.00	8.19	0.04
	Acquisition	0.00	0.44	0.01
	Inter-observer	0.00	0.00	0.00
	Intra-observer	0.00	91.36	0.13
	Total	0.00	100.00	0.14

Variance components, percentages of total variance, and repeatability coefficients were calculated for each variable using a nested random effects model. Dog, two different acquisitions, two different observers, and two repeated measurements from the same observer were used as effects. APD, antero-posterior annulus diameter; ALPMD, antero-lateral—posteromedial annulus diameter; CmD, commissural diameter; SI, annulus sphericity index calculated as APD/ALPMD; AnH, annulus height; AnCirc, annulus circumference; AnA, annulus area; TnH, tenting height; TnA, tenting area; TnV, tenting volume; ALL, anterior leaflet length; ALA, anterior leaflet area; PLL, posterior leaflet length; PLA, posterior leaflet area; NPA, non-planar angle; AHCWR, annulus height to commissural width ratio; RC, repeatability coefficient.

[a] Variables that demonstrated a significant association with body weight had been indexed using the allometric scaled body weight before the analysis, and are indicated followed by (i).

successfully utilized for evaluation of the left and right ventricle [24,25], left atrium [26], and to characterize congenital anomalies [27]. The feasibility reported in literature for using RT3DE for

assessing MVs in humans is variable. Some studies report percentages close to the one of this study, while others report feasibility of almost 100% [17,28,29]. In this study, in order to optimize the image quality, 3D datasets were created using a 4-beat acquisition, that means that the ultrasound unit stitches together information derived from four consecutive beats. As a consequence, panting and sinus arrhythmia can result in poor image quality. These phenomena are more common in dogs than in humans, therefore, when compared to human studies, the feasibility reported in this study should be considered in this context. Over time, there was an improvement in the quality of our datasets; although the difference was not statistically significant, the proportion of analyzable datasets was greater during the second period of the study. This suggests a learning curve in the acquisition and analysis process that should be taken into account when using this technology.

In this study, APD, ALPMD, CmD, AnCirc, AnA, TnV, ALL, ALA, PLA, were related to dogs' body sizes in an allometric fashion, with scaling exponents close to 1/3 for linear measurements and 2/3 for areas. The independence from dogs' BW of AnH, TnH, TnA, and PLL is unexpected, and requires further investigation. A possible explanation is that these variables are somehow intrinsic characteristics of the MV, which are preserved over the range of BW analyzed in this study. Another explanation could be that the strength of the association to body size is less than for the other variables, and the sample size was inadequate to identify a small but real linear association. The importance of annular geometry in diminishing MV stress, has been demonstrated in humans [5], and morphologic characteristics of the MV annulus had been extensively described in this and other species using different techniques [2,5,30—32]. This study reports for the first time that in vivo the MV annulus of normal dogs had a saddle shape, with an AHCWR of 0.21 $\pm$ 0.05. This value is approximately the same value reported in healthy humans [33]. The conservation of the saddle-shape morphology across species suggests that this morphology of MV provides a mechanical advantage for the function of the valve [5,7]. Our study also demonstrated that the MV annulus of normal dogs in vivo is elliptical, with an AP diameter smaller than the ALPM one. The ratio between the two annular diameters, referred here as SI, is commonly used to describe this characteristic of the annulus, and the value of 0.92 is higher than the one reported in dogs by anatomical measurements [3]. This difference is expected, and already reported by other investigators, and can be explained by an effect of the fixation process that shrinks the heart [34].

Most of the variables appeared to have an acceptable repeatability, with intra-observer, inter-observer and inter-acquisition CVs lower than 20%. The higher coefficients of variation reported for some variables measured from two datasets acquired from the same dog at different times, could reflect either an actual day-to-day physiologic variation, or a technical limitation due to the relatively low acquisition frame rate, that could lead to the measurement of the valve in slightly different time-points of the cardiac cycle in the two different acquisitions. However, when the variance components were analyzed, day-to-day variation was mainly responsible for the variability of the SI only, while the variation of the other variables was mainly attributable to operator and observer.

Limitations

The main limitation of this study is the small sample size, as the generation of more accurate and precise reference intervals would require a larger population; however, prediction intervals had been derived only for a range of weights close to the one represented by our population of dogs (4—40 kg). Moreover, the limited number of datasets analyzed, is partially due to the presence of a learning curve and, as we report, it could be improved with the consolidation of the new technique with time. The limited numbers of dogs (n = 6) chosen for performing the repeatability study was low but consistent with the extant veterinary literature [35—37]. Furthermore, the relatively low frame-rate could have caused some datasets to be measured in slightly different phases of the systole. Because changes in shape of the MV during systole have been reported in humans [29], the slightly different timing of the measurements could have influenced our results, and could have contributed to day-to-day variability.

Conclusions

In conclusion, evaluation of canine MVs using RT3DE is feasible, has an acceptable repeatability, and provides additional information compared to conventional echocardiography. Based on RT3DE assessment, MVs of healthy dogs analyzed are elliptical and saddle-shaped. Reference intervals for the measured MV variables are proposed. Given the importance of MV geometry, in the context of

pathophysiology of MMVD, and recent advancements in MV repair, the in-vivo study of MV morphology requires further attention.

Conflict of interest statement

The authors do not have any conflicts of interest to disclose.

Acknowledgments

This study has been funded by CEVA Santé Animale. The authors acknowledge Dr. Stephen Werre for the statistical support.

Supplementary data

Supplementary data associated with this article can be found, in the online version, at http://dx.doi.org/10.1016/j.jvc.2015.11.002.

Video number	Video title	Description
Video 1	Mitral model.	After identification of specific landmarks, a three-dimensional mitral model is generated by the software.
Video 2	Overlay of mitral model and three-dimensional image of the heart.	The video shows the three-dimensional image of the left atrium, mitral valve and left ventricle with the superimposition of the mitral model created using the same acquisition.

References

[1] Komeda M, Glasson JR, Bolger AF, Daughters GT, Niczyporuk MA, Ingels NB, Miller DC. Three-dimensional dynamic geometry of the normal canine mitral annulus and papillary muscles. Circulation 1996;94:II159—II163.
[2] Levine RA, Triulzi MO, Harrigan P, Weyman AE. The relationship of mitral annular shape to the diagnosis of mitral valve prolapse. Circulation 1987;75:756—767.
[3] Borgarelli M, Tursi M, La Rosa G, Savarino P, Galloni M. Anatomic, histologic, and two-dimensi onal-echocardiographic evaluation of mitral valve anatomy in dogs. Am J Vet Res 2011;72:1186—1192.
[4] Xu C, Brinster CJ, Jassar AS, Vergnat M, Eperjesi TJ, Gorman RC, Gorman III JH, Jackson BM. A novel approach to in vivo mitral valve stress analysis. Am J Physiol Heart Circ Physiol 2010;299:H1790—H1794.
[5] Salgo IS, Gorman III JH, Gorman RC, Jackson BM, Bowen FW, Plappert T, St John Sutton MG, Edmunds LH. Effect of annular shape on leaflet curvature in reducing mitral leaflet stress. Circulation 2002;106:711—717.
[6] Uechi M. Mitral valve repair in dogs. J Vet Cardiol 2012;14:185—192.
[7] Jensen MO, Jensen H, Smerup M, Levine RA, Yoganathan AP, Nygaard H, Hasenkam JM, Nielsen SL. Saddle-shaped mitral valve annuloplasty rings experience lower forces compared with flat rings. Circulation 2008;118:S250—S255.
[8] Mahmood F, Gorman III JH, Subramaniam B, Gorman RC, Panzica PJ, Hagberg RC, Lerner AB, Hess PE, Maslow A, Khabbaz KR. Changes in mitral valve annular geometry after repair: saddle-shaped versus flat annuloplasty rings. Ann Thorac Surg 2010;90:1212—1220.
[9] Lacerda CMR, MacLea HB, Kisiday JD, Orton EC. Static and cyclic tensile strain induce myxomatous effector proteins and serotonin in canine mitral valves. J Vet Cardiol 2012;14:223—230.
[10] Ljungvall I, Höglund K, Lilliehöök I, Oyama MA, Tidholm A, Tvedten H, Häggström J. Serum serotonin concentration is associated with severity of myxomatous mitral valve disease in dogs. J Vet Intern Med 2013;27:1105—1112.
[11] Aupperle H, Disatian S. Pathology, protein expression and signaling in myxomatous mitral valve degeneration: comparison of dogs and humans. J Vet Cardiol 2012;14:59—71.
[12] Orton EC, Lacerda CMR, MacLea HB. Signaling pathways in mitral valve degeneration. J Vet Cardiol 2012;14:7—17.
[13] Scruggs SM, Disatian S, Orton EC. Serotonin transmembrane transporter is down-regulated in late-stage canine degenerative mitral valve disease. J Vet Cardiol 2010;12:163—169.
[14] Mahmood F, Subramaniam B, Gorman III JH, Levine RM, Gorman RC, Maslow A, Panzica PJ, Hagberg RM, Karthik S, Khabbaz KR. Three-dimensional echocardiographic assessment of changes in mitral valve geometry after valve repair. Ann Thorac Surg 2009;88:1838—1844.
[15] Dal-Bianco JP, Levine RA. Anatomy of the mitral valve apparatus: role of 2D and 3D echocardiography. Cardiol Clin 2013;31:151—164.
[16] Takahashi K, Mackie AS, Rebeyka IM, Ross DB, Robertson M, Dyck JD, Inage A, Smallhorn JF. Two-dimensional versus transthoracic real-time three-dimensional echocardiography in the evaluation of the mechanisms and sites of atrioventricular valve regurgitation in a congenital heart disease population. J Am Soc Echocardiogr 2010;23:726—734.
[17] Pepi M, Tamborini G, Maltagliati A, Galli CA, Sisillo E, Salvi L, Naliato M, Porqueddu M, Parolari A, Zanobini M, Alamanni F. Head-to-head comparison of two- and three-dimensional transthoracic and transesophageal echocardiography in the localization of mitral valve prolapse. J Am Coll Cardiol 2006;48:2524—2530.
[18] Tsang W, Freed BH, Lang RM. The role of 3-dimensional echocardiography in the diagnosis and management of mitral valve disease: myxomatous valve disease. Cardiol Clin 2013;31:203—215.
[19] Chikwe J, Adams DH, Su KN, Anyanwu AC, Lin H-M, Goldstone AB, Lang RM, Fischer GW. Can three-dimensional echocardiography accurately predict complexity of mitral valve repair? Eur J Cardiothorac Surg 2012;41:518—524.

[20] Thomas WP, Gaber CE, Jacobs GJ, Kaplan PM, Lombard CW, Moise NS, Moses BL, Vet M. Recommendations for standards in transthoracic two-dimensional echocardiography in the dog and cat. J Vet Intern Med 1993;7:247—252.
[21] Hansson K, Häggström J, Kvart C, Lord P. Left atrial to aortic root indices using two-dimensional and M-mode echocardiography in cavalier King Charles spaniels with and without left atrial enlargement. Vet Radiol Ultrasound 2002;43:568—575.
[22] Bland JM, Altman DG. Measuring agreement in method comparison studies. Stat Methods Med Res 1999;8: 135—160.
[23] Cai Q, Ahmad M. Three-dimensional echocardiography in valvular heart disease. Echocardiography 2012;29:88—97.
[24] Ljungvall I, Höglund K, Carnabuci C, Tidholm A, Häggström J. Assessment of global and regional left ventricular volume and shape by real-time 3-dimensional echocardiography in dogs with myxomatous mitral valve disease. J Vet Intern Med 2011;25:1036—1043.
[25] Sieslack AK, Dziallas P, Nolte I, Wefstaedt P, Hungerbühler SO. Quantification of right ventricular volume in dogs: a comparative study between three-dimensional echocardiography and computed tomography with the reference method magnetic resonance imaging. BMC Vet Res 2014;10:242.
[26] Tidholm A, Bodegård-Westling A, Höglund K, Ljungvall I, Häggström J. Comparisons of 2- and 3-dimensional echocardiographic methods for estimation of left atrial size in dogs with and without myxomatous mitral valve disease. J Vet Intern Med 2011;25:1320—1327.
[27] Jung S, Orvalho J, Griffiths LG. Aortopulmonary window characterized with two- and three-dimensional echocardiogram in a dog. J Vet Cardiol 2012;14:371—375.
[28] Gutiérrez-Chico JL, Zamorano Gómez JL, Rodrigo-López JL, Mataix L, Pérez de Isla L, Almería-Valera C, Aubele A, Macaya-Miguel C. Accuracy of real-time 3-dimensional echocardiography in the assessment of mitral prolapse. Is transesophageal echocardiography still mandatory? Am Heart J 2008;155:694—698.
[29] Mihăilă S, Muraru D, Piasentini E, Miglioranza MH, Peluso D, Cucchini U, Iliceto S, Vinereanu D, Badano LP. Quantitative analysis of mitral annular geometry and function in healthy volunteers using transthoracic three-dimensional echocardiography. J Am Soc Echocardiogr 2014;27:846—857.
[30] Ryan LP, Jackson BM, Enomoto Y, Parish L, Plappert TJ, St John-Sutton MG, Gorman RC, Gorman III JH. Description of regional mitral annular nonplanarity in healthy human subjects: a novel methodology. J Thorac Cardiovasc Surg 2007;134:644—648.
[31] Gorman III JH, Gupta KB, Streicher JT, Gorman RC, Jackson BM, Ratcliffe MB, Bogen DK, Edmunds J. Dynamic three-dimensional imaging of the mitral valve and left ventricle by rapid sonomicrometry array localization. J Thorac Cardiovasc Surg 1996;112:712—726.
[32] Levine RA, Handschumacher MD, Sanfilippo AJ, Hagege AA, Harrigan P, Marshall JE, Weyman AE. Three-dimensional echocardiographic reconstruction of the mitral valve, with implications for the diagnosis of mitral valve prolapse. Circulation 1989;80:589—598.
[33] Lee AP-W, Hsiung MC, Salgo IS, Fang F, Xie J-M, Zhang Y-C, Lin Q-S, Looi J-L, Wan S, Wong RHL, Underwood MJ, Sun J-P, Yin W-H, Wei J, Tsai S-K, Yu C-M. Quantitative analysis of mitral valve morphology in mitral valve prolapse with real-time 3-dimensional echocardiography: importance of annular saddle shape in the pathogenesis of mitral regurgitation. Circulation 2013;127:832—841.
[34] Gutgesell HP, Bricker JT, Colvin EV, Latson LA, Hawkins EP. Atrioventricular valve anular diameter: two-dimensional echocardiographic-autopsy correlation. Am J Cardiol 1984;53:1652—1655.
[35] Schober K, Todd A. Echocardiographic assessment of left ventricular geometry and the mitral valve apparatus in cats with hypertrophic cardiomyopathy. J Vet Cardiol 2010;12:1—16.
[36] Smith DN, Bonagura JD, Culwell NM, Schober KE. Left ventricular function quantified by myocardial strain imaging in small-breed dogs with chronic mitral regurgitation. J Vet Cardiol 2012;14:231—242.
[37] Carnabuci C, Hanås S, Ljungvall I, Tidholm A, Bussadori C, Häggström J, Höglund K. Assessment of cardiac function using global and regional left ventricular endomyocardial and epimyocardial peak systolic strain and strain rate in healthy Labrador retriever dogs. Res Vet Sci 2013;95: 241—248.

Journal of Veterinary Cardiology (2017) **19**, 113—123

ELSEVIER

Journal of Veterinary Cardiology
ESVC

www.elsevier.com/locate/jvc

Mitral valve morphology assessed by three-dimensional transthoracic echocardiography in healthy dogs and dogs with myxomatous mitral valve disease

G. Menciotti, DVM [a,*], M. Borgarelli, DVM, PhD [a], M. Aherne, MVB, GradDipVetStud [a], S. Wesselowski, DVM, MS [a], J. Häggström, DVM, PhD [b], I. Ljungvall, DVM, PhD [b], S.M. Lahmers, DVM, PhD [a], J.A. Abbott, DVM [a]

[a] *Department of Small Animal Clinical Sciences, Virginia-Maryland College of Veterinary Medicine, Blacksburg, VA 24061, USA*
[b] *Department of Clinical Sciences, Swedish University of Agricultural Science, Uppsala, Sweden*

Received 30 March 2016; received in revised form 12 December 2016; accepted 2 January 2017

KEYWORDS
Heart;
Degeneration;
Diagnostic imaging

Abstract *Objective:* To assess differences in morphology of the mitral valve (MV) between healthy dogs and dogs affected by myxomatous mitral valve disease (MMVD) using real-time transthoracic three-dimensional echocardiography (RT3DE). *Animals:* Thirty-four were normal dogs and 79 dogs were affected by MMVD. *Methods:* Real-time transthoracic three-dimensional echocardiography mitral datasets were digitally recorded and analyzed using dedicated software. The following variables were obtained and compared between healthy dogs and dogs with MMVD at different stages: antero-posterior annulus diameter, anterolateral-posteromedial annulus diameter, commissural diameter, annulus height, annulus circumference, annulus area, anterior leaflet length, anterior leaflet area, posterior leaflet length, posterior leaflet area, non-planar angle, annulus sphericity index, tenting height, tenting area, tenting volume, the ratio of annulus height and commissural diameter.

* Corresponding author.
E-mail address: gmencio@gmail.com (G. Menciotti).

http://dx.doi.org/10.1016/j.jvc.2017.01.002

Results: Dogs with MMVD had a more circular MV annulus compared to healthy dogs as demonstrated by an increased annulus sphericity index (p=0.0179). Affected dogs had a less saddle-shaped MV manifest as a decreased annulus height to commissural width ratio (p=0.0004). Tenting height (p<0.0001), area (p<0.0001), and volume (p<0.0001) were less in affected dogs.
Conclusions: Real-time transthoracic three-dimensional echocardiography analysis demonstrated that dogs affected by MMVD had a more circular and less saddle-shaped MV annulus, as well as reduced tenting height area and volume, compared to healthy dogs. Multiple variables differed between dogs at different stages of MMVD. Diagnostic and prognostic utility of these variables, and the significance of these changes in the pathogenesis and natural history of MMVD, require further attention.

Abbreviations

AHCWR	annulus height to commissural width ratio
AnH	annulus height
BW	body weight
MMVD	myxomatous mitral valve disease
MR	mitral regurgitation
MV	mitral valve
nALA	normalized anterior leaflet area
nALL	normalized anterior leaflet length
nALPMD	normalized anterolateral-posteromedial annulus diameter
nAnA	normalized annulus area
nAnCirc	normalized annulus circumference
nAPD	normalized antero-posterior annulus diameter
nCmD	normalized commissural diameter
NPA	non-planar angle
nPLA	normalized posterior leaflet area
nTnV	normalized tenting volume
PLL	posterior leaflet length
RT3DE	real-time transthoracic three-dimensional echocardiography
SI	annulus sphericity index
TnA	tenting area
TnH	tenting height

Introduction

The morphology of the mitral valve (MV) is complex, with some morphologic characteristics considered fundamental to the maintenance of proper function [1—3]. Because normal MV morphology limits the stresses imposed on the valve during each cardiac cycle [4—6], a disruption of normal MV shape could be involved in the pathogenetic mechanisms that induce myxomatous degeneration of the valve, or predispose to this disease process [7—10]. In fact, alterations in MV morphology are known to result in abnormal stress on the valve [11—13]. These unbalanced mechanical forces acting on the valve, may induce signaling pathways that modulate myxomatous degeneration, and differences in MV morphology may explain variation in the propensity for disease development [7,10,14—16]. Real-time transthoracic three-dimensional echocardiography (RT3DE) allows a non-invasive and comprehensive assessment of cardiac structures in-vivo [17,18]. Off-line analysis of MV datasets acquired using RT3DE has provided new insights into MV morphology and function in human myxomatous mitral valve disease (MMVD) [19—21]. We recently reported the feasibility and repeatability of RT3DE for assessing the MV of dogs and provided reference values for this species [22]. The objective of this study was to compare, using RT3DE, the MV morphology of canine patients with different stages of MMVD to findings in healthy dogs.

Animals, materials and methods

Animals

In this study, we prospectively enrolled dogs presented for echocardiographic examination to the Veterinary Teaching Hospital of the Virginia—Maryland College of Veterinary Medicine, as well as dogs owned by students and staff of the same institution between August 2013 and September 2015. To be enrolled in this study, dogs had to be either healthy, or affected by MMVD; each dog's health status was determined by an owner interview, a physical examination that included thoracic auscultation, and echocardiography. Diagnosis of MMVD was based on the presence of thickened and/or prolapsing mitral leaflets on 2D

echocardiography and the presence of mitral regurgitation (MR) identified using color Doppler imaging. Dogs affected by MMVD were classified according to the guidelines of the American College of Veterinary Internal Medicine [23]. Left ventricular enlargement was defined as normalized left ventricular end-systolic or end-diastolic dimension exceeding 1.26 and 1.85, respectively [24]. Left atrial enlargement was defined as a left atrial volume indexed to body weight (BW) greater than 1.1mL/kg [25], or left atrium to aortic root ratio greater than 1.5 [26]. Dogs with clinical evidence of severe systemic diseases known to affect the cardiovascular system were excluded from this study. Dogs with other acquired or congenital cardiovascular abnormalities were excluded as well, even in cases in which the anomaly underwent correction.

Echocardiographic examination

The dogs underwent standard 2D, M-mode and Doppler echocardiographic examination while gently restrained in right and then left lateral recumbency [27]. An electrocardiogram (ECG) was acquired simultaneously. A right-parasternal long-axis view and a left-apical four-chamber view were used for 2D evaluation of MV thickening and prolapse, as well as for color Doppler identification of the presence or absence of MR. Left ventricular end-systolic and end-diastolic dimensions were measured from M-mode images that were directed by a 2D right-parasternal short-axis view. Left atrial to aortic root ratio and left atrial volumes were obtained as previously described [25]. Left-apical acoustic windows were used to acquire RT3DE datasets using a full matrix-array transducer with 3D capabilities[d] connected to the same ultrasound unit.[e] Three-dimensional datasets were acquired using a multi-plane view for guidance: two orthogonal long-axis planes and three short-axis sections were visualized and gain, field depth, focus, azimuth, and elevation were optimized for best visualization of the mitral apparatus. Care was taken to ensure inclusion of the aortic annulus in the acquisition volume. Switching then to full 4D mode, 3D volume datasets were acquired using four consecutive beats and at least three datasets were stored.

[c] 4D MV-Analysis 3.1, TomTec Imaging Systems, Unterschleissheim, Germany.
[d] PST-25SX matrix-array transducer, Toshiba Medical Systems, Tokyo, Japan.
[e] Artida, Toshiba Medical Systems, Tokyo, Japan.

Image analysis

Echocardiographic studies were evaluated for presence/absence of MMVD and disease staging by a board certified cardiologist (MB, JA, SL). Using commercially available software,[c] each RT3DE dataset was analyzed offline by a single operator (GM). Mitral models were created using a semi-automated procedure as previously described [22], and they were then reviewed to check and correct tracing errors. Variables relating to the MV apparatus were automatically measured and derived. Variables known to be significantly related to body size were indexed using the following formula:

$$normalized\ variable = \frac{variable}{BW^{exp}}$$

where 'exp' represents the scaling exponent derived from a previous study on 34 healthy dogs [22]. The following variables were then obtained: normalized antero-posterior annulus diameter (nAPD; exp = 0.308), normalized anterolateral-posteromedial annulus diameter (nALPMD; exp = 0.295), normalized commissural diameter (nCmD; exp = 0.315), annulus height (AnH), normalized annulus circumference (nAnCirc; exp = 0.303), normalized annulus area (nAnA; exp = 0.608), normalized anterior leaflet length (nALL; exp = 0.369), normalized anterior leaflet area (nALA; exp = 0.658), posterior leaflet length (PLL), normalized posterior leaflet area (nPLA; exp = 0.544), non-planar angle (NPA), annulus sphericity index (SI) calculated as APD/ALPMD, tenting height (TnH), tenting area (TnA), normalized tenting volume (nTnV; exp = 0.645). The ratio of AnH and CmD (AHCWR) was calculated as an index of saddle-shape and non-planarity of the mitral annulus [6]. The software used in this study reports TnH as absolute values; therefore, all datasets were reviewed and negative values were used to represent TnH that extended from the mitral annulus into the left atrium. TnV was measured only on the ventricular side of the annulus, and null values were reported by the software for volumes smaller than 0.

Data analysis

Data were analyzed using commercially available software.[f] Between groups, differences in the proportion of males were evaluated using Fisher's exact test. Normal distribution of data was

[f] JMP Pro 11, SAS Institute Inc., Cary, NC, 1989–2013.

assessed by visual inspection and confirmed using a Shapiro–Wilk test. Homoscedasticity was visually inspected and confirmed using a Levene's test. Normally distributed data are presented as mean ± standard deviation, while data that are not normally distributed are presented as median (min–max).

Two sets of comparisons were performed. We first compared the group of healthy dogs to one comprising all dogs affected by MMVD. We then classified MMVD affected dogs based on disease severity [23], and compared four different groups: healthy dogs, dogs in stage B1, dogs in stage B2 and dogs in stage C.

Healthy vs. all affected dogs: When the assumptions of homoscedasticity and normally distributed residuals were met (age, AnH, TnH, AHCWR), Student's *t*-test was used to compare variables obtained from healthy dogs to those from the group that comprised all affected dogs. For some variables, these assumptions were met only after square root transformation (PLL, TnA, nTnV). When these assumptions were not met despite transformation of the data, the Mann–Whitney U test (BW, SI) or Welch's *t*-test (nAPD, nALPMD, nCmD, nAnCirc, nAnA, nALL, nALA, nPLA, NPA) were used as appropriate.

Healthy vs. stages of MMVD: When the assumptions of homoscedasticity and normally distributed residuals were met (age, nALPMD, nCmD, AnH, nAnCirc, NPA), analysis of variance was used to compare variables obtained from healthy dogs to those from the groups that represented the different stages of MMVD. When the null hypothesis was rejected, post hoc analysis was through the use of the Tukey–Kramer honest significant difference test. For some variables, the assumptions of analysis of variance were met only after square root transformation (nAnA, nALL, nALA, nPLA, TnA, TnV, AHCWR). When these assumptions were not met despite transformation of the data (BW, nAPD, SI, PLL, TnH), the Kruskal–Wallis test was used, followed by Dunn's multiple comparisons test.

A corrected *p*-value of <0.05 was considered significant for all the tests.

Results

In this study, 113 dogs were enrolled; 61 were female and 52 male. The most represented breeds were mixed breed (25), Cavalier King Charles Spaniel (11), Beagle (7), Border Collie (7), Dachshund (5), Shih Tzu, (5) and less than five dogs for each of 33 other breeds. Thirty-four dogs were healthy, while 79 were affected by different stages of MMVD: 29 dogs were in stage B1, 39 in stage B2, and 11 in stage C. Sex, age, BW and most represented breeds of healthy dogs and dogs affected by MMVD are reported in Table 1. The proportion of males in the group of healthy dogs and dogs affected by MMVD did not differ, even when the latter group was subdivided based on disease stage. Healthy dogs were younger compared to dogs with MMVD grouped as a whole and also younger when compared to dogs in each of the disease stages. Dogs in stage B1 were younger than dogs in stage B2. Healthy dogs weighed more than dogs with MMVD and than the subgroup of dogs in stage B2 and in stage C. Likewise, dogs in stage B1 weighed more than dogs in stage B2 and in stage C.

Mean values of the measured and calculated RT3DE variables from healthy dogs and all dogs affected by MMVD are presented in Table 2. A significant difference between healthy dogs and dogs with MMVD was found for all variables analyzed except for nPLA. Compared to healthy dogs, dogs affected by MMVD had a greater nAPD, nALPMD, nCmD, nAnCirc, nAnA, nALL, nALA, NPA, and SI. On the other hand, AnH, PLL, TnH, TnA, nTnV, and AHCWR were smaller in dogs with MMVD, compared to healthy dogs (Fig. 1, Fig. 2A and Fig. 2B).

When disease stage was taken into account, dogs in stage B1 had a significantly smaller AnH, TnH, TnA, and nTnV compared to healthy dogs. Dogs in stage B2, compared to both healthy dogs and dogs in stage B1, had a significantly greater nAPD, nALPMD, nCmD, nAnCirc, nAnA, nALL, nALA, SI, and smaller TnH, TnA, nTnV. Furthermore, dogs in stage B2, compared to healthy dogs, had a smaller AnH and AHCWR, but a greater NPA. Dogs in stage C, compared to all the other groups, had a greater nALPMD, nAnCirc, nAnA, nPLA. Also, dogs in stage C had a significantly greater nAPD, nCmD, nALL, nALA, SI, and a smaller TnH, compared to healthy dogs and dogs in stage B1. Compared to healthy dogs, dogs in stage C also had a greater NPA, and smaller AnH, TnA, nTnV, and AHCWR. Values of TnH and SI among different stages of MMVD are presented in Figure 2C and D. Tenting volume was less than 0, and therefore not calculated by the software, in 18 dogs affected by MMVD (two in stage B1, thirteen in stage B2, and three in stage C). Tenting height was considered negative (i.e. measured on the atrial side of the APD) in 15 dogs affected by MMVD (two in stage B1, eight in stage B2, and five in stage C) (Table 3).

Table 1 Sex, age, body weight and the most commonly represented breeds of the dogs enrolled in the study by stage of severity of MMVD. Normal distributed data are presented as mean ± SD, not normally distributed data are presented as median (min–max).

Variable	Healthy dogs (n = 34)	MMVD dogs (n = 79)	MMVD dogs (stages of MMVD)		
			B1 (n = 29)	B2 (n = 39)	C (n = 11)
Sex (M/F)	12/22	40/39	15/14	20/19	5/6
Age (years)	4.5 ± 2.1	10.2 ± 2.6*	9.1 ± 2.9*	10.7 ± 2.3*,†	10.9 ± 2.1*
Body weight (Kg)	19.4 (5.6–29.5)	9.3 (4.1–33.2)*	14.0 (7.2–33.2)	8.0 (4.1–22.6)*,††	8.0 (6.0–11.9)*,†
Breed (n)	Mixed breed (14)	Cavalier King Charles Spaniel (13)	Mixed breed (5)	Cavalier King Charles Spaniel (8)	Miniature Schnauzer (2)
	Beagle (4)	Mixed breed (11)	Cavalier King Charles Spaniel (3)	Mixed breed (4)	Mixed breed (3)
	Australian Shepherd dog (2)	Border Collie (5)	Beagle (2)	Shih Tzu (4)	Cavalier King Charles Spaniel (2)
	Border Collie (2)	Dachshund (5)	Border Collie (2)	Border Collie (3)	Chihuahua (1)
	Boxer (2)	Shih Tzu (5)	Boston Terrier (2)	Other breeds (20)	Dachshund (1)
	Pit Bull (2)	Miniature Schnauzer (4)	Dachshund (2)		Japanese Chin (1)
	Other breeds (8)	Other breeds (36)	Labrador (2)		Lhasa Apso (1)
			Other breeds (11)		

MMVD, myxomatous mitral valve disease; SD, standard deviation.
*$p \leq 0.0001$ compared to healthy dogs.
†$p < 0.05$ compared to stage B1 dogs.
††$p < 0.001$ compared to stage B1 dogs.

Table 2 Measured and calculated variables in healthy dogs and dogs affected by MMVD. Normally distributed data are presented as mean ± SD, while not normally distributed data are presented as median (min–max).

Variable	Healthy dogs (n = 34)	MMVD dogs (n = 79)
nAPD[a]	1.07 (0.86–1.28)	1.22 (0.70–1.85)***
nALPMD[a]	1.21 ± 0.11	1.33 ± 0.19***
nCmD[a]	1.12 ± 0.12	1.25 ± 0.18***
AnH (cm)	0.58 ± 0.17	0.44 ± 0.18***
nAnCirc[a]	3.80 ± 0.33	4.19 ± 0.63***
nAnA[a]	1.08 (0.68–1.42)	1.28 (0.55–2.80)***
nALL[a]	0.62 ± 0.10	0.71 ± 0.15*
nALA[a]	0.56 (0.30–0.80)	0.67 (0.32–1.47)***
PLL (cm)	1.09 (0.69–1.50)	0.91 (0.43–2.02)**
nPLA[a]	0.70 (0.33–1.04)	0.71 (0.30–1.62)
NPA (°)[a]	151.48 ± 14.05	159.91 ± 10.17**
SI[b]	0.92 (0.80–1.11)	0.94 (0.75–1.13)*
TnH (cm)	0.43 ± 0.19	0.14 ± 0.16***
TnA (cm^2)	0.84 (0.25–1.56)	0.31 (0.01–1.41)***
nTnV (cm^3)	0.15 (0.04–0.39)	0.06 (0.00–0.21)*** (n = 61)
AHCWR	0.21 ± 0.05	0.17 ± 0.06***

nAPD, normalized antero-posterior annulus diameter; nALPMD, normalized anterolateral-posteromedial annulus diameter; nCmD, normalized commissural diameter; AnH, annulus height; nAnCirc, normalized annulus circumference; nAnA, normalized annulus area; nALL, normalized anterior leaflet length; nALA, normalized anterior leaflet area; PLL, posterior leaflet length; nPLA, normalized posterior leaflet area; NPA, non-planar angle; SI, annulus sphericity index; TnH, tenting height; TnA, tenting area; nTnV, normalized tenting volume; AHCWR, annulus height to commissural width ratio; MMVD, myxomatous mitral valve disease; SD, standard deviation.
*$p<0.05$ vs. healthy dogs.
**$p<0.01$ vs. healthy dogs.
***$p<0.001$ vs. healthy dogs.
[a] Groups have been compared using a Welch's *t*-test.
[b] Groups have been compared using a Mann–Whitney U test.

Discussion

For the first time in the veterinary literature, we report the results of an extensive, non-invasive in-vivo analysis of MV morphology using RT3DE in dogs affected by MMVD. This study showed that the morphology of the MV, assessed by RT3DE, of dogs affected by MMVD was different from that of healthy dogs; the morphology also differed in dogs at different stages of disease severity (Fig. 2C and D). These changes involved several aspects of the MV apparatus.

Mitral annulus: The annuli of affected dogs were larger than those of healthy dogs, as demonstrated by larger diameter, circumference and

Table 3 Measured and calculated variables in healthy dogs and dogs affected by MMVD at different stages of severity. Normally distributed data are presented as mean ± SD, and differences between groups analyzed using analysis of variance followed by a Tukey–Kramer honestly significant difference test.

Variable	Healthy dogs (n = 34)	Dogs affected by MMVD (stages of MMVD)		
		B1 (n = 29)	B2 (n = 39)	C (n = 11)
nAPD[a]	1.07 (0.86–1.28)	1.06 (0.70–1.33)	1.26 (1.06–1.85)***,†††	1.43 (1.05–1.81)***,†††
nALPMD	1.21 ± 0.11	1.22 ± 0.16	1.36 ± 0.17***,††	1.50 ± 0.20***,†††,¶
nCmD	1.12 ± 0.12	1.13 ± 0.14	1.29 ± 0.16***,†††	1.40 ± 0.20***,†††
AnH (cm)	0.58 ± 0.17	0.45 ± 0.16*	0.45 ± 0.19*	0.40 ± 0.16*
nAnCirc	3.80 ± 0.33	3.77 ± 0.48	4.34 ± 0.54***,†††	4.79 ± 0.63***,†††,¶
nAnA	1.08 (0.68–1.42)	1.05 (0.55–1.73)	1.39 (0.79–2.80)***,†††	1.71 (0.97–2.70)***,†††,¶
nALL	0.62 ± 0.10	0.60 ± 0.09	0.76 ± 0.16***,†††	0.81 ± 0.11***,†††
nALA	0.56 ± 0.13	0.54 ± 0.14	0.76 ± 0.23***,†††	0.88 ± 0.21***,†††
PLL (cm)[a]	1.09 (0.69–1.50)	0.89 (0.43–2.02)	0.91 (0.48–1.45)	0.97 (0.68–1.45)
nPLA	0.70 (0.33–1.04)	0.62 (0.30–1.40)	0.73 (0.36–1.62)	1.07 (0.60–1.59)**,†††,¶
NPA (°)	151.48 ± 14.05	157.38 ± 10.94	161.04 ± 9.70**	163.78 ± 8.59*
SI[a]	0.92 (0.80–1.11)	0.91 (0.75–1.02)	0.96 (0.87–1.09)**,††	0.95 (0.89–1.13)*,†
TnH (cm)[a]	0.43 (0.09–0.81)	0.23 (−0.07–0.62)*	0.09 (−0.35–0.29)***,††	0.02 (−0.08–0.51)***,†
TnA (cm^2)	0.84 (0.25–1.56)	0.38 (0.02–1.41)***	0.25 (0.04–0.78)***,†	0.27 (0.01–0.73)***
nTnV (cm^3)	0.16 ± 0.08	0.10 ± 0.05** (n = 27)	0.05 ± 0.03***,†† (n = 26)	0.08 ± 0.07** (n = 8)
AHCWR	0.21 (0.07–0.30)	0.17 (0.04–0.30)	0.17 (0.05–0.31)*	0.12 (0.06–0.23)**

nAPD, normalized antero-posterior annulus diameter; nALPMD, normalized anterolateral-posteromedial annulus diameter; nCmD, normalized commissural diameter; AnH, annulus height; nAnCirc, normalized annulus circumference; nAnA, normalized annulus area; nALL, normalized anterior leaflet length; nALA, normalized anterior leaflet area; PLL, posterior leaflet length; nPLA, normalized posterior leaflet area; NPA, non-planar angle; SI, annulus sphericity index; TnH, tenting height; TnA, tenting area; nTnV, normalized tenting volume; AHCWR, annulus height to commissural width ratio.

*$p<0.05$ vs. healthy dogs.

**$p<0.01$ vs. healthy dogs.

***$p<0.001$ vs. healthy dogs.

†$p<0.05$ vs. stage B1 dogs.

††$p<0.01$ vs. stage B1 dogs.

†††$p<0.001$ vs. stage B1 dogs.

¶$p<0.05$ vs. stage B2 dogs.

[a] Groups have been compared using a Kruskal–Wallis test followed by Dunn's multiple comparisons test.

area; moreover, dogs with MMVD had more circular annuli (Fig. 1B), compared to the elliptical annuli of healthy dogs (Fig. 1A), as suggested by the SI being closer to one. This finding is in accordance with results from studies in humans with MR [28,29]. These changes were found in dogs in stage B2 and stage C, while no difference was present between healthy dogs and dogs with stage B1, confirming 2D echocardiographic findings previously reported [30]. Interestingly, both healthy and affected dogs had an SI that was larger than that reported in healthy humans [20,31] and much closer to that of people with MR of different etiologies [5,32]. Although studies unbiased with respect to body size, referral, breed, and methodology are lacking, it is likely that the prevalence of MMVD is greater in dogs than in humans [33,34]. MV shape has a role in optimizing leaflet apposition and the forces exerted on the papillary muscles [35,36]; therefore, the findings of this investigation raise the possibility that morphometric characteristics of the MV could contribute to an increased risk of development of MMVD in the dog. However, this is merely speculation and further study would be required to address this.

The annulus of dogs affected by MMVD also lacked a saddle-shape, as demonstrated by smaller AnH, wider NPA, and smaller AHCWR (Fig. 1C and D). The height of the annulus was reduced in dogs without cardiac remodeling while it was not found to be different among the different stages of disease, suggesting that this change occurs either early in course of the disease, or that it is a predisposing factor for its development. The AHCWR is often used as single surrogate of the annular saddle-shape, and is reported to be smaller in humans with MR, although diverse values have been reported in the human literature both for normal individuals and for those with MR. The discrepant values for this variable between different studies could possibly be attributed to the use of different techniques for obtaining the measurement [6,37,38]. In this study the AHCWR values for healthy and diseased dogs were very

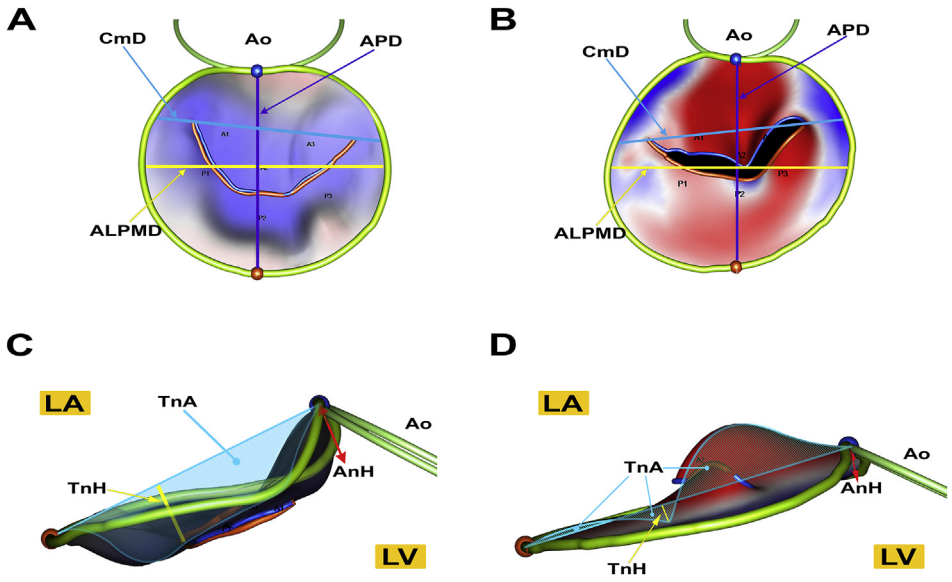

Figure 1 Atrial (A, B) and lateral (C, D) view of mitral valve models of a healthy dog (A, C) and a dog affected by myxomatous mitral valve disease (MMVD) (B, D). Healthy dogs have a more elliptical annulus (A) while dogs with MMVD have a more circular one (B). Furthermore, in healthy dogs the saddle shape is more evident (C) than in dogs with MMVD (D) that have a smaller annulus height. Tenting height and tenting area are reduced in dogs with MMVD (D) compared to healthy dogs (C). Ao, aortic annulus; APD, antero-posterior annulus diameter; ALPMD, anterolateral-posteromedial annulus diameter; CmD, commissural diameter; LA, left atrial side of the valve; TnA, tenting area (dashed); AnH, annulus height; LV, left ventricular side of the valve; TnH, tenting height.

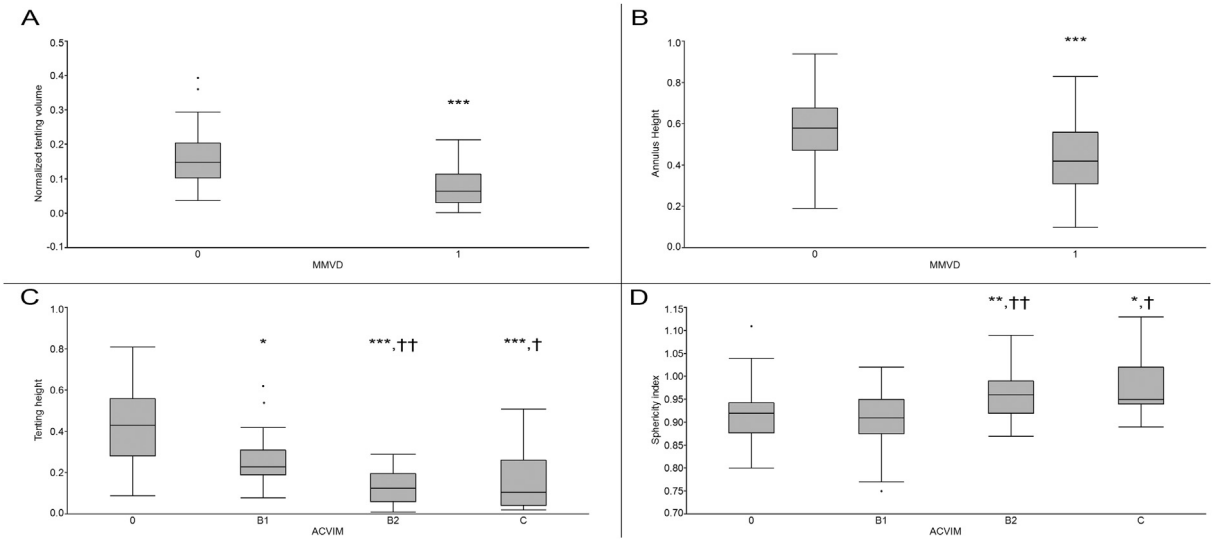

Figure 2 Box and whiskers plots of nTnV (A) and AnH (B) of dogs without (MMVD = 0) and with (MMVD = 1) MMVD, and TnH (C) and SI (D) of dogs at different stages of disease severity. The box encompasses the 3rd and 1st quartile and the horizontal line represents the median; whiskers extend from the end of the box to ±1.5 times the inter-quartile range. MMVD, myxomatous mitral valve disease; TnH, tenting height. *$p<0.05$ vs. healthy dogs; **$p<0.01$ vs. healthy dogs; ***$p<0.001$ vs. healthy dogs; †$p<0.05$ vs. stage B1 dogs; ††$p<0.01$ vs. stage B1 dogs.

similar to the ones recently reported using three-dimensional transesophageal echocardiography in humans with and without MR [37]. Normal AHCWR is known to provide an optimal distribution of stresses on the leaflets and chordae tendineae [6]. This is also supported by recent human studies, in which the choice of more physiologic, saddle-shaped annuloplasty rings is encouraged over flat ones [11,39—41], as saddle-shaped rings offer improved leaflet coaptation [42,43]. This finding suggests a possible role of annulus planarity in the predisposition and stratification of MMVD severity

and prognosis, and for this reason, further investigation is needed. Furthermore, it should be stressed that non-planarity of the MV annulus has important implications for the correct identification and evaluation of mitral prolapse using conventional 2D echocardiography, and should be taken into account when diagnosing prolapsing leaflets with this technique [1].

Mitral leaflets: The anterior mitral leaflets of dogs affected by MMVD had greater length and area (nALL and nALA) than did healthy dogs. However, both of these characteristics were evident only in dogs with more advanced stages of MMVD (stages B2 and C), while healthy dogs and dogs in stage B1 did not differ with respect to nALL and nALA; these findings are in agreement with 2D echocardiographic findings reported by Wesselowski et al. [30]. The posterior leaflet, on the other hand, was shorter in affected dogs than in normal ones, while differences in area were not found. When affected dogs were classified based on stage of MMVD, however, the PLL was not different between groups or when compared to healthy dogs, while the nPLA was greater in dogs in stage C compared to all the other groups. These differences between anterior and posterior MV leaflet, are probably related to the nature of the canine disease, known to affect the anterior leaflet more severely and more often than the posterior [44], while bi-leaflet involvement is more common in dogs with more advanced disease [45]. It is also noteworthy that the PLL was not indexed to the BW, because previous studies of healthy dogs failed to detect a relationship between PLL and body size [22]; however the dogs affected by MMVD in this study weighed significantly less than the healthy ones and a difference in PLL due to this difference cannot be excluded.

Tenting height, area and volume were significantly reduced in affected dogs compared to healthy ones. This finding can be explained by a combination of leaflet prolapse and flattening of the valvular apparatus. In fact, for the software used in this study, it is necessary to perform the analyses during mid-systole when prolapse, if present, reduces the space between the annular plane and leaflets (i.e. tenting). Our data contrast with what has been reported in humans with functional MR [46,47], where the lack of coaptation is caused by tethering and excess tenting of the valve. Surprisingly, our findings are also in contrast with what has been reported in humans with mitral prolapse, using a similar technique [48]. However, the variability in techniques of image acquisition, off-line analyses, and populations involved in these studies need to be taken into account and do not allow a straightforward comparison of these data.

Limitations

The relatively small number of dogs involved in this study, particularly in the stage C group that included just 11 dogs, was a limitation. Groups also differed with respect to age and BW, and although the effect of BW was minimized by appropriate standardization when necessary, controlling for the age of the subject was not attempted in this study. Additionally, as required by the software used, all measurements were performed during mid-systole; while this could be considered the optimal phase of the cardiac cycle for evaluation of annular structure and the presence of prolapse, the coapted position might not be optimal for evaluation of the individual leaflets. Moreover, the relatively low volume rate (i.e. volumes acquired per second, 3D analog of the frame rate in conventional 2D ultrasonography) reported for this technique in other studies, in association with the heart rate of dogs undergoing an echocardiographic examination, could cause the analyses to be performed at different phases of systole for different dogs. We did not attempt to standardize the therapy in the different groups, and evaluation of the effect of different therapies on MV morphology was beyond the scope of this study. The results must be considered in the context of multiple comparisons which increase the likelihood that a type I statistical error may occur. Statistical corrections that reduce the family wide error rate reduce power, and were not applied because the detected differences were directionally consistent, the *p*-values were generally very low and because the work is novel. Finally, the cross-sectional nature of this study did not allow us to determine whether the differences detected were the cause or the consequence of the pathophysiologic processes involved in MMVD, or if any of the variables have prognostic utility.

Conclusions

Use of RT3DE has allowed for further elucidation of the anatomy of the canine MV than previous imaging modalities have allowed. This study demonstrated that the MV of dogs affected by MMVD differed from that of healthy dogs in several morphological aspects. Affected dogs had an increased sphericity and a decreased saddle shape of the MV annulus, as well as a decreased tenting

height, area and volume. This study also demonstrated significant differences in multiple RT3DE MV measurements between dogs with varying severities of MMVD. Further studies are required to better elucidate the cause vs. effect relationship between the studied RT3DE measurements and their impact on both the predisposition to, and the progression of, MMVD in dogs.

Conflicts of Interest

The authors do not have any conflicts of interest to disclose.

References

[1] Levine RA, Triulzi MO, Harrigan P, Weyman AE. The relationship of mitral annular shape to the diagnosis of mitral valve prolapse. Circulation 1987;75:756—67. http://dx.doi.org/10.1161/01.CIR.75.4.756.

[2] Komeda M, Glasson JR, Bolger AF, Daughters GT, Niczyporuk MA, Ingels NB, Miller DC. Three-dimensional dynamic geometry of the normal canine mitral annulus and papillary muscles. Circulation 1996;94:II159—63.

[3] Uechi M. Mitral valve repair in dogs. J Vet Cardiol 2012;14:185—92. http://dx.doi.org/10.1016/j.jvc.2012.01.004.

[4] Spinner EM, Buice D, Yap CH, Yoganathan AP. The effects of a three-dimensional, saddle-shaped annulus on anterior and posterior leaflet stretch and regurgitation of the tricuspid valve. Ann Biomed Eng 2012;40:996—1005. http://dx.doi.org/10.1007/s10439-011-0471-6.

[5] Mahmood F, Gorman III JH, Subramaniam B, Gorman RC, Panzica PJ, Hagberg RC, Lerner AB, Hess PE, Maslow A, Khabbaz KR. Changes in mitral valve annular geometry after repair: saddle-shaped versus flat annuloplasty rings. Ann Thorac Surg 2010;90:1212—20. http://dx.doi.org/10.1016/j.athoracsur.2010.03.119.

[6] Salgo IS, Gorman III JH, Gorman RC, Jackson BM, Bowen FW, Plappert T, St John Sutton MG, Edmunds LH, Gorman JH, Gorman RC, Jackson BM, Bowen FW, Plappert T, St John Sutton MG, Edmunds LH. Effect of annular shape on leaflet curvature in reducing mitral leaflet stress. Circulation 2002;106:711—7. http://dx.doi.org/10.1161/01.CIR.0000025426.39426.83.

[7] Lacerda CMR, MacLea HB, Kisiday JD, Orton EC. Static and cyclic tensile strain induce myxomatous effector proteins and serotonin in canine mitral valves. J Vet Cardiol 2012;14:223—30. http://dx.doi.org/10.1016/j.jvc.2011.12.002.

[8] Grashow JS, Yoganathan AP, Sacks MS. Biaixal stress-stretch behavior of the mitral valve anterior leaflet at physiologic strain rates. Ann Biomed Eng 2006;34:315—25. http://dx.doi.org/10.1007/s10439-005-9027-y.

[9] Waxman AS, Kornreich BG, Gould RA, Moïse NS, Butcher JT. Interactions between TGFβ1 and cyclic strain in modulation of myofibroblastic differentiation of canine mitral valve interstitial cells in 3D culture. J Vet Cardiol 2012;14:211—21. http://dx.doi.org/10.1016/j.jvc.2012.02.006.

[10] Oyama MA, Levy RJ. Insights into serotonin signaling mechanisms associated with canine degenerative mitral valve disease. J Vet Intern Med 2010;24:27—36. http://dx.doi.org/10.1111/j.1939-1676.2009.0411.x.

[11] Ryan LP, Jackson BM, Hamamoto H, Eperjesi TJ, Plappert TJ, St. John-Sutton M, Gorman RC, Gorman III JH. The influence of annuloplasty ring geometry on mitral leaflet curvature. Ann Thorac Surg 2008;86:749—60. http://dx.doi.org/10.1016/j.athoracsur.2008.03.079.

[12] Stevanella M, Krishnamurthy G, Votta E, Swanson JC, Redaelli A, Ingels NB. Mitral leaflet modeling: importance of in vivo shape and material properties. J Biomech 2011;44:2229—35. http://dx.doi.org/10.1016/j.jbiomech.2011.06.005.

[13] Ryan LP, Jackson BM, Enomoto Y, Parish L, Plappert TJ, St. John-Sutton MG, Gorman RC, Gorman III JH. Description of regional mitral annular nonplanarity in healthy human subjects: a novel methodology. J Thorac Cardiovasc Surg 2007;134:644—8. http://dx.doi.org/10.1016/j.jtcvs.2007.04.001.

[14] Orton EC, Lacerda CMR, MacLea HB. Signaling pathways in mitral valve degeneration. J Vet Cardiol 2012;14:7—17. http://dx.doi.org/10.1016/j.jvc.2011.12.001.

[15] Lacerda CMR, Kisiday J, Johnson B, Orton EC. Local serotonin mediates cyclic strain-induced phenotype transformation, matrix degradation, and glycosaminoglycan synthesis in cultured sheep mitral valves. AJP Heart Circ Physiol 2012;302:H1983—90. http://dx.doi.org/10.1152/ajpheart.00987.2011.

[16] Oyama M, Chittur S. Genomic expression patterns of mitral valve tissues from dogs with degenerative mitral valve disease. Am J Vet Res 2006;67:1307—18. http://dx.doi.org/10.2460/ajvr.67.8.1307.

[17] Lang RM, Mor-Avi V, Sugeng L, Nieman PS, Sahn DJ. Three-dimensional echocardiography. J Am Coll Cardiol 2006;48:2053—69. http://dx.doi.org/10.1016/j.jacc.2006.07.047.

[18] Ljungvall I, Höglund K, Carnabuci C, Tidholm A, Häggström J. Assessment of global and regional left ventricular volume and shape by real-time 3-dimensional echocardiography in dogs with myxomatous mitral valve disease. J Vet Intern Med 2011;25:1036—43. http://dx.doi.org/10.1111/j.1939-1676.2011.0774.x.

[19] Khabbaz KR, Mahmood F, Shakil O, Warraich HJ, Gorman III JH, Gorman RC, Matyal R, Panzica P, Hess PE. Dynamic 3-dimensional echocardiographic assessment of mitral annular geometry in patients with functional mitral regurgitation. Ann Thorac Surg 2013;95:105—10. http://dx.doi.org/10.1016/j.athoracsur.2012.08.078.

[20] Mihăilă S, Muraru D, Piasentini E, Miglioranza MH, Peluso D, Cucchini U, Iliceto S, Vinereanu D, Badano LP, Mih, Muraru D, Piasentini E, Miglioranza MH, Peluso D, Cucchini U, Iliceto S, Vinereanu D, Badano LP. Quantitative analysis of mitral annular geometry and function in healthy volunteers using transthoracic three-dimensional echocardiography. J Am Soc Echocardiogr 2014;27:846—57. http://dx.doi.org/10.1016/j.echo.2014.04.017.

[21] Burri MV, Gupta D, Kerber RE, Weiss RM. Review of novel clinical applications of advanced, real-time, 3-dimensional echocardiography. Transl Res 2012;159:149—64. http://dx.doi.org/10.1016/j.trsl.2011.12.008.

[22] Menciotti G, Borgarelli M, Aherne M, Häggström J, Ljungvall I, Lahmers SM, Abbott JA. Assessment of mitral valve morphology using three-dimensional echocardiography. Feasibility and reference values. J Vet Cardiol 2016;18:156—67. http://dx.doi.org/10.1016/j.jvc.2015.11.002.

[23] Atkins C, Bonagura J, Ettinger S, Fox P, Gordon S, Haggstrom J, Hamlin R, Keene B, Luis-Fuentes V, Stepien R. Guidelines for the diagnosis and treatment of canine chronic valvular heart disease. J Vet Intern Med 2009;23:1142—50. http://dx.doi.org/10.1111/j.1939-1676.2009.0392.x.

[24] Cornell CC, Kittleson MD, Della Torre P, Häggström J, Lombard CW, Pedersen HD, Vollmar A, Wey A. Allometric scaling of m-mode cardiac measurements in normal adult dogs. J Vet Intern Med 2004;18:311—21. http://dx.doi.org/10.1111/j.1939-1676.2004.tb02551.x.

[25] Wesselowski S, Borgarelli M, Bello NM, Abbott J. Discrepancies in identification of left atrial enlargement using left atrial volume versus left atrial-to-aortic root ratio in dogs. J Vet Intern Med 2014;28:1527—33. http://dx.doi.org/10.1111/jvim.12410.

[26] Hansson K, Häggström J, Kvart C, Lord P. Left atrial to aortic root indices using two-dimensional and M-mode echocardiography in cavalier King Charles spaniels with and without left atrial enlargement. Vet Radiol Ultrasound 2002;43:568—75. http://dx.doi.org/10.1111/j.1740-8261.2002.tb01051.x.

[27] Thomas WP, Gaber CE, Jacobs GJ, Kaplan PM, Lombard CW, Moise NS, Moses BL, Vet M. Recommendations for standards in transthoracic two-dimensional echocardiography in the dog and cat. J Vet Intern Med 1993;7:247—52. http://dx.doi.org/10.1111/j.1939-1676.1993.tb01015.x.

[28] Moustafa SE, Mookadam F, Alharthi M, Kansal M, Bansal RC, Chandrasekaran K. Mitral annular geometry in normal and myxomatous mitral valves: three-dimensional transesophageal echocardiographic quantification. J Heart Valve Dis 2012;21:299—310.

[29] Kaplan SR, Bashein G, Sheehan FH, Legget ME, Munt B, Li X-N, Sivarajan M, Bolson EL, Zeppa M, Archa M, Martin RW. Three-dimensional echocardiographic assessment of annular shape changes in the normal and regurgitant mitral valve. Am Heart J 2000;139:378—87. http://dx.doi.org/10.1016/S0002-8703(00)90077-2.

[30] Wesselowski S, Borgarelli M, Menciotti G, Abbott J. Echocardiographic anatomy of the mitral valve in healthy dogs and dogs with myxomatous mitral valve disease. J Vet Cardiol 2015;17:97—106. http://dx.doi.org/10.1016/j.jvc.2015.01.003.

[31] Mihaila S, Muraru D, Miglioranza MH, Piasentini E, Peluso D, Cucchini U, Iliceto S, Vinereanu D, Badano LP. Normal mitral annulus dynamics and its relationships with left ventricular and left atrial function. Int J Cardiovasc Imaging 2014:279—90. http://dx.doi.org/10.1007/s10554-014-0547-0.

[32] Schueler R, Momcilovic D, Weber M, Welz A, Werner N, Mueller C, Ghanem A, Nickenig G, Hammerstingl C. Acute changes of mitral valve geometry during interventional edge-to-edge repair with the mitraclip system are associated with midterm outcomes in patients with functional valve disease: preliminary results from a prospective single-center study. Circ Cardiovasc Interv 2014;7:390—9. http://dx.doi.org/10.1161/CIRCINTERVENTIONS.113.001098.

[33] Detweiler DK, Patterson DF. The prevalence and types of cardiovascular disease in dogs. Ann N Y Acad Sci 1965;127:481—516. http://dx.doi.org/10.1111/j.1749-6632.1965.tb49421.x.

[34] Delling FN, Vasan RS. Epidemiology and pathophysiology of mitral valve prolapse: new insights into disease progression, genetics, and molecular basis. Circulation 2014;129:2158—70. http://dx.doi.org/10.1161/CIRCULATIONAHA.113.006702.

[35] Burch GE, Giles TD. Angle of traction of the papillary muscle in normal and dilated hearts: a theoretic analysis of its importance in mitral valve dynamics. Am Heart J 1972;84:141—4. http://dx.doi.org/10.1016/0002-8703(72)90319-5.

[36] Espino DM, Shepherd DET, Buchan KG. Effect of mitral valve geometry on valve competence. Heart Vessels 2007;22:109—15. http://dx.doi.org/10.1007/s00380-006-0937-x.

[37] Lee AP-W, Hsiung MC, Salgo IS, Fang F, Xie J-M, Zhang Y-C, Lin Q-S, Looi J-L, Wan S, Wong RHL, Underwood MJ, Sun J-P, Yin W-H, Wei J, Tsai S-K, Yu C-M. Quantitative analysis of mitral valve morphology in mitral valve prolapse with real-time 3-dimensional echocardiography: importance of annular saddle shape in the pathogenesis of mitral regurgitation. Circulation 2013;127:832—41. http://dx.doi.org/10.1161/CIRCULATIONAHA.112.118083.

[38] Gorman III JH, Jackson BM, Enomoto Y, Gorman RC. The effect of regional ischemia on mitral valve annular saddle shape. Ann Thorac Surg 2004;77:544—8. http://dx.doi.org/10.1016/S0003-4975(03)01354-7.

[39] Timek TA, Glasson JR, Lai DT, Liang D, Daughters GT, Ingels NB, Miller DC. Annular height-to-commissural width ratio of annulolasty rings in vivo. Circulation 2005;112:I423—8. http://dx.doi.org/10.1161/CIRCULATIONAHA.104.525485.

[40] Jensen MO, Jensen H, Smerup M, Levine RA, Yoganathan AP, Nygaard H, Hasenkam JM, Nielsen SL. Saddle-shaped mitral valve annuloplasty rings experience lower forces compared with flat rings. Circulation 2008;118:S250—5. http://dx.doi.org/10.1161/CIRCULATIONAHA.107.746776.

[41] Jassar AS, Vergnat M, Jackson BM, McGarvey JR, Cheung AT, Ferrari G, Woo YJ, Acker MA, Gorman RC, Gorman III JH. Regional annular geometry in patients with mitral regurgitation: implications for annuloplasty ring selection. Ann Thorac Surg 2014;97:64—70. http://dx.doi.org/10.1016/j.athoracsur.2013.07.048.

[42] Vergnat M, Jackson BM, Cheung AT, Weiss SJ, Ratcliffe SJ, Gillespie MJ, Woo YJ, Bavaria JE, Acker MA, Gorman RC, Gorman JH. Saddle-shape annuloplasty increases mitral leaflet coaptation after repair for flail posterior leaflet. Ann Thorac Surg 2011;92:797—803. http://dx.doi.org/10.1016/j.athoracsur.2011.04.047.

[43] Bouma W, Aoki C, Vergnat M, Pouch AM, Sprinkle SR, Gillespie MJ, Mariani MA, Jackson BM, Gorman RC, Gorman JH. Saddle-shaped annuloplasty improves leaflet coaptation in repair for ischemic mitral regurgitation. Ann Thorac Surg 2015;100:1360—6. http://dx.doi.org/10.1016/j.athoracsur.2015.03.096.

[44] Terzo E, Di Marcello M, McAllister H, Glazier B, Lo Coco D, Locatelli C, Palermo V, Brambilla PG. Echocardiographic assessment of 537 dogs with mitral valve prolapse and leaflet involvement. Vet Radiol Ultrasound 2009;50:416—22. http://dx.doi.org/10.1111/j.1740-8261.2009.01559.x.

[45] Borgarelli M, Savarino P, Crosara S, Santilli RA, Chiavegato D, Poggi M, Bellino C, La Rosa G, Zanatta R, Haggstrom J, Tarducci A, La Rosa G. Survival characteristics and prognostic variables of dogs with mitral regurgitation attributable to myxomatous valve disease. J Vet Intern Med 2008;22:120—8. http://dx.doi.org/10.1111/j.1939-1676.2007.0008.x.

[46] Watanabe N, Ogasawara Y, Yamaura Y, Kawamoto T, Toyota E, Akasaka T, Yoshida K. Quantitation of mitral valve tenting in ischemic mitral regurgitation by transthoracic real-time three-dimensional echocardiography. J Am Coll Cardiol 2005;45:763—9. http://dx.doi.org/10.1016/j.jacc.2004.11.048.

[47] Ciarka A, Braun J, Delgado V, Versteegh M, Boersma E, Klautz R, Dion R, Bax JJ, Van de Veire N. Predictors of mitral regurgitation recurrence in patients with heart failure undergoing mitral valve annuloplasty. Am J Cardiol 2010;106: 395—401. http://dx.doi.org/10.1016/j.amjcard.2010.03.042.

[48] Song J-M, Jung Y-J, Jung Y-J, Ji H-W, Kim D-H, Kang D-H, Song J-K. Three-dimensional remodeling of mitral valve in patients with significant regurgitation secondary to rheumatic versus prolapse etiology. Am J Cardiol 2013;111: 1631—7. http://dx.doi.org/10.1016/j.amjcard.2013.02.006.

This manuscript is currently under preparation

Comparison of the Mitral Valve Morphologies of Cavalier King Charles Spaniels and Dogs of other Breeds using Real-time 3D Transthoracic Echocardiography

G. Menciotti, DVM;[a] M. Borgarelli, DVM, PhD;[a] M. Aherne, MVB, GradDipVetStud;[a] P. Camacho;[a] J. Häggström, DVM, PhD;[b] I. Ljungvall, DVM, PhD;[b] S. M. Lahmers, DVM, PhD;[a] J. A. Abbott, DVM.[a]

[a] Department of Small Animal Clinical Sciences, Virginia-Maryland College of Veterinary Medicine, Blacksburg, VA 24061, USA

[b] Department of Clinical Sciences, Swedish University of Agricultural Science, Uppsala, Sweden

Short title for running head: mitral valve morphology in CKCS

Corresponding author: Giulio Menciotti, gmencio@gmail.com

Abstract

Objectives: To determine whether the mitral valve (MV) morphology of healthy Cavalier King Charles Spaniels (CKCSs) differs from the morphology of healthy dogs of other breeds using transthoracic real time 3D echocardiography (RT–3DTTE).

Animals: 35 healthy CKCSs and 41 healthy dogs of other breeds.

Methods: Dogs underwent physical examination, conventional echocardiography, and RT–3DTTE. RT–3DTTE datasets were analyzed using dedicated software for MV morphologic analysis. Morphologic variables were compared between CKCSs and dogs of other breeds.

Results: The MV of healthy CKCSs has a smaller anterolateral-posteromedial diameter ($p=0.0387$), annulus height ($p=0.0021$), tenting height ($p<0.0001$), tenting area ($p<0.0001$), tenting volume ($p=0.0001$) and area of the posterior leaflet ($p=0.0080$) compared to healthy dogs of other breeds.

Conclusions: The MV of CKCSs is flatter and has reduced tenting compared to the MV of other breeds. These morphologic features could confer a mechanical disadvantage, and play a role in the predisposition of this breed to the early development of myxomatous mitral valve disease.

Abbreviations

AHCWR	annulus height to commissural width ratio
AnH	annulus height
ANOVA	analysis of variance
BW	body weight
CKCS	Cavalier King Charles Spaniel
MMVD	myxomatous mitral valve disease
MR	mitral regurgitation
MV	mitral valve
nALA	normalized anterior leaflet area
nALL	normalized anterior leaflet length
nALPMD	normalized anterolateral-posteromedial annulus diameter
nAnA	normalized annulus area
nAnCirc	normalized annulus circumference
nAPD	normalized antero-posterior annulus diameter
nCmD	normalized commissural diameter
NPA	non-planar angle
nPLA	normalized posterior leaflet area
nTnV	normalized tenting volume
PLL	posterior leaflet length
RT–3DTTE	real-time transthoracic three-dimensional echocardiography
SI	annulus sphericity index
SLU	Swedish University of Agricultural Sciences
TnA	tenting area
TnH	tenting height
VMCVM	VA-MD College of Veterinary Medicine

Introduction

Compared to other breeds of dogs, Cavalier King Charles Spaniels (CKCSs) have an earlier onset of myxomatous mitral valve disease (MMVD), and a higher prevalence of the disease at a given age [1–3]. Fifty percent of CKCSs are affected by the age of 6-7 years, and almost 100% are affected by the age of 11 [2–4]. Also, it is known that the development and severity of MMVD in CKCSs is highly heritable [5].

The pathology of MMVD has been extensively described, but little is known of the cause or mechanisms that trigger the observed pathologic changes. The mitral valve (MV) annulus is a hyperbolic paraboloid (commonly described as "saddle-shaped") [9,10]. This geometry, consistent across a number of mammalian species [11], confers a mechanical advantage and is important for optimizing leaflet curvature, reducing leaflet stress, and maintaining valve competency [11–14]. Differences in MV apparatus morphology and presumably, the mechanical forces acting on the valve were suggested as a stimulus for signaling pathways that contribute to myxomatous degeneration and its progression [6–8]. Abnormal stresses on canine MV have been postulated to play a role in the pathogenesis and progression of MMVD in dogs, since they have been directly linked in vitro to an increased expression of myxomatous effector proteins [15]. Therefore, a breed-specific difference in MV apparatus morphology may alter mechanical stresses on valve leaflets that can activate signaling pathways that contribute to myxomatous degeneration and its progression. Data from our laboratory show that the analysis of canine MV using RT–3DTTE is feasible and repeatable, and that healthy dogs have an elliptical, saddle-shaped MV, with parameters defining this shape very similar to those described in healthy humans [10,11,16]. In contrast, dogs affected by MMVD have a more circular and flatter MV [17], therefore lacking some of the aforementioned favorable geometric characteristics. Based on the results of these

studies, we wanted to analyze the MV morphology of healthy CKCSs and compare it to the MV morphology of healthy dogs of other breeds. We hypothesized that the MV of CKCSs would have morphologic differences compared to dogs of other breeds.

Animals, Materials and Methods

Animals: In this study, we prospectively enrolled dogs from two institutions: VA-MD College of Veterinary Medicine (VMCVM), and Swedish University of Agricultural Sciences (SLU). After interview of the pet-owner, each dog was subject to: physical examination including comprehensive cardiac auscultation, conventional 2D / color Doppler echocardiography, and acquisition of a RT–3DTTE dataset. To be enrolled in the study, dogs had to be older than 1 year of age, and without a history of cardiac disease. Additional inclusion criteria comprised: tolerance of a complete echocardiographic examination without need of sedation, absence of evidence of MMVD at conventional 2D and color Doppler examination, and acquisition of RT–3DTTE datasets free from stitching artifacts. Dogs with murmurs graded 1/6 or 2/6 were not excluded provided all inclusion criteria were met.

Methods: The RT–3DTTE datasets were acquired using two different ultrasound units[c,d] equipped with matrix probes[e,f,g]. MMVD was identified when color Doppler echocardiography demonstrated a mitral regurgitant jet that was consistently evident in a right parasternal four-chamber view, and/or a left apical four chamber view, and associated with MV thickening and/or prolapse. All RT–3DTTE datasets were imported into a computer workstation equipped with a dedicated software for MV analysis[h], and analyzed offline by a single operator (GM). Mitral models were created using a semi-automated procedure, and manually reviewed to identify and correct tracing errors, as previously described [10]. Morphologic variables were automatically measured and calculated on the MV models, and variables known to be significantly related to body size

were scaled using allometric equations reported elsewhere [10]. The following variables were obtained: normalized antero-posterior annulus diameter (nAPD), normalized anterolateral-posteromedial annulus diameter (nALPMD), normalized commissural diameter (nCmD), annulus sphericity index (SI) calculated as APD/ALPMD, annulus height (AnH), normalized annulus circumference (nAnCirc), normalized annulus area (nAnA), normalized anterior leaflet length (nALL), normalized anterior leaflet area (nALA), posterior leaflet length (PLL), normalized posterior leaflet area (nPLA), non-planar angle (NPA), tenting height (TnH), tenting area (TnA), normalized tenting volume (nTnV). The ratio of AnH and CmD (AHCWR) was calculated as an index of non-planarity of the mitral annulus [11]. This study was approved by the Institutional Animal Care and Use Committee at Virginia Tech, VA, and by the Ethical Committee for Animal Welfare in Uppsala.

Data analysis: Data describing sex, age, body weight (BW), breed, institution of image acquisition, and the values of the MV morphologic variables, were entered into a spreadsheet and analyzed using commercially available software[i]. Dogs were divided in two groups: *CKCSs* and *dogs of other breeds*. CKCSs were subdivided based on the institution at which images were acquired - VMCVM (VMCVM-CKCSs), or SLU (SLU-CKCSs). Proportions of males, age, BW, and the MV morphologic variables were compared between CKCSs and dogs of other breeds, and between VMCVM-CKCSs and SLU-CKCSs. Normal distribution of data was assessed by visual inspection of normal quantile plots. Homoscedasticity of data was assessed using a Levene's test. Normally distributed data are presented as mean ± standard deviation, while data that were not normally distributed are presented as median (25^{th} – 75^{th} percentile).

Differences in the proportion of males between two groups were assessed using Fisher's exact test. Differences in continuous variables between two groups were assessed using an unpaired

Student's t-test when data followed a normal distribution, Mann–Whitney U test when data were not normally distributed, and Welch's test when the homoscedasticity assumption was not met. Given the finding of an age difference between CKCSs and dogs of other breeds, a possible relationship between the MV morphologic variables and age was investigated using simple linear regression. A p-value corrected for multiple comparisons ≤ 0.05 was considered significant for all tests.

Results

Seventy-six dogs were enrolled in the study: 35 CKCSs and 41 dogs of other breeds, of which the most represented (count ≥ 3) breeds were mixed breed (n=17), Beagle (n=4), and Border Collie (n=3). Forty-seven dogs (of which 14 were CKCSs) were enrolled at the VA-MD College of Veterinary Medicine, and 29 (of which 21 were CKCSs) were enrolled at the Swedish University of Agricultural Sciences. Fifty-three dogs were females (of which 28 were CKCSs), and 23 were males (of which 7 were CKCSs).

CKCSs vs dogs of other breeds: Differences between CKCSs and dogs of other breeds are summarized in Table 1. There was no difference in proportion of males between CKCSs and dogs of other breeds (p=0.085). The median age for all dogs was 3.4 years (2.6 – 5.8 years), and CKCSs were significantly younger than dogs of other breeds. The median BW for all dogs was 10.1 kg (8.5 – 19.5 kg), and CKCSs weighed significantly less than dogs of other breeds. No difference was found between CKCSs and dogs of other breeds regarding nAPD, nCmD, SI, nAnCirc, nAnA, nALL, nALA, nPLL, NPA, and AHCWR. The nALPMD was significantly smaller in CKCSs than in dogs of other breeds. The AnH was smaller in CKCSs, compared to dogs of

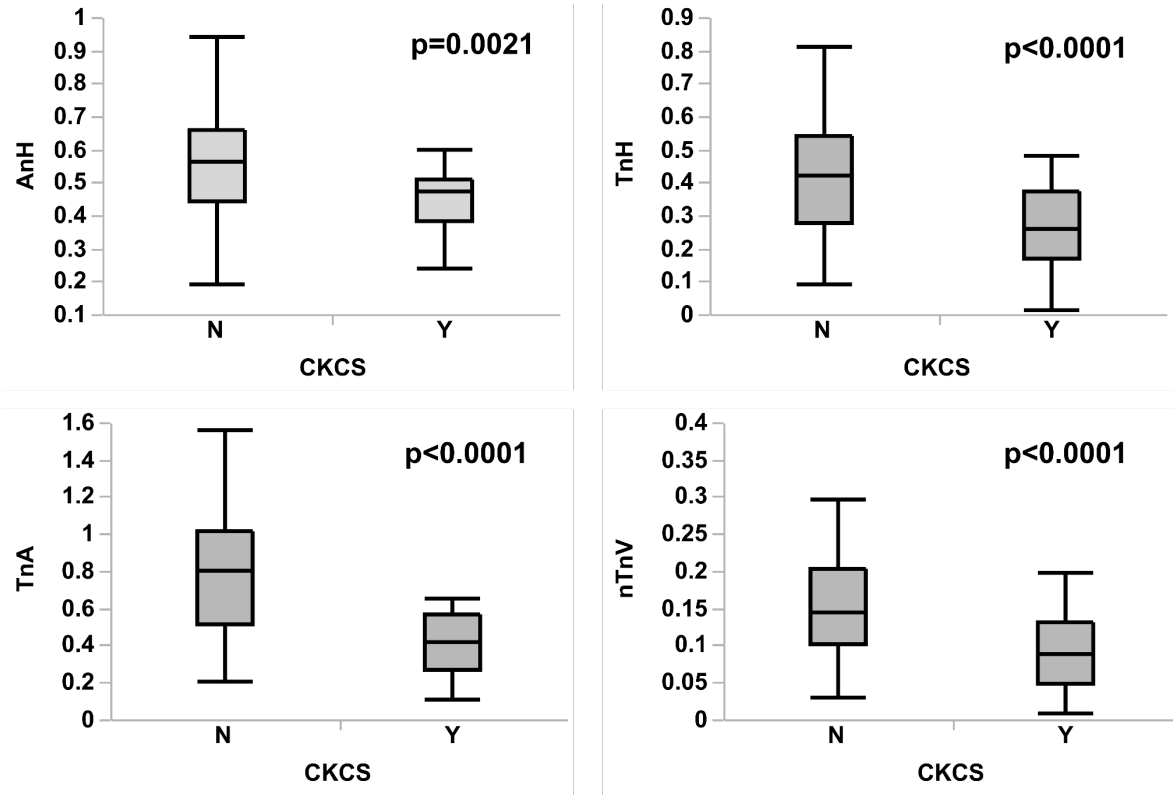

Figure 1 Box and whiskers plots of annulus height and tenting variables in Cavalier King Charles Spaniels and dogs of other breeds. CKCS=N: Dogs of other breeds; CKCS=Y: Cavalier King Charles Spaniels dogs; AnH: Annulus height; TnH: Tenting height; TnA: Tenting area; nTnV: normalized tenting volume. The boxes contain the 25th – 75th percentile and the horizontal line within each box represents the median. The whiskers extend from the 5th to the 95th percentile.

other breeds (Figure 1), as well as the nPLA was smaller in CKCSs than in dogs of other breeds. TnH, TnA, and nTnV were smaller in CKCSs than in dogs of other breeds (Figure 1).

VMCVM-CKCSs vs SLU-CKCSs: Differences between VMCVM-CKCSs and SLU-CKCSs are summarized in Table 2. There was no difference in proportions of males between VMCVM-CKCSs and SLU-CKCSs (p=0.40). The ages of the VMCVM-CKCs and SLU-CKCS were not significantly different, and there was no difference in BW between these two groups. No difference was found between VMCVM-CKCSs and SLU-CKCSs in regard to nAPD, nALPMD, nCmD, SI, AnH, nAnCirc, nAnA, nALL, nALA, nPLA, NPA, AHCWR. The PLL was significantly greater in VMCVM-CKCSs than in SLU-CKCSs. Tenting height, TnA, and nTnV were significantly smaller in SLU-CKCSs compared to VMCVM-CKCSs. There was no relationship between age

and any MV morphologic variable in the entire study population (all p values >0.16), nor among CKCSs (all p values >0.13) and dogs of other breeds (all p values >0.11).

Table 1 Differences in body weight, age, and MV morphologic variables between Cavalier King Charles Spaniels and dogs of other breeds. Normally distributed data are presented as mean ± SD, not normally distributed data are presented as median (25^{th} – 75^{th} percentile). Groups were compared with an unpaired Student's t–test unless indicated by a superscript letter beside the variable.
a = differences analyzed using a Mann–Whitney U test
b = differences analyzed using a Welch's test

Variable	CKCSs	Other breeds	p-value
Age[a]	2.83 (2.00 – 4.42)	4.67 (3.04 – 6.33)	**0.0042**
BW[b]	8.44 ± 1.19	17.70 ± 5.78	**<0.0001**
nAPD	1.03 ± 0.12	1.05 ± 0.11	0.3077
nALPMD	1.13 ± 0.12	1.18 ± 0.13	**0.0387**
nCmD	1.07 ± 0.11	1.10 ± 0.13	0.1374
SI[a]	0.95 (0.91 – 0.98)	0.92 (0.88 – 0.95)	0.0725
AnH[b]	0.46 ± 0.11	0.56 ± 0.17	**0.0021**
nAnnCirc	3.63 ± 0.37	3.73 ± 0.36	0.1307
nAnA	0.98 ± 0.19	1.03 ± 0.19	0.1301
nALL	0.63 ± 0.11	0.62 ± 0.10	0.5932
nALA	0.53 ± 0.13	0.55 ± 0.13	0.2569
PLL[b]	1.06 ± 0.36	1.05 ± 0.27	0.8449
nPLA	0.57 ± 0.15	0.66 ± 0.18	**0.0080**
NPA	151.27 ± 11.26	151.71 ± 14.14	0.4401
TnH[b]	0.26 ± 0.12	0.42 ± 0.18	**<0.0001**
TnA[b]	0.42 ± 0.15	0.79 ± 0.34	**<0.0001**
nTnV[a]	0.09 (0.05 – 0.13)	0.14 (0.10 – 0.20)	**<0.0001**
AHCWR	0.22 ± 0.05	0.21 ± 0.05	0.8294

Table 2 Differences in body weight, age, and MV morphologic variables between Cavalier King Charles Spaniels enrolled at the VA-MD College of Veterinary Medicine (VMCVM–CKCSs) and CKCSs enrolled at the Swedish University of Agricultural Studies (SLU–CKCSs). Normally distributed data are presented as mean±SD, not normally distributed data are presented as median (25^{th} – 75^{th} percentile). Groups were compared with an unpaired Student's t–test unless indicated by a superscript letter beside the variable.
a = differences analyzed using a Mann–Whitney U test

Variable	VMCVM–CKCSs	SLU–CKCSs	p-value
Age[a]	2.92 (1.27 – 4.46)	2.83 (2.13 – 3.79)	0.8926
BW	8.49 ± 1.27	8.41 ± 1.17	0.8590
nAPD	1.04 ± 0.14	1.03 ± 0.11	0.3684
nALPMD	1.16 ± 0.13	1.11 ± 0.11	0.1359
nCmD	1.09 ± 0.12	1.05 ± 0.10	0.1187
SI	0.92 ± 0.06	0.95 ± 0.06	0.9001
AnH	0.45 ± 0.09	0.47 ± 0.12	0.7179
nAnnCirc	3.71 ± 0.40	3.58 ± 0.34	0.1736
nAnA	1.02 ± 0.21	0.95 ± 0.18	0.1710
nALL	0.66 ± 0.11	0.61 ± 0.11	0.1050
nALA	0.56 ± 0.13	0.50 ± 0.13	0.0942
PLL	1.43 ± 0.22	0.82 ± 0.19	**<0.0001**
nPLA	0.58 ± 0.18	0.55 ± 0.13	0.2937
NPA	152.05 ± 10.72	150.76 ± 11.84	0.3702
TnH	0.30 ± 0.11	0.23 ± 0.12	**0.0401**
TnA	0.47 ± 0.14	0.38 ± 0.15	**0.0290**
nTnV	0.11 ± 0.05	0.08 ± 0.05	**0.0212**
AHCWR	0.21 ± 0.04	0.23 ± 0.06	0.8968

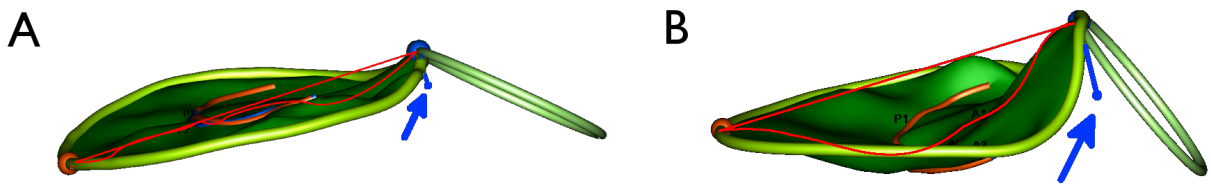

Figure 2 Mitral valve model obtained using RT–3DTTE and offline analysis of a Cavalier King Charles Spaniel (left, A) and a dog of another breed (i.e. Basenji) (right, B). It can be noticed that the leaflet tenting (space contained in the red line) and the height of the annulus (blue bar pointed by the blue arrow) are reduced in the Cavalier King Charles Spaniel.

Discussion

This study demonstrates that the MV morphology of healthy CKCSs differs from that of healthy dogs of other breeds. Specifically, the MV of CKCSs was flatter than in dogs of other breeds, having a reduced AnH and reduced leaflet tenting, as demonstrated by reduced TnH, TnA, and nTnV (Figure 2). It is known that the morphology of the MV has an effect on the stress acting on the leaflets and on the tensioning apparatus [11–14], and therefore an abnormal valvular shape could alter the forces applied on the MV during each cardiac cycle. These abnormal stresses on canine MV have been postulated to play a role in the pathogenesis and progression of MMVD in dogs, since they have been directly linked to an increased expression of myxomatous effector proteins (such as α-smooth muscle actin and matrix metalloproteinases), chondrogenic markers (such as bone morphogenic protein and collagen type 2), and endogenous serotonin synthesis (up-regulation of tryptophan hydroxylase 1) [15]. The differences between the MV morphology of CKCSs and dogs of other breeds did not include 3D indexes of annular non-planarity, such as AHCWR or NPA, that have been associated with increased leaflet stress [11,13]. However, leaflets' spatial configuration, is another fundamental characteristic that potentially minimizes valvular peak stress [11,18]. Interestingly, the four variables found to differ between healthy CKCSs and healthy dogs of other breeds (AnH, TnH, TnA, nTnV), are the same four MV

morphologic variables that our group found altered in a mixed population of dogs affected by MMVD without cardiac remodeling (i.e. ACVIM Stage B1) [17]. This finding supports the hypothesis that morphologic alterations of the valve could represent factors that predispose to the development of the disease, rather than changes that result from disease status, as has been proposed in humans [19]. However, a longitudinal study is needed in order to test this hypothesis. The tenting variables were also significantly reduced in the CKCSs enrolled at SLU, when compared to the ones enrolled at VMCVM. This difference could arise from several sources. First, it might be that the lineages of the two study populations were different. However, evaluation of pedigrees was not part of this study, and therefore this is speculation. Also, there is no report regarding an earlier development of MMVD among CKCSs in Sweden, compared to CKCSs in the Unites States [2,20]. Second, the difference between these two populations of CKCSs could reflect inter-operator variability, or differences in equipment used at the two centers.

The differences in age between CKCSs and dogs of other breeds, and between CKCSs of the two institutions, should not have had an impact on the results of this study. In fact, simple linear regression analysis failed to identify a significant linear relationship between MV morphologic variables and the age of the dogs, both among the entire population, and in the four subpopulations used for data analysis. Interestingly, this might also suggest that the morphologic variables measured in this and previous studies [10,21] are intrinsic characteristics of the MV and of its apparatus that do not change throughout the life of the dogs, at least in the range of ages analyzed in this study (1 – 10 years); however, given the cross-sectional nature of the study, and the fact that dogs were selected based on disease status and therefore have a comparably narrow distribution in age, this is speculation.

There was also a difference in BW between CKCSs and dogs of other breeds and as previously reported, some measurements of MV morphology are significantly related to BW [10]. However, in the current study, the variables known to be significantly related to body sizes had been standardized using allometric indexes derived from a population of healthy dogs [10], therefore eliminating the effect of body sizes on the morphologic variables.

Limitations

Datasets analyzed in this study were acquired in two different centers, equipped with two different ultrasound units, and by multiple operators. This could have introduced some variability in the data. Therefore, the differences in MV morphologies found between CKCSs examined in the two centers, could be attributed to a center bias. The influence of these factors should have been minimized by the nature of the three-dimensional technique, in which the operator has very limited influence on the final dataset. Moreover, one operator using the same software, analyzed all the datasets, which should have further minimized the variability. However, an influence of a parameter intrinsic to the two different acquisition platforms, such as the volume-rate of the acquisition, cannot be excluded. An assessment of the inter-center variation, would require the same dog to be examined in both institutions, which was not feasible. Furthermore, dog's pedigrees information were not acquired, therefore whether the CKCSs examined belong to different lineages is unknown.

Conclusion

The MV of CKCSs, as assessed by RT–3DTTE and offline dedicated analysis, is shorter, has reduced leaflet tenting, and has a smaller posterior leaflet, compared to dogs of other breeds.

These morphologic differences could represent factors that predispose to early onset of MMVD in this breed, but a longitudinal investigation is required in order to confirm this hypothesis.

Footnotes

c) Artida, Toshiba Medical Systems, Tokyo, Japan
d) IE33, Philips Medical Systems, Andover, MA
e) PST-25SX matrix-array transducer, Toshiba Medical Systems, Tokyo, Japan
f) X2-7, Philips Medical Systems, Andover, MA
g) X1-3, Philips Medical Systems, Andover, MA
h) 4D MV-Analysis 2.3, TomTec Imaging Systems, Unterschleissheim, Germany
i) JMP Pro 11, SAS Institute Inc., Cary, NC, 1989-2013

References

[1] Egenvall A, Bonnett BN, Häggström J. Heart Disease as a Cause of Death in Insured Swedish Dogs Younger Than 10 Years of Age. J Vet Intern Med 2006;20:894–903.

[2] Häggström J, Hansson K, Kvart C, Swenson L. Chronic valvular disease in the cavalier King Charles spaniel in Sweden. Vet Rec 1992;131:549–53.

[3] Darke P. Valvular incompetence in Cavalier King Charles Spaniels. Vet Rec 1987;120:365–6.

[4] Malik R, Hunt G, Allan G. Prevalence of mitral valve insufficiency in cavalier King Charles spaniels. Vet Rec 1992;130:302–3.

[5] Lewis T, Swift S, Woolliams J a, Blott S. Heritability of premature mitral valve disease in Cavalier King Charles spaniels. Vet J 2011;188:73–6.

[6] Waxman AS, Kornreich BG, Gould RA, Moïse NS, Butcher JT. Interactions between TGFβ1 and cyclic strain in modulation of myofibroblastic differentiation of canine mitral valve interstitial cells in 3D culture. J Vet Cardiol 2012;14:211–21.

[7] Aupperle H, Disatian S. Pathology, protein expression and signaling in myxomatous mitral valve degeneration: comparison of dogs and humans. J Vet Cardiol 2012;14:59–71.

[8] Orton EC, Lacerda CMR, MacLea HB. Signaling pathways in mitral valve degeneration. J Vet Cardiol 2012;14:7–17.

[9] Levine RA, Handschumacher MD, Sanfilippo AJ, Hagege AA, Harrigan P, Marshall JE, Weyman AE. Three-dimensional echocardiographic reconstruction of the mitral valve, with implications for the diagnosis of mitral valve prolapse. Circulation 1989;80:589–98.

[10] Menciotti G, Borgarelli M, Aherne M, Häggström J, Ljungvall I, Lahmers SM, Abbott JA. Assessment of mitral valve morphology using three-dimensional echocardiography. Feasibility and reference values. J Vet Cardiol 2016;18:156–67.

[11] Salgo IS, Gorman III JH, Gorman RC, Jackson BM, Bowen FW, Plappert T, St John Sutton MG, Edmunds LH, Gorman JH, Gorman RC, Jackson BM, Bowen FW, Plappert T, St John Sutton MG, Edmunds LH. Effect of Annular Shape on Leaflet Curvature in Reducing Mitral Leaflet Stress. Circulation 2002;106:711–7.

[12] Mahmood F, Gorman III JH, Subramaniam B, Gorman RC, Panzica PJ, Hagberg RC, Lerner AB, Hess PE, Maslow A, Khabbaz KR. Changes in mitral valve annular geometry after repair: Saddle-shaped versus flat annuloplasty rings. Ann Thorac Surg 2010;90:1212–20.

[13] Jensen MO, Jensen H, Smerup M, Levine R a., Yoganathan AP, Nygaard H, Hasenkam JM, Nielsen SL. Saddle-Shaped Mitral Valve Annuloplasty Rings Experience Lower Forces Compared With Flat Rings. Circulation 2008;118:S250–5.

[14] Ryan LP, Jackson BM, Hamamoto H, Eperjesi TJ, Plappert TJ, St. John-Sutton M, Gorman RC, Gorman III JH. The Influence of Annuloplasty Ring Geometry on Mitral Leaflet Curvature. Ann Thorac Surg 2008;86:749–60.

[15] Lacerda CMR, MacLea HB, Kisiday JD, Orton EC. Static and cyclic tensile strain induce myxomatous effector proteins and serotonin in canine mitral valves. J Vet Cardiol 2012;14:223–30.

[16] Lee AP-W, Hsiung MC, Salgo IS, Fang F, Xie J-M, Zhang Y-C, Lin Q-S, Looi J-L, Wan S, Wong RHL, Underwood MJ, Sun J-P, Yin W-H, Wei J, Tsai S-K, Yu C-M. Quantitative Analysis of Mitral Valve Morphology in Mitral Valve Prolapse With Real-Time 3-Dimensional Echocardiography: Importance of Annular Saddle Shape in the Pathogenesis of Mitral Regurgitation. Circulation 2013;127:832–41.

[17] Menciotti G, Borgarelli M, Aherne M, Wesselowski S, Häggström J, Ljungvall I, Lahmers SM, Abbott JA. Mitral valve morphology assessed by three-dimensional transthoracic echocardiography in healthy dogs and dogs with myxomatous mitral valve disease. J Vet Cardiol 2017;In Press.

[18] Arts T, Meerbaum S, Reneman R, Corday E. Stresses in the closed mitral valve: A model study. J Biomech 1983;16.

[19] Jassar AS, Vergnat M, Jackson BM, McGarvey JR, Cheung AT, Ferrari G, Woo YJ, Acker M a, Gorman RC, Gorman III JH. Regional annular geometry in patients with mitral regurgitation: implications for annuloplasty ring selection. Ann Thorac Surg 2014;97:64–70.

[20] Beardow AW, Buchanan JW. Chronic mitral valve disease in cavalier King Charles spaniels: 95 cases (1987-1991). J Am Vet Med Assoc 1993;203:1023–9.

[21] Menciotti G, Häggström J, Ljungvall I, Aherne M, Wesselowski S, Abbott JA, Borgarelli M. Three-dimensional echocardiographic comparison of mitral valve morphology in Cavalier King Charles Spaniels to mitral valve morphology in dogs of other breeds. Res. Commun. 24th ECVIM-CA Congr., Journal of Veterinary Internal Medicine; 2017, p. 212.

This manuscript is currently accepted subject to minor revision on Journal of Veterinary Cardiology

Anatomic Regurgitant Orifice Area Obtained Using 3D-Echocardiography As An Indicator of Severity of Mitral Regurgitation in Dogs With Myxomatous Mitral Valve Disease

Sandra Müller, DVM;[a] Giulio Menciotti, DVM;[b] Michele Borgarelli, DVM, PhD;[b]

[a] Department of Clinical Sciences of Companion Animals, Faculty of Veterinary Medicine, Utrecht University, Utrecht, The Netherlands
[b] Department of Small Animal Clinical Sciences, Virginia-Maryland College of Veterinary Medicine, Blacksburg, VA 24061, USA

Corresponding author: Giulio Menciotti, gmencio@gmail.com

Short title: AROA in dogs with MMVD

Presented in part at the 2016 ACVIM Forum, Denver, CO.

Acknowledgments: Sandra Müller performed this study at the Department of Small Animal Clinical Sciences, Virginia-Maryland College of Veterinary Medicine, Blacksburg, VA as part of the Merial Veterinary Scholars Program 2015. The authors acknowledge the help of Dr. Mark Dirven from Utrecht University in the manuscript preparation.

Abstract

Objectives: to determine feasibility and repeatability of measuring the anatomical regurgitant orifice area (AROA) using real-time 3D transthoracic echocardiography (RT3DE) in dogs with myxomatous mitral valve disease (MMVD), and to investigate differences in the AROA of dogs with different disease severity and in different American College of Veterinary Internal Medicine (ACVIM) stages.

Animals: 81 privately-owned dogs diagnosed with MMVD.

Methods: the echocardiographic database of our institution was retrospectively searched for dogs diagnosed with MMVD and RT3DE dataset acquisition. Dogs were classified into mild, moderate or severe MMVD according to a Mitral Regurgitation Severity Score (MRSS), and into stage B1, B2 or C according to ACVIM staging. The RT3DE datasets were imported into dedicated software and a short axis plane crossing the regurgitant orifice was used to measure the AROA. Feasibility, inter- and intra- observer variability of measuring the AROA was calculated. Differences in the AROA between dogs in different MRSS and ACVIM stages were investigated.

Results: The AROA was measurable in 60 datasets out of 81 selected to be included in the study (74.1%). The inter- and intra-observer coefficients of variation were 26% and 21%, respectively. The AROA was significantly greater in dogs with a severe MRSS compared to dogs with mild MRSS ($p=0.045$). There was no difference between the AROA of dogs in different ACVIM clinical stages.

Conclusions: obtaining the AROA using RT3DE is feasible and might provide additional information to stratify mitral regurgitation severity in dogs with MMVD. Diagnostic and prognostic utility of the AROA deserves further investigation.

Key Words

Heart, ultrasound, atrio-ventricular valve, canine, three dimensional

Abbreviation Table

%CV	Coefficient of variation
2DE	Two-dimensional echocardiography
ACVIM	American College of Veterinary Internal Medicine
AROA	Anatomic regurgitant orifice area
BW	Body weight
EROA	Effective regurgitant orifice area
LA	Left atrial
LA:Ao	Left atrial to aortic root ratio
LA Vol/BW	Left atrial volume indexed to body weight
MMVD	Myxomatous mitral valve disease
MR	Mitral regurgitation
MRSS	Mitral regurgitation severity score
MV	Mitral valve
RT–3DTTE	Real-time three-dimensional transthoracic echocardiography

Introduction

Myxomatous mitral valve disease (MMVD) is the most common acquired cardiac disease in dogs, and the most common cause of congestive heart failure in this species [1,2]. Current classification of severity of MMVD in dogs is based on both clinical signs and identification of cardiac remodeling by radiographs and echocardiography [3]. In humans, classification of severity of MMVD is mainly based on echocardiographic criteria [4] with particular attention posed on quantification of mitral regurgitation (MR) [5,6]. In fact, in humans the severity of MR is associated with prognosis in patients with MMVD [5,7]. It is unclear whether the severity of MR is an independent predictor of survival in dogs with MMVD, however, several studies indirectly suggest that this is also true in this species [8–10].

One of the main factors affecting MR severity is the size of the orifice through which MR occurs [11,12]**.** Cardiac Magnetic Resonance Imaging is considered the gold standard to assess the mitral regurgitant orifice, but this technique has several limitations in veterinary medicine including requirement for general anesthesia, time, and specific personnel and equipment, therefore resulting in elevated costs and poor applicability in clinical settings. Two-dimensional echocardiography (2DE), in combination with Doppler based techniques is currently the method of choice for non-invasive evaluation of MR in both humans and dogs [4,9,11,13]. However, obtaining information about the size of the orifice using 2DE and Doppler techniques could be time-consuming, and is demonstrated to suffer from limitations that could arise from misalignment of the scanning plane with the regurgitant jet, and shape and direction of the MR jet [11].

In humans, measuring the area of the regurgitant orifice during systole, i.e. planimetry of the anatomic regurgitant orifice area (AROA), using real-time three-dimensional echocardiography

(RT3DE), proved to be a feasible and accurate way to assess MR [12,14]. Moreover, analysis of the AROA has demonstrated several advantages compared to other conventional techniques, as it is relatively fast and non-invasive [4,12,13]. To the best of our knowledge, no attempt has been made in veterinary medicine to calculate the AROA using RT3DE in dogs affected by MMVD.

The aims of this study were: 1) to determine feasibility and repeatability of the AROA measurements using real-time 3D transthoracic echocardiography (RT3DE) in dogs affected by MMVD; 2) to determine whether the AROA obtained using RT3DE relates to the severity of MR assessed by an echocardiographic scoring system (MRSS) [15] and to the American College of Veterinary Medicine (ACVIM) clinical staging.

Animals, Materials and Methods

The echocardiographic database of the Comparative Cardiovascular Research Lab of the Virginia-Maryland College of Veterinary Medicine was searched for client-owned dogs referred to the Cardiology service of the same institution in a period comprised between July 2013 and June 2015. Inclusion criteria were: echocardiographic diagnosis of MMVD, availability of RT3DE datasets, and availability of a complete echocardiographic examination. The conventional echocardiographic examination comprised acquisition of standard M-mode, 2D, and Doppler blood flow measurements using standard planes [16] with continuous electrocardiographic monitoring using an ultrasound unit[c] equipped with 1.5–10 MHz phased array transducers. Additionally, RT3DE datasets of the mitral valve (MV) were acquired from a left apical acoustic window using the same ultrasound unit[c] equipped with a matrix array transducer.[d] All the RT3DE datasets were acquired using a full-volume four beats acquisition. Myxomatous mitral valve disease in included dogs was diagnosed based on the echocardiographic identification of MV thickening and/or prolapse in combination with the presence of MR identified by color Doppler.

Exclusion criteria were the use of sedative drugs during echocardiographic examination and the presence of other acquired or congenital cardiovascular disorders other than MMVD.

In all dogs, the AROA was measured using commercial dedicated software.[e] Three-dimensional datasets optimized for acquisition of the MV were sorted, and a dataset of appropriate quality and free from stitching artifacts crossing the MV was selected for measuring the AROA. Two orthogonal long-axis planes and a third plane, orthogonal to the other two, and therefore representing a short axis plane, were simultaneously visualized. A mid systolic frame was selected for the analysis. When the number of systolic frame was even, the operator arbitrarily chose one of the two central frames of the sequence. The long-axis planes were aligned perpendicular to the MV leaflets, in order to identify the assumed location of the regurgitant orifice. From this view the short axis plane was aligned so that it crosses the center of the regurgitant orifice. In this latter plane, the area (in cm^2) of the orifice in the MV (AROA) was manually tracked [14] (*Fig. 1*). One observer conducted the measurements in all dogs. The number of datasets in which it was possible to measure the AROA was recorded and the feasibility of this technique was expressed as the percentage of datasets in which the AROA could be obtained over the total dogs fulfilling the inclusion criteria. In addition, 9 volume loops from 9 different patients were randomly selected among the ones in which the AROA was obtained, and, on these loops, the AROA measurement was performed twice by the same observer and also twice by a second observer. These data were used to assess intra-observer repeatability and inter-observer reproducibility of the AROA.

All patients were classified according to the ACVIM staging guidelines [3]. Cardiac remodeling was defined as presence of echocardiographic evidence of left atrial (LA) enlargement (left atrial volume calculated the biplane area-length method [17] indexed to body weight (LA Vol/BW) >1.1

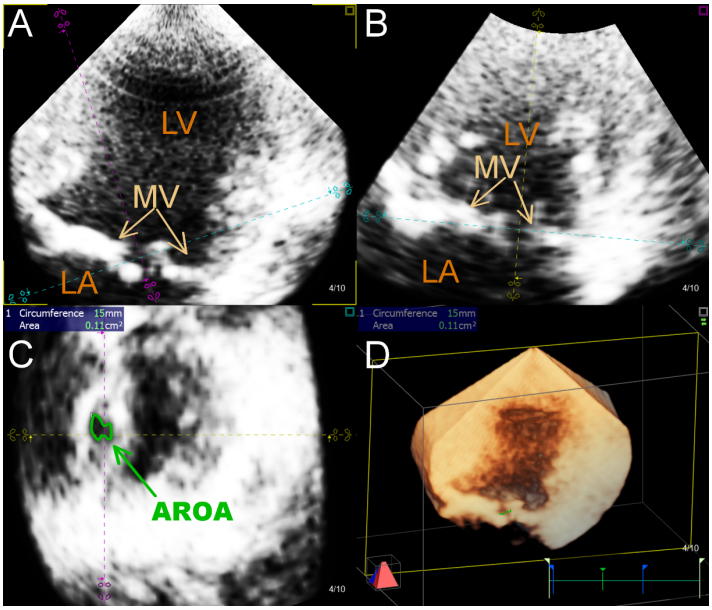

Fig. 1 Obtaining the AROA from RT3DE data set. In a mid-systolic frame, two orthogonal long-axis planes are moved using the pink and the yellow dotted lines parallel to the supposed regurgitation orifice and perpendicular to the MV leaflets (A and B). The short axis plane (light blue line) is aligned so that it crosses the center of the regurgitant orifice so that planimetry of the regurgitant orifice area can be performed in the short axis surgical view of the mitral valve obtained (C). The lower right image shows a 3D overview (D). LV, left ventricle; MV, mitral valve leaflets; LA, left atrium; AROA, anatomic regurgitant orifice area.

ml/kg and/or left atrial to aortic root ratio (LA:Ao) >1.5) [15], and increased left ventricular end-diastolic dimensions (compared to expected dimensions) [17]. For each patient, a MR severity score (MRSS) was also calculated using a previously reported method [15] integrated with the LA dimensions, to assess overall MR severity. The MRSS of this study was therefore determined using the following parameters: Color Doppler regurgitant jet area [18], peak velocity of the mitral inflow [19], left ventricular internal dimension in diastole [20], leaflet anatomy [21], density of the continuous wave Doppler MR signal [13], and LA enlargement using LA volume (LA Vol/BW) and/or the left atrial aortic root ratio (LA:Ao), prioritizing LA Vol/BW (Table 1) [15]. Individual scores for each of the parameters were summed to obtain the MRSS, and total score assigned patients to their MR severity class (mild: 4-7, moderate: 8-12, severe: >12). Due to our inclusion criteria, dogs in this study could have a MRSS ranging from 6 to 17.

Table 1 Classification system for mitral regurgitation severity (MRSS) for dogs with MMVD, based on echocardiographic parameters. The score for each variable is calculated and the sum of the scores provides the MRSS. Four MRSS categories are defined: Normal (MRSS=3), Mild (4≤MRSS≤7), Moderate (8≤MRSS≤12), Severe (MRSS>12). (Modified from Wesselowski S, Borgarelli M, Bello NM, Abbott J. Discrepancies in Identification of Left Atrial Enlargement Using Left Atrial Volume versus Left Atrial-to-Aortic Root Ratio in Dogs. J Vet Intern Med 2014;28:1527–1533.)

	Score			
Echocardiographic Parameter	**0**	**1**	**2**	**3**
Color Doppler regurgitant jet area	None, or trivial	<20% of LA area	20-40% of LA area	>40% of LA area
Mitral inflow		E wave <1.2 m/s	E wave >1.2 m/s (dec. time >80 ms)	E wave >1.2 m/s (dec. time <80 ms)
Left ventricular internal dimension in diastole		Normal	Enlarged (<20% over upper reference limit for BW)	Enlarged (>20% over upper reference limit for BW)
Leaflet anatomy		Normal	Thickening / mitral valve prolapse	Flail leaflet
CW Doppler MR jet density	None	Incomplete/faint	Dense	
LA enlargement: LA:Ao and LA volume	LA:Ao ≤ 1.5 AND LAvol ≤ 1.1 ml/Kg	1.5 < LA:Ao ≤ 1.7, OR 1.1 < LAvol ≤ 1.3 ml/Kg	1.7 < LA:Ao ≤ 2.0, OR 1.3 < LAvol ≤ 1.5 ml/Kg	LA:Ao > 2.0, OR LAvol > 1.5 ml/Kg

Statistical Analysis

Intra- and inter-observer repeatability of the AROA measurements was calculated as % coefficient of variation (%CV). The %CV was calculated for each dog, and is presented as mean (min – max). More, a variance component analysis was performed, using a nested random effect model. The effects of dog, observer (inter-observer), and measurement instance (i.e. repeated measure on the same image by the same observer) were evaluated and are reported as % of total variance. The distributions of age, BW and AROA were tested using the Shapiro-Wilk test. Normally distributed data are presented as mean ±SD, while non-normally distributed data are presented as median (25^{th} – 75^{th} percentile). Baseline characteristics of dogs in which measuring the AROA was possible or not were compared using a Chi-Square test, an unpaired Student's T-test, or a Wilcoxon signed rank test, as appropriate for data characteristics and distribution.

Differences in the AROA between dogs in different MRSS classes, as well as in different ACVIM clinical stages were evaluated using a Kruskall-Wallis test. When this test disclosed statistically significant differences, post-hoc evaluation with a Dunn's Test was performed to determine differences between individual groups. A level of $p \leq 0.05$ was considered significant for all the statistical tests.

Results

Eighty-one dogs were enrolled in the study, of which 46 (57%) were males and 35 (43%) were females, with a mean age of 10.05 ± 2.63 years, and median BW of 9.8 kg (7.3 – 15.2 kg). In 21 patients the AROA could not be obtained because of poor dataset quality or presence of stitching artifacts in the RT3DE examinations. The feasibility of the technique was therefore 74%.

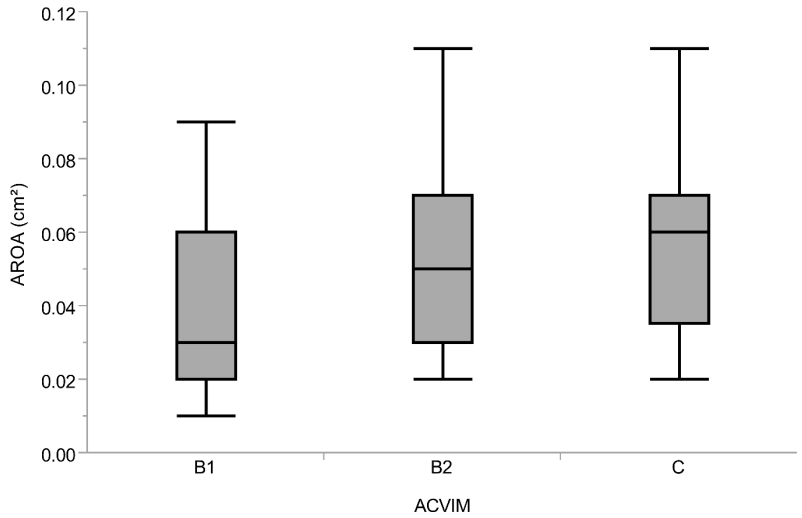

Fig. 2 Box-and-Whiskers plot of the AROA in different ACVIM clinical stages.

The remaining 60 dogs in which the AROA was measurable consisted of 32 males and 28 females, with a mean age of 10.25 ± 2.63 years and median BW of 9.6 kg (7.23 – 13.08). Twenty-five breeds were represented. 11 dogs were of mixed breed origin. The most common breed was Cavalier King Charles Spaniel (n=11), followed by Shih Tzu (n=4), Beagle (n=3), Dachshund (n=3) and Lhasa Apso (n=3). The remaining 19 breeds were represented by two or less dogs each. Twenty-two dogs were classified as ACVIM Stage B1, 29 as Stage B2, and 9 were classified as Stage C. Of the 60 patients, 15 dogs were classified as mild MRSS, 28 dogs as moderate MRSS and 17 as severe MRSS.

Dogs in which it was feasible to measure the AROA had a lower BW than dogs in which the AROA was not measurable (p=0.03). Between dogs with or without planimetry of the AROA, there was no difference in sex proportions (p=0.28) or age (p=0.27).

The inter- and intra-observer coefficients of variation of measuring the AROA were 26% (0 - 64%) and 21% (0 – 35%), respectively. Variance component analysis showed that most of the variation was due to observer (41.1%), followed by measurement instance (31.6%) and dog (27.3%).

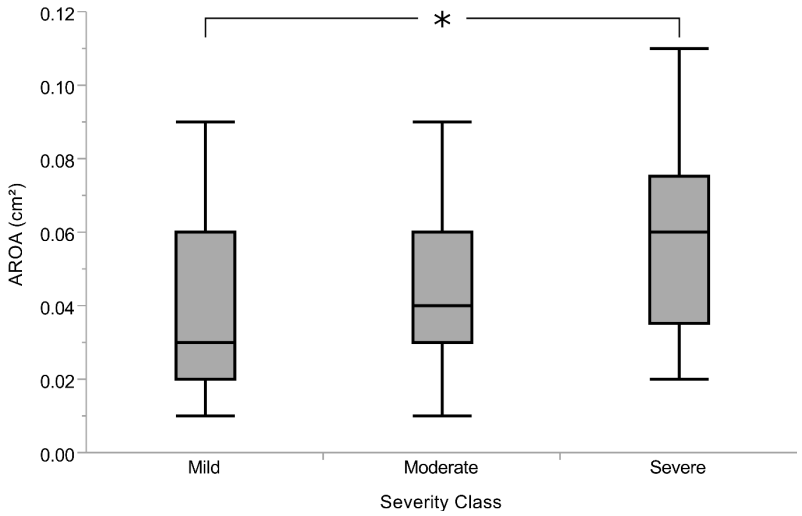

Fig. 3 Box-and-Whiskers plot of the AROA in different MRSS classes. The asterisk indicates a significant difference.

There was no significant difference between the AROA of dogs in different ACVIM stages (p=0.170, Fig. 2). A statistically significant difference was found between the AROA and different MRSS classes (p=0.046). The AROA was significantly greater (p=0.045) in dogs with a severe MRSS [0.06 cm^2 (0.04 – 0.08 cm^2)] compared to the ones with mild MRSS [0.03 cm^2 (0.02 – 0.06 cm^2)]. There was no significant difference in the AROA between dogs in mild and moderate [0.04 cm^2 (0.03 – 0.06 cm^2)] MRSS class (p=0.84) or moderate and severe MRSS (p=0.28) (Fig. 3).

Discussion

This is the first study aimed to measure the AROA in dogs affected by MMVD using RT3DE. In 74% of the RT3DE datasets it was feasible to measure the AROA. In the other 26% (21 patients) poor image resolution or stitching artifacts did not allow measuring the AROA. The feasibility of measuring the AROA reported in human studies is generally higher [4,14,22]. Particularly, Lange and colleagues found a feasibility of 95% when measured from the atrial side and 89% when measured from the ventricle [4]. This higher feasibility is likely due to the fact that those studies were performed using transesophageal echocardiography, which increases resolution and

therefore the quality of the datasets, compared to RT3DE. Dogs in which it was feasible to measure AROA had a significantly lower BW compared to the ones in which AROA was not measurable and this could hypothetically be due to the fact that the same matrix-array transducer was used in all patients, which might provide a better resolution and less stitching artifacts in smaller patients. This finding is in accordance with a previous report on RT3DE in dogs using the same equipment, where the technique proved to be more feasible in smaller dogs, when used for analyzing the MV of a mixed canine population.[f]

The inter- and intra-observer %CVs for the AROA, and the variance component analysis, suggest that the observer contributed the most to the variability. Individual observer preferences on the level of zooming, brightness and contrast of the images, and the accuracy in tracing the AROA could have contributed to this. Standardizing the technique of measuring the AROA and providing more training to observers should be considered in order to improve the variability. However, part of the variability could be intrinsic of the technique and equipment used. In fact, the relatively low volume rate, when compared to the heart rate of dogs undergoing an echocardiographic examination, allows the acquisition of only few systolic frames. The AROA was measured in what appeared as a mid-systolic frame but, given the low temporal resolution, it is possible that the AROA was measured in different phases of the systole. Since the regurgitant orifice is dynamic during the systole [23,24], this could cause variability in the AROA measurement in the same dog, or also among our population of dogs. Also, we did not attempt to evaluate intra-patient beat-to-beat variability of AROA, which could introduce another source of variation. More, individual patients do vary in BW, thoracic conformation, fat percentage and cooperation during ultrasound, which causes variation in resolution.

In this study patients were classified by both ACVIM staging and MRSS. Although there is little conclusive evidence that MR severity can be used as a prognostic factor in veterinary medicine as it is in human medicine, there are various studies that support this hypothesis [26–28]. Currently, no gold standard exists for quantification of MR severity in veterinary medicine. Therefore, a combined assessment with 2DE and Doppler echocardiography is still the method of choice for noninvasive evaluation of MR severity [13,25]. The scoring system used in this study, is attempting this by combining several established echocardiographic parameters which are either associated with a worse prognosis in both pre-clinical and clinical dogs with MMVD [9,26,27], or are validated to assess MR severity [13,18,19]. The system has been used in veterinary medicine before [15], and it is based on previously published recommendations for echocardiographic evaluation of the MR severity in humans and dogs [13,30,31]. Combining the parameters allows internal verification of interpretation and takes physiologic conditions that could alter the accuracy of certain parameters into account. Ultimately, the MRSS gives the opportunity to compare MR severity with the AROA.

The AROA did not show any difference between ACVIM Stages. This is not an unexpected result. In fact, this classification is meant for linking appropriate treatment recommendations to the clinical stages, and it does not strictly evaluate MR severity. Although partially related to development of clinical sign, MR severity is not the only determinant for the development of clinical signs. Hence, it was not expected that the AROA would have been related to ACVIM staging, while the difference found between the AROA and MRSS classes mild and severe was expected, as it can be hypothesized that a bigger AROA would result in a more severe MR and therefore more severe MRSS.

Most limitations of this study are related to its retrospective design. Some dogs were excluded because they had incomplete echocardiographic studies or RT3DE datasets where of insufficient quality. Also, the AROA was not compared to other echocardiographic methods for evaluating MR, like the effective regurgitant orifice area (EROA) or the vena contracta width. In human medicine, there is good correlation between AROA and EROA and in one study the former was found to be more reproducible than the latter, although the bias between the two techniques increases in patients with eccentric jets [4,28]. However, it is necessary to underline that in the referenced studies AROA was calculated using three-dimensional transesophageal echocardiography which has a better spatial resolution compare to RT3DE, but would have limited application in clinical veterinary settings.

Another limitation is that we cannot rule out unconscious bias due to the lack of a blind study design. Although ACVIM stage and MRSS score could have been blinded, it is not possible to avoid expectations on disease severity based on subjective echocardiographic findings while measuring the AROA. Lastly, there is a limited number of dogs enrolled in the study and an imbalance in patient groups. In fact, only 9 dogs were in Stage C, against 22 and 29 in B1 and B2, respectively. This might have limited our ability to detect differences between these groups. According to MRSS classes instead, dogs are more equally distributed, but each individual class comprises relatively few dogs.

Conclusions

This study shows that it is feasible to obtain the AROA in dogs with MMVD using RT3DE. The AROA of patients with severe MR, as assessed by a combination of conventional echocardiographic variables, is greater than the one of patients with mild MR. Further

standardization of the technique is required to improve inter- and intra-observer variability, and investigate the diagnostic and prognostic potential of this variable.

Footnotes

c. Artida, Toshiba Medical Systems, Tokyo, Japan

d. PST-25SX matrix-array transducer, Toshiba Medical Systems, Tokyo, Japan

e. 4D Cardio-View 3.0 TomTec Imaging Systems, Unterschleisssheim, Germany

f. G. Menciotti, M. Borgarelli, S. Wesselowski, J. Abbott. Quantitative evaluation of canine mitral valve in dogs using three-dimensional echocardiography. In: Research Communications of the 24th ECVIM-CA Congress. J Vet Intern Med 2015;29:423–484

References

[1] Detweiler DK, Patterson DF. The prevalence and types of cardiovascular disease in dogs. Ann N Y Acad Sci 1965;127:481–516.

[2] Darke P. Valvular incompetence in Cavalier King Charles Spaniels. Vet Rec 1987;120:365–6.

[3] Atkins C, Bonagura J, Ettinger S, Fox P, Gordon S, Haggstrom J, Hamlin R, Keene B, Luis-Fuentes V, Stepien R. Guidelines for the diagnosis and treatment of canine chronic valvular heart disease. J Vet Intern Med 2009;23:1142–50.

[4] Lange A, Palka P, Donnelly JE, Burstow DJ. Quantification of mitral regurgitation orifice area by 3-dimensional echocardiography: Comparison with effective regurgitant orifice area by PISA method and proximal regurgitant jet diameter. Int J Cardiol 2002;86:87–98.

[5] Grigioni F, Enriquez-Sarano M, Zehr KJ, Bailey KR, Tajik AJ. Ischemic Mitral Regurgitation : Long-Term Outcome and Prognostic Implications With Quantitative Doppler Assessment. Circulation 2001;103:1759–64.

[6] Thavendiranathan P, Phelan D, Collier P, Thomas JD, Flamm SD, Marwick TH. Quantitative assessment of mitral regurgitation: How best to do it. JACC Cardiovasc Imaging 2012;5:1161–75.

[7] Enriquez-Sarano M, Avierinos J-F, Messika-Zeitoun D, Detaint D, Capps M, Nkomo V, Scott C, Schaff H V, Tajik a J. Quantitative determinants of the outcome of asymptomatic mitral regurgitation. N Engl J Med 2005;352:875–83.

[8] Wesselowski S, Borgarelli M, Menciotti G, Abbott J. Echocardiographic anatomy of the mitral valve in healthy dogs and dogs with myxomatous mitral valve disease. J Vet Cardiol 2015;17:97–106.

[9] Sargent J, Muzzi R, Mukherjee R, Somarathne S, Schranz K, Stephenson H, Connolly D, Brodbelt D, Fuentes VL. Echocardiographic predictors of survival in dogs with myxomatous mitral valve disease. J Vet Cardiol 2015;17:1–12.

[10] Ljungvall I, Höglund K, Carnabuci C, Tidholm A, Häggstrom J. Assessment of Global and Regional Left Ventricular Volume and Shape by RealTime 3-Dimensional Echocardiography in Dogs with Myxomatous Mitral Valve Disease. J Vet Intern Med 2011;25:1036–43.

[11] Di Marcello M, Terzo E, Locatelli C, Palermo V, Sala E, Dall'Aglio E, Bussadori CM, Spalla I, Brambilla PG. Assessment of mitral regurgitation severity by Doppler color flow mapping of the vena contracta in dogs. J Vet Intern Med 2014;28:1206–13.

[12] Hamada S, Altiok E, Frick M, Almalla M, Becker M, Marx N, Hoffmann R. Comparison of accuracy of mitral valve regurgitation volume determined by three-dimensional

transesophageal echocardiography versus cardiac magnetic resonance imaging. Am J Cardiol 2012;110:1015–20.

[13] Zoghbi WA, Enriquez-Sarano M, Foster E, Grayburn PA, Kraft CD, Levine RA, Nihoyannopoulos P, Otto CM, Quinones MA, Rakowski H, Stewart WJ, Waggoner A, Weissman NJ, Grayburn MD, William J. Recommendations for evaluation of the severity of native valvular regurgitation with two-dimensional and Doppler echocardiography. J Am Soc Echocardiogr 2003;16:777–802.

[14] Altiok E, Hamada S, van Hall S, Hanenberg M, Dohmen G, Almalla M, Grabskaya E, Becker M, Marx N, Hoffmann R. Comparison of direct planimetry of mitral valve regurgitation orifice area by three-dimensional transesophageal echocardiography to effective regurgitant orifice area obtained by proximal flow convergence method and vena contracta area determined by color. Am J Cardiol 2011;107:452–8.

[15] Wesselowski S, Borgarelli M, Bello NM, Abbott J. Discrepancies in Identification of Left Atrial Enlargement Using Left Atrial Volume versus Left Atrial-to-Aortic Root Ratio in Dogs. J Vet Intern Med 2014;28:1527–33.

[16] Thomas WP, Gaber CE, Jacobs GJ, Kaplan PM, Lombard CW, Moise NS, Moses BL, Vet M. Recommendations for Standards in Transthoracic Two-Dimensional Echocardiography in the Dog and Cat. J Vet Intern Med 1993;7:247–52.

[17] Lang RM, Bierig M, Devereux RB, Flachskampf F a, Foster E, Pellikka P a, Picard MH, Roman MJ, Seward J, Shanewise JS, Solomon SD, Spencer KT, Sutton MSJ, Stewart WJ. Recommendations for chamber quantification: a report from the American Society of Echocardiography's Guidelines and Standards Committee and the Chamber Quantification Writing Group, developed in conjunction with the European Association of Echocardiograph. J Am Soc Echocardiogr 2005;18:1440–63.

[18] Cornell CC, Kittleson MD, Torre P Della, Häggström J, Lombard CW, Pedersen HD, Vollmar A, Wey A. Allometric Scaling of M-Mode Cardiac Measurements in Normal Adult Dogs. J Vet Intern Med 2004;18:311–21.

[19] Muzzi RAL, de Araújo RB, Muzzi LAL, Pena JLB, Silva EF. Regurgitant jet area by Doppler color flow mapping: quantitative assessment of mitral regurgitation severity in dogs. J Vet Cardiol 2003;5:33–8.

[20] Kim J-H, Park H-M. Usefulness of Conventional and Tissue Doppler Echocardiography to Predict Congestive Heart Failure in Dogs with Myxomatous Mitral Valve Disease. J Vet Intern Med 2015;29:132–40.

[21] Stewart JA, Wei CC, Brower GL, Rynders PE, Hankes GH, Dillon AR, Lucchesi PA, Janicki JS, Dell'Italia LJ. Cardiac mast cell- and chymase-mediated matrix metalloproteinase activity and left ventricular remodeling in mitral regurgitation in the dog. J Mol Cell Cardiol 2003;35:311–9.

[22] Terzo E, Di Marcello M, McAllister H, Glazier B, Lo Coco D, Locatelli C, Palermo V, Brambilla PG. Echocardiographic Assessment of 537 Dogs With Mitral Valve Prolapse and Leaflet Involvement. Vet Radiol Ultrasound 2009;50:416–22.

[23] Breburda CS, Griffin BP, Pu M, Rodriguez L, Cosgrove DM, Thomas JD. Three-dimensional echocardiographic planimetry of maximal regurgitant orifice area in myxomatous mitral regurgitation: intraoperative comparison with proximal flow convergence. J Am Coll Cardiol 1998;32:432–7.

[24] Buck T, Plicht B, Kahlert P, Schenk IM, Hunold P, Erbel R. Effect of Dynamic Flow Rate and Orifice Area on Mitral Regurgitant Stroke Volume Quantification Using the Proximal Isovelocity Surface Area Method. J Am Coll Cardiol 2008;52:767–78.

[25] Paiva RMP, Garcia-Guasch L, Manubens J, Montoya-Alonso JA. Proximal isovelocity surface area variability during systole in dogs with mitral valve prolapse. J Vet Cardiol 2011;13:267–70.

[26] Borgarelli M, Savarino P, Crosara S, Santilli RA, Chiavegato D, Poggi M, Bellino C, Rosa G La, Zanatta R, Haggstrom J, Tarducci A, La Rosa G. Survival characteristics and prognostic variables of dogs with mitral regurgitation attributable to myxomatous valve disease. J Vet Intern Med 2008;22:120–8.

[27] Chandra S, Salgo IS, Sugeng L, Weinert L, Settlemier SH, Mor-Avi V, Lang RM. A three-dimensional insight into the complexity of flow convergence in mitral regurgitation: adjunctive benefit of anatomic regurgitant orifice area. Am J Physiol Heart Circ Physiol 2011;301:H1015-24.

[28] Olsen LH, Mow T, Koch J, Pedersen HD. Heart rate variability in young, clinically healthy Dachshunds: influence of sex, mitral valve prolapse status, sampling period and time of day. J Vet Cardiol 1999;1:7–16.

[29] Gouni V, Serres FJ, Pouchelon J-L, Tissier R, Lefebvre HP, Nicolle AP, Sampedrano CC, Chetboul V. Quantification of mitral valve regurgitation in dogs with degenerative mitral valve disease by use of the proximal isovelocity surface area method. J Am Vet Med Assoc 2007;231:399–406.

[30] Borgarelli M, Crosara S, Lamb K, Savarino P, La Rosa G, Tarducci A, Haggstrom J, Santilli RA, Chiavegato D, Poggi M, Bellino C, Rosa G La, Zanatta R, Haggstrom J. Survival characteristics and prognostic variables of dogs with preclinical chronic degenerative mitral valve disease attributable to myxomatous degeneration. J Vet Intern Med 2012;26:69–75.

[31] Häggström J, Boswood A, O'Grady M, Jöns O, Smith S, Swift S, Borgarelli M, Gavaghan B, DiFruscia R, et al. Effect of pimobendan or benazepril hydrochloride on survival times in dogs with congestive heart failure caused by naturally occurring myxomatous mitral valve disease: the QUEST study. J Vet Intern Med 2008;22:1124–35.

Accuracy of Noninvasively Determined Pulmonary Artery Pressure in Dogs with Myxomatous Mitral Valve Disease (MMVD)

G. Menciotti,[a] M. Borgarelli,[a] M. Aherne,[a] J.A. Abbott[a]

[a] Department of Small Animal Clinical Sciences, VA–MD College of Veterinary Medicine, Blacksburg, VA.

Disclosure: The present study is still ongoing, and only preliminary results are presented in this dissertation. Two different observers measured the invasive pressure tracings and the echocardiographic images (JA and MB, respectively), blind to the results obtained by the other observer. The pressure values obtained from the same dog with the two techniques were then matched by a third observer unrelated to the study, and both dogs' identity and the nature of the technique used for obtaining each value were anonymized. The resulting table of matched pairs of pressures was then analyzed.

Materials and methods

Animals: Data presented in this report had been collected from dogs presented for cardiac evaluation to the cardiology service of the VA–MD College of Veterinary Medicine. To be enrolled in this study, dogs had to weigh 5 kg or more and be affected by MMVD in ACVIM Stage B2 or "stable" Stage C [1]. Echocardiographic criteria defining MMVD were: presence of a consistent MR jet assessed by Doppler echocardiography associated with evidence of thickened and/or prolapsing MV leaflets at 2D echocardiographic examination. Stage B2 was defined by a left atrium to aortic root ratio $\geq$ 1.7 [2] and a normalized left ventricular diameter > 1.7 (according to Cornell's method) [3], provided that the patient never had clinical signs of heart disease or had never been treated with cardiovascular drugs. Stable stage C was defined as dogs with MMVD that have, or have had, radiographic pulmonary edema. Before enrollment, patients receiving cardiovascular drugs had to be stable in their treatment, without a change in dosages of any drug, for at least 1 month. All dogs enrolled had to have measurable tricuspid regurgitant (TR) jet. All dogs enrolled had a normal renal function assessed by blood evaluation of creatinine and urea. Dogs with PH not due to MMVD were excluded from the study.

All dogs enrolled in the study had a consent form signed by the owner. The study was approved by the Virginia Tech Institutional Animal Care and Use Committee (IACUC #16-092).

Methods: *Clinical variables*: The following clinical variables were collected: breed, sex, age, presence/absence of dyspnea, presence/absence of cough, presence/absence of syncope, presence/absence of exercise intolerance, drugs currently administered.

Blood pressure measurement: a cuff of appropriate size was positioned on right or left limb. A Doppler probe was positioned under the cuff and once the sound of blood flow was clearly heard the cuff was be inflated. The cuff was then slowly de-inflated until blood flow sounds were

detected. Dogs were minimally restrained in lateral recumbency during this procedure to prevent excessive movement.

Sedation: To obtain uniform, comparable and more accurate measurements, and to mitigate stress during the procedures, all patients were sedated prior to echocardiographic examination and cardiac catheterization: an IV catheter was placed in the cephalic or saphenous vein and dogs were administered acepromazine (0.03 mg/kg IV) and buprenorphine (0.007 mg/kg IV). This sedation protocol is reported not to have significant hemodynamic effects [4].

Doppler estimation of systolic pulmonary artery (PA) pressure: Systolic PA pressure was estimated by the simplified Bernoulli equation using the peak velocity of TR ($PASP = 4 \times TR^2$). No attempt to add a clinical estimate of right atrial pressure was performed in this preliminary report. Echocardiographic examination and cardiac catheterization were performed simultaneously.

Right ventricular catheterization: Cefazolin (20 mg/kg/IV) was administered immediately before, and 90 minutes and 8 hours after, catheterization. Dogs were positioned in left lateral recumbency, and after infiltration of the subcutis with lidocaine, a sheath-introducer system was aseptically placed into the right external jugular vein using the modified Seldinger technique. For recordings of intracardiac and intravascular pressures, a multi-lumen, flow-directed catheter equipped with a thermistor was connected to a fluid-filled pressure transducer system. Atmospheric pressure, with the transducer positioned at the level of the right atrium, was taken as zero-pressure reference. The analogue pressure signal was amplified and subject to digital conversion (MP150 – BioPac) for display and then storage on a laptop computer. A simultaneously recorded electrocardiogram was also digitally stored. Commercially available software (Acqknowledge – BioPac) was used to view and analyze the digitally stored data. The catheter was also attached to a dedicated cardiac output (CO) computer (Baxter Healthcare Corporation [Edwards Com-2])

for determination of CO by thermodilution, averaging the values obtained by 3 to 5 injections of iced 5% dextrose (5cc per injection). The tip of the catheter was sequentially advanced to the right atrium, right ventricle, PA and then to the "wedge" position. In general, catheter manipulations were guided by observation of the distinctive pressure contours of the relevant chambers and vessels. However, fluoroscopy was available to guide or confirm catheter placement if necessary.

Statistical Analysis: Data were visually assessed for normality using normal quantile plots. All continuous data followed a normal distribution and are therefore presented as mean ± SD. Pearson correlation was generated to evaluate association of between the two methods. Linear regression equations were determined and evaluated for goodness of fit (r^2). Bland-Altman analysis was used to describe the agreement between the two methods, reported as the bias and 95% limits of agreement. Given the concealed nature of the two methods during this preliminary analysis, it was impossible to determine which of the two methods represented the "gold standard", therefore the analysis of receiver operating characteristic curves to determine the accuracy of Doppler estimation of systolic PA pressure was not attempted.

Results

Thirteen dogs were enrolled in the study in a period comprised between 5/14/2014 to 2/23/2017. Cardiac catheterization failed in 1 of the dogs, due to the impossibility of percutaneously puncturing the right jugular vein despite several attempts. One dog was excluded from the data analysis because of the impossibility to obtain a clean PA trace.

Data regarding breed, sex, age, presence/absence of dyspnea, respiratory rate, heart rate, presence/absence of cough, presence/absence of syncope, presence/absence of exercise intolerance, and treatment are reported in Table 1. The mean age of the examined dogs was 10.86 ± 3.23 years and the mean body weight was 12.60 ± 6.12 kg. The most represented breeds were CKCSs, Whippet, and Mixed breed, with two dogs enrolled per each breed. The remaining dogs enrolled in the study were one Bichon Frisee, one Border Collie, one Dachshund, one Miniature Schnauzer and one Shetland Sheepdog. The mean blood pressure was 128.61 ± 30.02 mmHg. At enrollment, 1 dog was reported to have dyspnea, 4 cough, 3 syncope, and 3 exercise intolerance. Nine dogs were classified as ACVIM Stage B2 and 2 as ACVIM Stage C at the moment of enrollment. Three dogs were receiving pimobendan, 1 dogs an ace-inhibitor (enalapril), and 2 furosemide. The mean CO was 1.36 ± 0.78 L/min, which represents a mean cardiac index (CO/Body Weight) of 113 ± 4 mL/Kg/min. Table 2 represents the 22 matched PA pressures obtained from the 11 analyzed dogs. The mean pressure resulting from using "Method X" was 23.92 ± 9.86 mmHg, while the one resulting from using "Method Y" was 24.67 ± 7.75 mmHg.

Variable	Value
Age (years)	10.86 ± 3.23
Weight (Kg)	12.60 ± 6.12
Sex (M/F)	5/6
Breeds	CKCS (2), Whippet (2), Mixed Breed (2), Bichon Frisee (1), Border Collie (1), Dachshund (1), Min Schnauzer (1), Shetland Sheepdog (1)
IBP	128.61 ± 30.02
Dyspnea (Y/N)	1/10
Cough (Y/N)	4/7
Syncope (Y/N)	3/8
Exerc. Int. (Y/N)	3/8
ACVIM (B2/C)	9/2
Pimobendan (n.)	3
Ace-I (n.)	1
Furosemide (n.)	2

Table 1 – Characteristics of the 11 examined dogs. Data are presented as mean ± SD. IBP: Invasive blood pressure. The rows relative to Pimobendan, Ace-I and Furosemide report how many dogs were treated with the drug.

Table 2 – Measured and estimated systolic PA pressure. Each row reports the systolic PA pressure measured invasively and the one estimated using the modified Bernoulli equation applied to peak tricuspid regurgitant jet. The type of measurement and the dog identifier were anonymized before analysis.

Method X (mmHg)	Method Y (mmHg)
11.6	22.2
22.6	22.3
40.8	34.9
9.5	13.5
25.8	25.3
38.7	28.9
17.0	30.7
22.3	21.5
19.6	10.8
29.6	34.6

Pearson correlation coefficient between the two techniques was 0.6725 (p=0.0234) and the linear regression between the measurements obtained with the two techniques is represented in Fig. 1.

Fig. 2 represents a Bland-Altman plot of the PA measurements obtained with the two techniques. The mean difference between the measurements obtained with the two techniques (Method Y - Method X) was 0.75mmHg. The 95% confidence interval of the mean difference included 0, indicating the absence of a significant bias. Visual analysis of the plot indicated also absence of a trend towards under- or overestimation of one technique respect to the other in the range of pressures measured. The upper and lower 95% limits of agreement between the two techniques were +15.98mmHg and -14.47mmHg, respectively, which indicates that results obtained by Method Y may be 15.98mmHg above or 14.47mmHg below the measurement obtained by Method X.

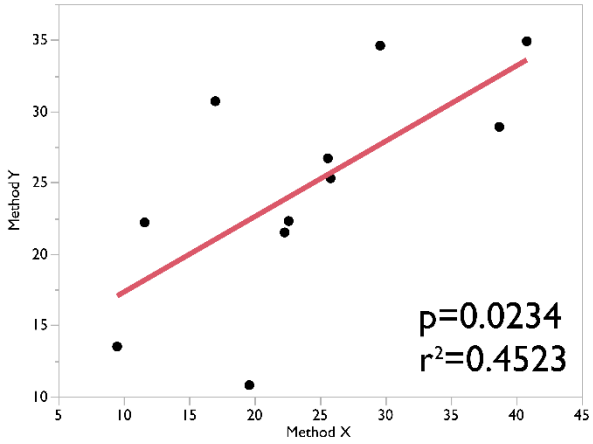

Fig. 1 Measurements obtained using Method X plotted against measurements obtained using Method Y. A linear regression line is fitted to the data.

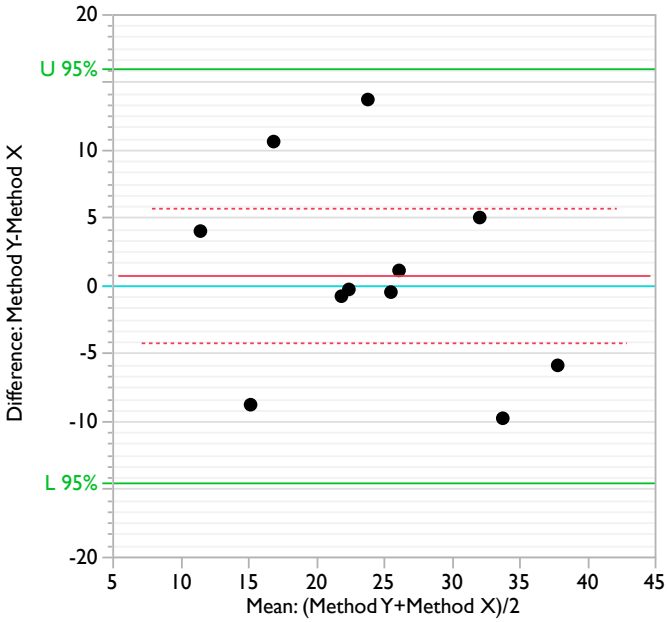

Fig. 2 Bland–Altman plot. The mean of the measurements obtained with the two methods is plotted against the difference between the two measurements. The red line represents the mean difference, and the dotted red line represent the 95% confidence interval of the mean difference. The green lines represent the upper (U 95%) and lower (L 95%) limits of agreement.

Comment

The preliminary analysis reported here indicates that the two techniques used for obtaining the systolic PA pressure are significantly related, but they do not present good agreement. The 95% limits of agreement reported here are narrower than what previously reported in a canine experimental model of pulmonary embolism [5], but it must be noticed that the range of pressures examined in the present study is significantly narrower than the one in the experimental model. However, the entity of the limits of agreement reported here indicates that one method could either underestimate or overestimate the other by about 15mmHg. Given the order of magnitude of systolic PA pressures in normal dogs, and dogs with PH, this represent a clinically relevant error that can be introduced in the patient's evaluation.

References

[1] Atkins C, Bonagura J, Ettinger S, Fox P, Gordon S, Haggstrom J, Hamlin R, Keene B, Luis-Fuentes V, Stepien R. Guidelines for the diagnosis and treatment of canine chronic valvular heart disease. J Vet Intern Med 2009;23:1142–50.

[2] Rishniw M, Erb HN. Evaluation of four 2-dimensional echocardiographic methods of assessing left atrial size in dogs. J Vet Intern Med 2000;14:429–35.

[3] Cornell CC, Kittleson MD, Torre P Della, Häggström J, Lombard CW, Pedersen HD, Vollmar A, Wey A. Allometric Scaling of M-Mode Cardiac Measurements in Normal Adult Dogs. J Vet Intern Med 2004;18:311–21.

[4] Stepien RL, Bonagura JD, Bednarski RM, Muir WW. Cardiorespiratory effects of acepromazine maleate and buprenorphine hydrochloride in clinically normal dogs. Am J Vet Res 1995;56:78–84.

[5] Soydan LC, Kellihan HB, Bates ML, Stepien RL, Consigny DW, Bellofiore A, Francois CJ, Chesler NC. Accuracy of Doppler echocardiographic estimates of pulmonary artery pressures in a canine model of pulmonary hypertension. J Vet Cardiol 2014.

Conclusions

In conclusion, analyzing the MV of dogs using RT–3DTTE is feasible, repeatable, and provides valuable information. The morphology of the MV is generally elliptical and saddle-shaped in healthy dogs, with most of the morphologic variables related to the size of the dogs in an allometric fashion. Dogs affected by MMVD have a MV with a disrupted morphology, which is overall more circular and flatter than the MV of healthy dogs. Some morphologic characteristics are related to the severity of the disease. The height of the annulus and the degree of leaflets' tenting are reduced in dogs at early stages of the disease, before significant cardiac remodeling has occurred. The MV of healthy CKCSs presents the same morphologic alterations when compared to the MV of a mixed population of healthy dogs of other breeds. Given the importance of MV biomechanics, and the known link between abnormal valvular stress and development of myxomatous degeneration, this supports speculations on whether these morphologic characteristics represent predisposing factors for the disease development in dogs. A longitudinal study is required in order to confirm this hypothesis.

From the results of the studies reported here, we can also conclude that RT–3DTTE is a feasible way to measure AROA in dogs with MMVD, and that AROA is different between dogs with mild and severe MMVD. However, we must also conclude that the technique used in our study is poorly repeatable and reproducible, most likely for a lack of standardization of the technique and for technical constraints.

The preliminary and blind nature of the data regarding the accuracy of pulmonary arterial pressure estimation using Doppler echocardiography allows for only limited conclusion: the two

techniques have wide 95% limits of agreement. Both under- and over-estimation of one of the two techniques is present, in some cases reaching magnitudes of 15mmHg.

Future directions

In the future, we would like to prospectively enroll CKCSs for a longitudinal study of MV morphology and age of onset of the disease. Given the results presented in this dissertation, we hypothesize that there will be a relationship between morphologic aspects of the MV and the age of onset of MMVD in this breed, with dogs that present a flatter valve presenting an earlier onset of the disease.

We also would like to better standardize the 3D evaluation of the regurgitant orifice of dogs affected by MMVD, in order to obtain a reliable index of the severity of the regurgitation, which could also have important diagnostic and prognostic implications.

Lastly, we will continue to enroll dogs in the study evaluating the accuracy of Doppler echocardiography for estimating pulmonary artery pressure. When 20 dogs will be enrolled, we will analyze the data and we will be able to calculate the accuracy of the Doppler estimation of pulmonary artery pressure in dogs with MMVD.

References

[1] Detweiler DK, Patterson DF. The prevalence and types of cardiovascular disease in dogs. Ann N Y Acad Sci 1965;127:481–516.

[2] Detweiler DK, Patterson DF, Hubben K, Botts RP. The prevalence of spontaneously occurring cardiovascular disease in dogs. Am J Public Health Nations Health 1961;51:228–41.

[3] Darke P. Valvular incompetence in Cavalier King Charles Spaniels. Vet Rec 1987;120:365–6.

[4] Malik R, Hunt G, Allan G. Prevalence of mitral valve insufficiency in cavalier King Charles spaniels. Vet Rec 1992;130:302–3.

[5] Häggström J, Hansson K, Kvart C, Swenson L. Chronic valvular disease in the cavalier King Charles spaniel in Sweden. Vet Rec 1992;131:549–53.

[6] Beardow AW, Buchanan JW. Chronic mitral valve disease in cavalier King Charles spaniels: 95 cases (1987-1991). J Am Vet Med Assoc 1993;203:1023–9.

[7] Aupperle H, März I, Thielebein J, Kiefer B, Kappe A, Schoon H-A. Immunohistochemical characterization of the extracellular matrix in normal mitral valves and in chronic valve disease (endocardiosis) in dogs. Res Vet Sci 2009;87:277–83.

[8] Aupperle H, Disatian S. Pathology, protein expression and signaling in myxomatous mitral valve degeneration: comparison of dogs and humans. J Vet Cardiol 2012;14:59–71.

[9] Han RI, Black A, Culshaw GJ, French AT, Else RW, Corcoran BM. Distribution of myofibroblasts, smooth muscle–like cells, macrophages, and mast cells in mitral valve leaflets of dogs with myxomatous mitral valve disease. Am J Vet Res 2008;69:763–9.

[10] Disatian S, Ehrhart EJ, Zimmerman S, Orton EC. Interstitial cells from dogs with naturally occurring myxomatous mitral valve disease undergo phenotype transformation. J Heart Valve Dis 2008;17:402–11; discussion 412.

[11] Han RI, Black A, Culshaw G, French AT, Corcoran BM. Structural and cellular changes in canine myxomatous mitral valve disease: an image analysis study. J Heart Valve Dis 2010;19:60–70.

[12] Hadian M, Corcoran BM, Han RI, Grossmann JG, Bradshaw JP. Collagen organization in canine myxomatous mitral valve disease: an x-ray diffraction study. Biophys J 2007;93:2472–6.

[13] Pomerance A, Whitney JC. Heart valve changes common to man and dog: a comparative study. Cardiovasc Res 1970;4:61–6.

[14] Stephens EH, Nguyen TC, Itoh A, Ingels NB, Miller DC, Grande-Allen KJ. The effects of mitral regurgitation alone are sufficient for leaflet remodeling. Circulation 2008;118:S243-9.

[15] Nguyen TC, Itoh A, Carlhäll CJ, Bothe W, Timek TA, Ennis DB, Oakes RA, Liang D,

Daughters GT, Ingels NB, Miller DC. The effect of pure mitral regurgitation on mitral annular geometry and three-dimensional saddle shape. J Thorac Cardiovasc Surg 2008;136:557–65.

[16] Moustafa SE, Mookadam F, Alharthi M, Kansal M, Bansal RC, Chandrasekaran K. Mitral annular geometry in normal and myxomatous mitral valves: three-dimensional transesophageal echocardiographic quantification. J Heart Valve Dis 2012;21:299–310.

[17] Lewis T, Swift S, Woolliams J a, Blott S. Heritability of premature mitral valve disease in Cavalier King Charles spaniels. Vet J 2011;188:73–6.

[18] Swenson L, Häggström J, Kvart C, Juneja RK. Relationship between parental cardiac status in Cavalier King Charles spaniels and prevalence and severity of chronic valvular disease in offspring. J Am Vet Med Assoc 1996;208:2009–12.

[19] Olsen LH, Fredholm M, Pedersen HD. Epidemiology and inheritance of mitral valve prolapse in Dachshunds. J Vet Intern Med 1999;13:448–56.

[20] Swift S, Baldin A, Cripps P. Degenerative Valvular Disease in the Cavalier King Charles Spaniel: Results of the UK Breed Scheme 1991-2010. J Vet Intern Med 2017:9–14.

[21] Lundin T, Kvart C. Evaluation of the Swedish breeding program for cavalier King Charles spaniels. Acta Vet Scand 2010;52:54.

[22] Birkegård AC, Reimann MJ, Martinussen T, Häggström J, Pedersen HD, Olsen LH. Breeding Restrictions Decrease the Prevalence of Myxomatous Mitral Valve Disease in Cavalier King Charles Spaniels over an 8- to 10-Year Period. J Vet Intern Med 2016;30:63–8.

[23] Perloff JK, Roberts WC. The mitral apparatus. Functional anatomy of mitral regurgitation. Circulation 1972;46:227–39.

[24] Tsakiris AG, Von Bernuth G, Rastelli GC, Bourgeois MJ, Titus JL, Wood EH. Size and motion of the mitral valve annulus in anesthetized intact dogs. J Appl Physiol 1971;30:611–8.

[25] Levine RA, Triulzi MO, Harrigan P, Weyman AE. The relationship of mitral annular shape to the diagnosis of mitral valve prolapse. Circulation 1987;75:756–67.

[26] Levine RA, Handschumacher MD, Sanfilippo AJ, Hagege AA, Harrigan P, Marshall JE, Weyman AE. Three-dimensional echocardiographic reconstruction of the mitral valve, with implications for the diagnosis of mitral valve prolapse. Circulation 1989;80:589–98.

[27] Gillinov AM, Cosgrove DM, Blackstone EH, Diaz R, Arnold JH, Lytle BW, Smedira NG, Sabik JF, McCarthy PM, Loop FD. Durability of mitral valve repair for degenerative disease. J Thorac Cardiovasc Surg 1998;116:734–43.

[28] Ryan LP, Jackson BM, Hamamoto H, Eperjesi TJ, Plappert TJ, St. John-Sutton M, Gorman RC, Gorman III JH. The Influence of Annuloplasty Ring Geometry on Mitral Leaflet Curvature. Ann Thorac Surg 2008;86:749–60.

[29] Jensen MO, Jensen H, Smerup M, Levine R a., Yoganathan AP, Nygaard H, Hasenkam JM, Nielsen SL. Saddle-Shaped Mitral Valve Annuloplasty Rings Experience Lower Forces Compared With Flat Rings. Circulation 2008;118:S250–5.

[30] Spinner EM, Buice D, Yap CH, Yoganathan AP. The effects of a three-dimensional, saddle-

shaped annulus on anterior and posterior leaflet stretch and regurgitation of the tricuspid valve. Ann Biomed Eng 2012;40:996–1005.

[31] Bouma W, Aoki C, Vergnat M, Pouch AM, Sprinkle SR, Gillespie MJ, Mariani MA, Jackson BM, Gorman RC, Gorman JH. Saddle-Shaped Annuloplasty Improves Leaflet Coaptation in Repair for Ischemic Mitral Regurgitation. Ann Thorac Surg 2015;100:1360–6.

[32] Mahmood F, Gorman III JH, Subramaniam B, Gorman RC, Panzica PJ, Hagberg RC, Lerner AB, Hess PE, Maslow A, Khabbaz KR. Changes in mitral valve annular geometry after repair: Saddle-shaped versus flat annuloplasty rings. Ann Thorac Surg 2010;90:1212–20.

[33] Jassar AS, Vergnat M, Jackson BM, McGarvey JR, Cheung AT, Ferrari G, Woo YJ, Acker M a, Gorman RC, Gorman III JH. Regional annular geometry in patients with mitral regurgitation: implications for annuloplasty ring selection. Ann Thorac Surg 2014;97:64–70.

[34] Gorman III JH, Jackson BM, Enomoto Y, Gorman RC. The effect of regional ischemia on mitral valve annular saddle shape. Ann Thorac Surg 2004;77:544–8.

[35] Salgo IS, Gorman III JH, Gorman RC, Jackson BM, Bowen FW, Plappert T, St John Sutton MG, Edmunds LH, Gorman JH, Gorman RC, Jackson BM, Bowen FW, Plappert T, St John Sutton MG, Edmunds LH. Effect of Annular Shape on Leaflet Curvature in Reducing Mitral Leaflet Stress. Circulation 2002;106:711–7.

[36] Arts T, Meerbaum S, Reneman R, Corday E. Stresses in the closed mitral valve: A model study. J Biomech 1983;16.

[37] Lacerda CMR, MacLea HB, Kisiday JD, Orton EC. Static and cyclic tensile strain induce myxomatous effector proteins and serotonin in canine mitral valves. J Vet Cardiol 2012;14:223–30.

[38] Dekker DL, Piziali RL, Dong E. A system for ultrasonically imaging the human heart in three dimensions. Comput Biomed Res 1974;7:544–53.

[39] Buck T, Plicht B. Real-Time Three-Dimensional Echocardiographic Assessment of Severity of Mitral Regurgitation Using Proximal Isovelocity Surface Area and Vena Contracta Area Method. Lessons We Learned and Clinical Implications. Curr Cardiovasc Imaging Rep 2015;8:38.

[40] Tidholm A, Westling a B, Höglund K, Ljungvall I, Häggström J. Comparisons of 3-, 2-dimensional, and M-mode echocardiographical methods for estimation of left chamber volumes in dogs with and without acquired heart disease. J Vet Intern Med 2010;24:1414–20.

[41] Tidholm A, Bodegård-Westling A, Höglund K, Ljungvall I, Häggström J. Comparisons of 2- and 3-Dimensional Echocardiographic Methods for Estimation of Left Atrial Size in Dogs with and without Myxomatous Mitral Valve Disease. J Vet Intern Med 2011;25:1320–7.

[42] Ljungvall I, Höglund K, Carnabuci C, Tidholm A, Häggström J. Assessment of global and regional left ventricular volume and shape by real-time 3-dimensional echocardiography in dogs with myxomatous mitral valve disease. J Vet Intern Med 2011;25:1036–43.

[43] Menciotti G, Borgarelli M, Aherne M, Häggström J, Ljungvall I, Lahmers SM, Abbott JA.

Assessment of mitral valve morphology using three-dimensional echocardiography. Feasibility and reference values. J Vet Cardiol 2016;18:156–67.

[44] Whitney JC. Cardiovascular Pathology. J Small Anim Pract 1967;8:459–65.

[45] Buck T, Franke A, Monaghan MJ. Three-dimensional Echocardiography. Berlin, Heidelberg: Springer Berlin Heidelberg; 2015.

[46] Kellihan HB, Stepien RL. Pulmonary hypertension in canine degenerative mitral valve disease. J Vet Cardiol 2012;14:149–64.

[47] Johnson L, Boon J, Orton EC. Clinical characteristics of 53 dogs with Doppler-derived evidence of pulmonary hypertension: 1992-1996. J Vet Intern Med 1999;13:440–7.

[48] Pyle R, Abbott JA, MacLean H. Pulmonary hypertension and cardiovascular sequelae in 54 dogs. Intern J Appl Res Vet Med 2004:99–109.

[49] Bach JF, Rozanski EA, MacGregor J, Betkowski JM, Rush JE. Retrospective evaluation of sildenafil citrate as a therapy for pulmonary hypertension in dogs. J Vet Intern Med 2006;20:1132–5.

[50] Guglielmini C, Civitella C, Diana A, Tommaso M Di, Cipone M, Luciani A, Di Tommaso M. Serum cardiac troponin I concentration in dogs with precapillary and postcapillary pulmonary hypertension. J Vet Intern Med 2010;24:145–52.

[51] Borgarelli M, Zini E, D'Agnolo G, Tarducci A, Santilli RA, Chiavegato D, Tursi M, Prunotto M, Häggström J. Comparison of primary mitral valve disease in German Shepherd dogs and in small breeds. J Vet Cardiol 2004;6:27–34.

[52] Serres FJ, Chetboul V, Tissier R, Sampedrano CC, Gouni V, Nicolle AP, Pouchelon JL. Doppler echocardiography–derived evidence of pulmonary arterial hypertension in dogs with degenerative mitral valve disease: 86 cases (2001–2005). J Am Vet Med Assoc 2006;229:1772–8.

[53] Delgado JF, Conde E, Sánchez V, López-Ríos F, Gómez-Sánchez MA, Escribano P, Sotelo T, de la Cámara AG, Cortina J, de la Calzada CS. Pulmonary vascular remodeling in pulmonary hypertension due to chronic heart failure. Eur J Heart Fail 2005;7:1011–6.

[54] Guazzi M, Arena R. Pulmonary hypertension with left-sided heart disease. Nat Rev Cardiol 2010;7:648–59.

[55] Delgado JF. The pulmonary circulation in heart failure. Rev Esp Cardiol (Engl Ed) 2010;63:334–45.

[56] Chiavegato D, Borgarelli M, D'Agnolo G, Santilli R a. Pulmonary hypertension in dogs with mitral regurgitation attributable to myxomatous valve disease. Vet Radiol Ultrasound 2009;50:253–8.

[57] Barbieri A, Bursi F, Grigioni F, Tribouilloy C, Avierinos JF, Michelena HI, Rusinaru D, Szymansky C, Russo A, Suri R, Bacchi Reggiani ML, Branzi A, Modena MG, Enriquez-Sarano M, Tribouilloy C, Rusinaru D, Szymanski C, Fournier A, Trojette F, Touati G, Remadi JP, Grigioni F, Russo A, Piovaccari G, Ferlito M, Ionico T, Barbaresi E, Branzi A, Savini C, Martin-Suarez S, Marinelli G, Di Bartolomeo R, Avierinos JF, Tafanelli L, Habib G, Collard F, Riberi A, Metras D, Barbieri A, Bursi F, Grimaldi T, Nuzzo A, Modena MG, Enriquez-

Sarano M, Michelena HI, Suri R, Bacchi-Reggiani ML. Prognostic and therapeutic implications of pulmonary hypertension complicating degenerative mitral regurgitation due to flail leaflet: A Multicenter Long-term International Study. Eur Heart J 2011;32:751–9.

[58] Cappola TP, Felker GM, Kao WHL, Hare JM, Baughman KL, Kasper EK. Pulmonary hypertension and risk of death in cardiomyopathy: Patients with myocarditis are at higher risk. Circulation 2002;105:1663–8.

[59] Ghio S, Gavazzi A, Campana C, Inserra C, Klersy C, Sebastiani R, Arbustini E, Recusani F, Tavazzi L. Independent and additive prognostic value of right ventricular systolic function and pulmonary artery pressure in patients with chronic heart failure. J Am Coll Cardiol 2001;37:183–8.

[60] Borgarelli M, Abbott J, Braz-Ruivo L, Chiavegato D, Crosara S, Lamb K, Ljungvall I, Poggi M, Santilli R a., Haggstrom J. Prevalence and Prognostic Importance of Pulmonary Hypertension in Dogs with Myxomatous Mitral Valve Disease. J Vet Intern Med 2015;29:569–74.

[61] Galiè N, Hoeper MM, Humbert M, Torbicki A, Vachiery J-L, Barbera JA, Beghetti M, Corris P, Gaine S, Gibbs JS, Gomez-Sanchez M a, Jondeau G, Klepetko W, Opitz C, Peacock A, Rubin L, Zellweger M, Simonneau G. Guidelines for the diagnosis and treatment of pulmonary hypertension. Eur Respir J 2009;34:1219–63.

[62] Fisher MR, Forfia PR, Chamera E, Housten-Harris T, Champion HC, Girgis RE, Corretti MC, Hassoun PM. Accuracy of doppler echocardiography in the hemodynamic assessment of pulmonary hypertension. Am J Respir Crit Care Med 2009;179:615–21.

[63] Brecker SJ, Gibbs JS, Fox KM, Yacoub MH, Gibson DG. Comparison of Doppler derived haemodynamic variables and simultaneous high fidelity pressure measurements in severe pulmonary hypertension. Heart 1994;72:384–9.

[64] Henik RA. Pulmonary Hypertension. In: Bonagura JD, Tweedt DC, editors. Kirk's Curr. Vet. Ther. 14th ed., St. Louis, Missouri: Saunders Elsevier; 2009, p. 697–708.

[65] Kellum HB, Stepien RL. Sildenafil citrate therapy in 22 dogs with pulmonary hypertension. J Vet Intern Med 2007;21:1258–64.

[66] Skjaerpe T, Hatle L. Noninvasive estimation of systolic pressure in the right ventricle in patients with tricuspid regurgitation. Eur Heart J 1986;7:704–10.

[67] Yock PG, Popp RL. Noninvasive estimation of right ventricular systolic pressure by Doppler ultrasound in patients with tricuspid regurgitation. Circulation 1984;70:657–62.

[68] Testani JM, St John Sutton MG, Wiegers SE, Khera A V, Shannon RP, Kirkpatrick JN. Accuracy of noninvasively determined pulmonary artery systolic pressure. Am J Cardiol 2010;105:1192–7.

[69] Altman DG, Bland JM. Measurement in medicine: the analysis of method comparison studies. Statistician 1983;32:307–17.

[70] Zhang RF, Zhou L, Ma GF, Shao FC, Wu XH, Ying KJ. Diagnostic value of transthoracic Doppler echocardiography in pulmonary hypertension: a meta-analysis. Am J Hypertens 2010;23:1261–4.

[71] Janda S, Shahidi N, Gin K, Swiston J. Diagnostic accuracy of echocardiography for pulmonary hypertension: a systematic review and meta-analysis. Heart 2011;97:612–22.

[72] Soydan LC, Kellihan HB, Bates ML, Stepien RL, Consigny DW, Bellofiore A, Francois CJ, Chesler NC. Accuracy of Doppler echocardiographic estimates of pulmonary artery pressures in a canine model of pulmonary hypertension. J Vet Cardiol 2014.